

The curvature sensitivity of membrane-binding amphipathic helices can be modulated by the electrostatics of their flanking regions

by

Sharon Shin Yin Chong

B.Sc., University of British Columbia, 2010

Thesis Submitted in Partial Fulfillment of the
Requirements for the Degree of
Master of Science

in the

Department of Molecular Biology and Biochemistry
Faculty of Science

© Sharon Shin Yin Chong 2013

SIMON FRASER UNIVERSITY

Fall 2013

All rights reserved.

However, in accordance with the *Copyright Act of Canada*, this work may be reproduced, without authorization, under the conditions for "Fair Dealing." Therefore, limited reproduction of this work for the purposes of private study, research, criticism, review and news reporting is likely to be in accordance with the law, particularly if cited appropriately.

Approval

Name: Sharon Shin Yin Chong

Degree: Master of Science

Title of Thesis: *The curvature sensitivity of membrane-binding amphipathic helices can be modulated by the electrostatics of their flanking regions*

Examining Committee: **Chair:** Dr. Barry Honda
Professor
Department of Molecular Biology and Biochemistry

Dr. Rosemary B. Cornell
Senior Supervisor
Professor
Department of Molecular Biology and Biochemistry, Department of Chemistry

Dr. Jenifer Thewalt
Supervisor
Professor
Department of Molecular Biology and Biochemistry, Department of Physics

Dr. Frederic F. Pio
Supervisor
Associate Professor
Department of Molecular Biology and Biochemistry

Dr. Martin Zuckermann
Internal Examiner
Adjunct Professor
Department of Physics, Simon Fraser University
Professor Emeritus
Department of Physics, McGill University

Date Defended/Approved: December 5, 2013

Partial Copyright Licence



The author, whose copyright is declared on the title page of this work, has granted to Simon Fraser University the non-exclusive, royalty-free right to include a digital copy of this thesis, project or extended essay[s] and associated supplemental files (“Work”) (title[s] below) in Summit, the Institutional Research Repository at SFU. SFU may also make copies of the Work for purposes of a scholarly or research nature; for users of the SFU Library; or in response to a request from another library, or educational institution, on SFU’s own behalf or for one of its users. Distribution may be in any form.

The author has further agreed that SFU may keep more than one copy of the Work for purposes of back-up and security; and that SFU may, without changing the content, translate, if technically possible, the Work to any medium or format for the purpose of preserving the Work and facilitating the exercise of SFU’s rights under this licence.

It is understood that copying, publication, or public performance of the Work for commercial purposes shall not be allowed without the author’s written permission.

While granting the above uses to SFU, the author retains copyright ownership and moral rights in the Work, and may deal with the copyright in the Work in any way consistent with the terms of this licence, including the right to change the Work for subsequent purposes, including editing and publishing the Work in whole or in part, and licensing the content to other parties as the author may desire.

The author represents and warrants that he/she has the right to grant the rights contained in this licence and that the Work does not, to the best of the author’s knowledge, infringe upon anyone’s copyright. The author has obtained written copyright permission, where required, for the use of any third-party copyrighted material contained in the Work. The author represents and warrants that the Work is his/her own original work and that he/she has not previously assigned or relinquished the rights conferred in this licence.

Simon Fraser University Library
Burnaby, British Columbia, Canada

revised Fall 2013

Abstract

Membrane-induced amphipathic helices (m-AH) can act as membrane curvature sensors by binding preferentially to hydrophobic lipid packing defects enriched in curved surfaces. Weak electrostatic interactions can impart a greater reliance on hydrophobicity and membrane curvature for binding. I probed the role of modifying membrane and protein charge on the curvature sensing of two m-AH containing proteins, CTP:phosphocholine cytidyltransferase (CCT) and alpha-synuclein (alpha-syn). The m-AH in both proteins are flanked by disordered tails with multiple phosphoserines (CCT) or acidic residues (alpha-syn), which I mutated to glutamate or serine to modify protein charge. Analysis of binding to vesicles of varying curvature showed that increasing negative charge of the tail region decreased binding strength and augmented curvature dependence, which I attribute to charge repulsion. Conversely, increasing the membrane negative charge dampened the curvature dependence. Our data show that discrimination of curved vs. flat membranes with high negative charge could be modulated by phosphorylation.

Keywords: CTP:phosphocholine cytidyltransferase; alpha-synuclein; membrane curvature sensing; phosphorylation; amphipathic helices, fluorescence, circular dichroism, lipid vesicles

*To my family, friends and the members of the
Cornell Lab for their support and enthusiasm.*

Acknowledgements

This work was supported by a grant to Rosemary B. Cornell from the Natural Sciences and Engineering Research Council. Thank you to Dr. Rosemary B. Cornell for her guidance and support throughout the entire project and to members of my committee, Dr. Jenifer Thewalt and Dr. Frederic Pio for their input and timely advice. Thank you to Svetla G. Taneva for her help in all aspects of this project. I thank Ziwei Ding and Jaeyong Lee for the construction of several plasmids and advice on transformation and expression conditions, Dr. B. Frisken and her students Gabriel Espinosa, and Rasoul Narimani for their assistance with DLS measurements, and Mohammad Javad Tabesh for his assistance with data collection and analysis. Finally, thank you to Joseph Lee for piloting this project and developing many of the protocols used in my thesis.

Table of Contents

Approval.....	ii
Partial Copyright Licence	iii
Abstract.....	iv
Dedication.....	v
Acknowledgements.....	vi
Table of Contents.....	vii
List of Tables.....	x
List of Figures.....	xi
List of Acronyms.....	xiii

Chapter 1. Introduction..... 1

1.1. Membrane territories in the cell feature different physical assets	1
1.1.1. The Electrostatic surface of the membrane	2
1.1.2. Membrane curvature and lipid packing defects	3
1.2. Amphitropic proteins.....	4
1.2.1. Polybasic / lipidated anchors and regulation by modulation of protein electrostatic and hydrophobic character.....	6
1.2.2. Membrane-induced amphipathic helices	6
1.2.3. Curvature sensing m-AH.....	8
1.3. Other protein motifs that can display membrane curvature sensing.....	9
1.4. Membrane curvature induction and sensing may be related.....	11
1.5. CTP:phosphocholine cytidyltransferase (CCT).....	12
1.5.1. CCT is the key regulatory enzyme in PC synthesis.....	12
1.5.2. CCT genes, localization and domain organization.....	13
1.5.3. The CCT M domain amphipathic helix	16
1.5.4. The CCT P region	18
1.5.5. Curvature-related functions of CCT.....	18
1.6. α -Synuclein (α -syn)	19
1.6.1. α -Synuclein: Physiological function, folding and roles in disease	19
1.6.2. α -Synuclein: Domain structure and similarity to the CCT tail region	21
1.6.3. Curvature sensing of synuclein	22
1.6.4. Differences between α -synuclein and CCT	23
1.7. Overview of research objectives.....	23

Chapter 2. Experimental Procedures..... 25

2.1. Materials.....	25
2.2. Cloning.....	25
2.2.1. Preparation of plasmids for transformation.....	25
2.3. Protein overexpression.....	28
2.3.1. Expression conditions	28
2.3.2. General large scale overexpression	30
2.4. Protein purification.....	30
2.4.1. Cell lysis.....	30
2.4.2. Purification	31

2.4.3.	Thrombin Digestion	31
2.4.4.	Protein quantification methods	32
2.5.	Phospholipid vesicle preparation	33
2.5.1.	Preparation of single lamellar vesicles (SUVs) and extruded vesicles (LUVs)	33
2.5.2.	Vesicle sizing	34
2.5.2.1.	Vesicle sizing using dynamic light scattering (DLS)	34
2.5.2.2.	Vesicle sizing using transmission electron microscopy (TEM)	36
2.6.	Membrane binding analyses	38
2.6.1.	Circular Dichroism and deconvolution	38
2.6.1.1.	Theory	38
2.6.1.2.	Sample preparation and data collection	39
2.6.2.	Fluorescence	39
2.6.2.1.	Theory	39
2.6.2.2.	Tryptophan fluorescence: Sample preparation and data collection	40
2.6.3.	NBD fluorescence	40
2.6.3.1.	NBD labeling procedure	41
2.6.3.2.	Sample preparation and data collection	42
2.6.4.	Procedure for constructing binding curves and obtaining partition coefficients (K_p)	43
2.6.5.	Assessment of the reliability of K_p values	43

Chapter 3. Results: Comparison of the curvature dependence of CCT and α -synuclein and the role of their negatively charged tails 45

3.1.	Curvature-sensitivity of the m-AH is modulated by the charge of its flanking region.	45
3.1.1.	Curvature dependent binding as probed by circular dichroism	45
3.1.2.	Curvature dependent binding as probed by Trp fluorescence	49
3.1.3.	Curvature dependent partitioning as probed by NBD fluorescence	53
3.2.	The curvature sensitivity of CCT (UP) is influenced by the membrane charge.	57
3.3.	Negative charge flanking the CCT m-AH reduces the electrostatic component of binding.	60
3.4.	α -Synuclein is less sensitive to electrostatic modulation.	62

Chapter 4. Concluding Discussion and Future Directions: The significance of curvature sensing for CCT and α -syn proteins 67

4.1.	Mechanism for modulation of curvature sensing by change in protein electrostatic character	67
4.2.	The impact of a repulsively charged tail on curvature sensitivity may depend on the electrostatic / hydrophobic balance.	68
4.3.	Potential role of acidic tails in targeting m-AH segments to curved or flat membranes in cells.....	71

4.3.1. α -Synuclein may have evolved to have a charged tail to weaken its binding strength.	71
4.3.2. Regulation of curvature sensing by phosphorylation of CCT tail could serve to direct CCT to highly curved membranes.	72
4.4. Role of phosphorylation in regions flanking m-AHs on the curvature-sensing of other proteins	72
4.5. Critique and Future Work.....	73
References	76

List of Tables

Table 2.1. CCT M+P and α -syn proteins used in vesicle binding experiments.....	27
Table 2.2. Induction times and temperatures for expression of CCT and α -syn.....	28
Table 2.3. Protein physical parameters	33
Table 2.4. Summary of results for DLS and TEM vesicle sizing measurements.	38
Table 2.5. Equations used to normalize binding curves	43
Table 3.1. Summary of K_p values for CCT (UP) and (PM) using NBD fluorescence: Effect of varying anionic lipid and size of vesicles.	59
Table 3.2. Summary of K_p values for CCT (UP) and (PM) using Trp fluorescence: Varying ionic strength.....	62
Table 3.3. K_p values for α -syn and α -syn12S.	66
Table 4.1. Properties of the m-AH in CCT α and α -syn.....	69
Table 4.2. Δ Net charge of the proteins with negative vs. neutralized tails.....	71

List of Figures

Figure 1.1. m-AH interactions with the bilayer are promoted by electrostatics and/or membrane curvature and lipid packing defects.	3
Figure 1.2. General strategies amphitropic proteins use to associate with membranes.	5
Figure 1.3. The m-AH of CCT α and α -syn have a polar and non-polar face.	8
Figure 1.4. Examples of curvature sensing motifs found in proteins.	10
Figure 1.5. CCT is the rate limiting enzyme in the CDP-choline pathway of PC synthesis.	13
Figure 1.6. Comparison of the M + P region of CCT α and α -synuclein.	15
Figure 1.7. CCT is an amphitropic protein that uses an m-AH to associate with membranes.	17
Figure 2.1. Overexpression and purification of His ₆ -tagged CCT M+P and α -syn proteins.	29
Figure 2.2. Purification and thrombin cleavage of His ₆ -tag.	32
Figure 2.3. The hydrodynamic radius of sonicated and extruded vesicles were measured using DLS.	35
Figure 2.4. The sizes of SUV and 100 nm extruded vesicles were measured using TEM.	37
Figure 2.5. Labelling of protein with NBD fluorophore.	41
Figure 2.6. NBD labelling was confirmed by fluorescence imaging of CCT band on gel.	42
Figure 3.1. Curvature dependence of CCT and α -syn as probed by CD.	46
Figure 3.2. Deconvolution of CD spectra show a transition from unordered structure to alpha-helix with increasing lipid concentration.	48
Figure 3.3. CCT (PM) and α -syn are more curvature dependent than CCT (UP).	49
Figure 3.4. The fluorescence of the native Trp in CCT shows a blue-shift and increase in intensity upon titration with vesicles of varying sizes.	51
Figure 3.5. Binding curves from Trp fluorescence show that CCT (PM) is more curvature sensitive than CCT (UP).	52

Figure 3.6. The fluorescence emission maxima of the NBD labeled CCT shows a blue-shift and increase in intensity upon titration with 30% PG vesicles of varying sizes.....	55
Figure 3.7. Binding curves from NBD fluorescence show that CCT (PM) is more curvature sensitive than CCT (UP).....	56
Figure 3.8. Curvature sensing of CCT can be modulated by protein and/or membrane electrostatic properties.	58
Figure 3.9. Membrane binding of CCT (UP) is sensitive to changes in medium ionic strength whereas CCT (PM) is insensitive.....	61
Figure 3.10. The fluorescence of the engineered Trp in α -syn and α -syn12S shows a blue-shift upon titration with vesicles of varying sizes.	64
Figure 3.11. Curvature dependence of α -syn and α -syn12S probed by Trp fluorescence.....	66
Figure 4.1. The m-AH of CCT α and α -syn have similar distributions of charged residues.	70

List of Acronyms

AH	Amphipathic helix
m-AH	Membrane-induced amphipathic helix
CCT	CTP: phosphocholine cytidyltransferase
α -syn	α -synuclein
PC	Phosphatidylcholine
PG	Phosphatidylglycerol
CD	Circular Dichroism
PD	Parkinson's Disease
K_p	Partition coefficient
ALPS	Amphipathic lipid packing sensor
UP	Unphosphorylated
PM	phosphomimic
Da	Dalton (1 Dalton = 1 g/mol)
PDB	Protein Data Bank
PBR	Polybasic Region
MARCKS	myristoylated alanine-rich protein kinase c substrate
EC50	Effective Concentration of lipid for half maximal binding

Chapter 1. Introduction

When surrounded by membrane surfaces of all types, what strategies do peripheral proteins use to specify their function on the correct membrane in the cell and how can this membrane localization be modulated? In this thesis I focus my studies on the curvature sensing ability of the CTP:phosphocholine cytidyltransferase (CCT) and α -synuclein (α -syn) membrane-induced amphipathic helix (m-AH) and how their curvature dependence may be modulated by changes in the negative charge of regions flanking their m-AH. This is the first time an electrostatic switch mechanism adjacent to an amphipathic helix has been implicated in modulating curvature sensitivity. In the following sections, I will review current knowledge of membrane and protein electrostatic and hydrophobic driving forces and their implication in membrane curvature sensing and generation.

1.1. Membrane territories in the cell feature different physical assets

Some cellular processes that occur on membrane surfaces (e.g. vesicle budding and fusion, lipid biosynthesis) can be regulated both spatially and temporally by two basic membrane physicochemical parameters: membrane electrostatics and curvature (lipid packing) (Antonny, 2011). Organelles possess dynamic membranes whose dominating physical characteristics alternate between a combination of these two parameters at various times in the lifecycle of a cell, causing their membrane-associating proteins to switch localization and function. Acquiring a broad view of the various membrane landscapes in a cell is important for understanding the many mechanisms that underlie protein sorting, trafficking and signalling.

1.1.1. *The Electrostatic surface of the membrane*

The electrostatic nature of the cell membrane surface is primarily controlled by the prevalence and distribution of anionic phospholipids such as phosphatidylserine (PS) and phosphatidylinositides in eukaryotic cells (Goldenberg and Steinberg, 2010) and phosphatidylglycerol (PG) in prokaryotic cells (Dowhan, 1997). In eukaryotes, PS distribution ranges from ~5% in the endoplasmic reticulum (ER) membrane to greater than 10% in the plasma membrane (PM) (Leventis and Grinstein, 2010). Adding further negative charge density are the phosphoinositides which are mostly confined to the inner leaflets of the endomembrane network (Kutateladze, 2010). Certain peripheral proteins that translocate from the cytosol onto the cytosolic-facing leaflets of these various membranes can differentiate between membrane territories rich in anionic lipids (e.g. PM) and regions of intermediate anionic lipid content (e.g. ER and endomembrane system) and modulate their activity accordingly (Goldenberg and Steinberg, 2010). Such proteins may rely on modules that interact with specific anionic lipid headgroups (e.g. Pleckstrin Homology domains that bind PIPs (Harlan et al., 1994)). Or proteins may use non-specific sensing of negative charge density. The sensing devices include poly basic regions found for example in MARCKS, K-ras or src proteins involved in cell signalling processes (Heo et al., 2006), and the amphipathic helix (Figure 1.1 A), found in proteins such as the antimicrobial peptide magainin 2, a bacterial division site-selection protein, MinD, the rate-limiting enzyme in PC synthesis (CCT), and disease-linked proteins like α -synuclein (Cornell and Taneva, 2006; Drin and Antonny, 2010). In all cases changes in the negative surface charge density via change in the content of acidic lipids such as PIPs and PS directly affect the magnitude of the membrane's negative surface potential, thereby modulating the electrostatic attraction between the basic residues of the proteins and the membrane surface (Murray et al., 1998).

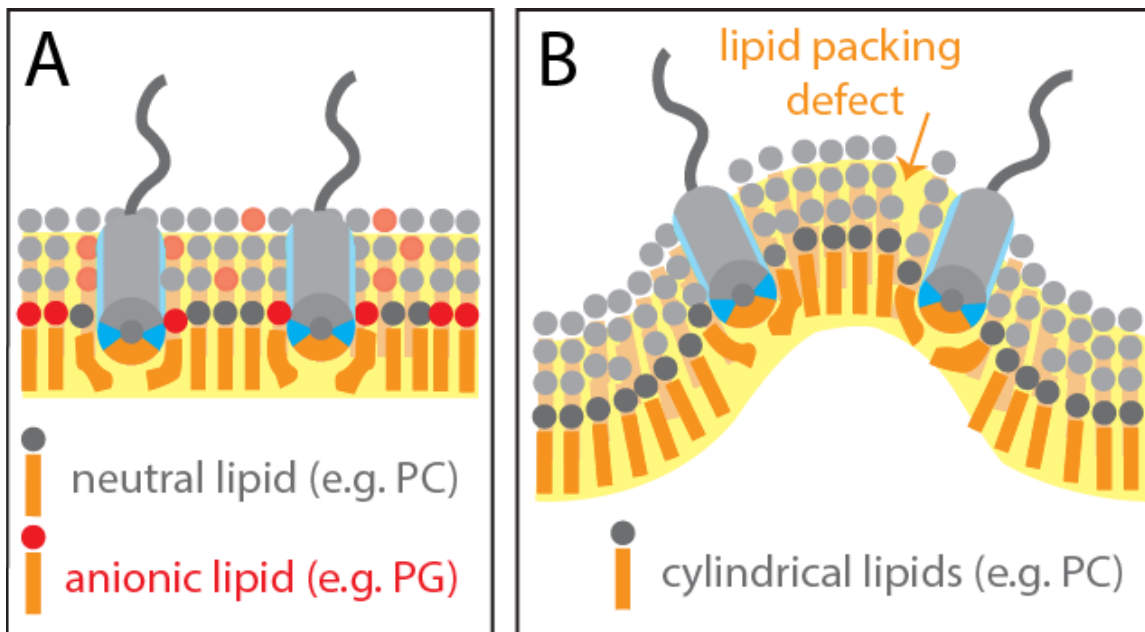


Figure 1.1. m-AH interactions with the bilayer are promoted by electrostatics and/or membrane curvature and lipid packing defects.

(A) Schematic of an m-AH inserted into the lipid backbone of an anionic membrane. Red represents negatively charged and blue positively charged species, yellow represents hydrophobic character. (B) Schematic of a region of highly curved membrane. Cylindrical lipids pack poorly in such regions, creating lipid packing defects exposing the hydrophobic membrane interior. Insertion of the m-AH into these packing defects alleviates lipid packing stress.

1.1.2. Membrane curvature and lipid packing defects

Aside from charge distribution, another simple way to identify an organelle is by the shape of its membrane. The ER membrane, for example, can be distinguished by its diverse curvatures, ranging from highly curved tubules to flatter cisternal structures (Hu et al., 2008) whereas the nuclear envelope and plasma membrane are relatively flat in comparison. A major feature of curved membrane surfaces is an increase in the size of lipid packing defects that expose hydrophobic binding sites (Cui et al., 2011). These lipid packing defects arise when there is a mismatch between the lipid's individual shape and the membrane's overall curvature (Drin and Antonny, 2010). Depending on the relative volumes of their acyl chain and head group, lipids can be classified as conical (e.g. lysolipids), cylindrical (e.g. phosphatidylcholine) or even inverted cone (e.g. unsaturated phosphatidylethanolamine) (Dowhan, 1997; Escriba et al., 1997). If allowed to assemble spontaneously, cylindrical lipids will form bilayers whereas conical and inverted conical lipids will favour formation of non-bilayer structures (such as micelles or inverted

hexagonal forms) to optimize packing and minimize stress (Gruner et al., 1985). When these non-bilayer lipids accumulate in a cell membrane which must be constrained as a bilayer, the spontaneous curvature will be thwarted, generating packing defects that expose the hydrophobic interior of the membrane. Moreover, when sequestered into a positively curved membrane surface, even the cylindrical bilayer-favouring PC would generate a membrane with high lipid packing stress and many hydrophobic surface patches (Figure 1.1 B). Certain peripheral proteins may sense these lipid packing defects using hydrophobic domains, thus discriminating between flat and curved membrane territories.

Based on the distributions of various lipids, the cell's membrane landscape can be broadly divided into major territories: the ER membrane (and membranes of the early secretory pathway) which are weakly charged but highly curved (with many lipid packing defects) and the plasma membrane (and membranes of the late secretory pathway) which can be highly charged but contain more regions that are flat (with less lipid packing defects) (Bigay and Antonny, 2012; Pranke et al., 2011). In addition, the nuclear membranes have low surface charge and lipids with monounsaturated fatty acyl chains (Pranke et al., 2011; van Meer et al., 2008). Given a membrane topology that has already been established, how do proteins interact and differentiate between these different membrane landscapes in the cell?

1.2. Amphitropic proteins

The term amphitropism was coined by Burn (1988) to describe proteins that localize between aqueous and membranous compartments (Johnson and Cornell, 1999). Many kinases, phosphatases and phospholipases are amphitropic proteins that respond to membrane generated signals. They bind membranes in a weak and reversible manner which is subject to regulation by membrane and/or protein physical properties, a topic which was discussed in section 1.1. Typically, membrane binding is associated with the active state of the protein whereas the soluble form is the inactive state (Johnson and Cornell, 1999). Amphitropic proteins can interact with membranes via three essential strategies: hydrophobic anchors, lipid clamps or amphipathic helices (Figure 1.2) (Johnson and Cornell, 1999). Combinations of these devices are also

frequently used for anchoring on membranes. As mentioned earlier, MARCKS and the Src family of kinases fall under the category of hydrophobic anchors, combining lipid anchors with polybasic sites to facilitate electrostatic interactions with negative membrane surfaces (Kim et al., 1994). In this case, the lipid anchor may be buried in the soluble form but extruded into the membrane upon binding (Johnson and Cornell, 1999). Alternatively, peripheral proteins may contain a binding pocket for a specific lipid head group – called a lipid clamp. Examples of motifs that fall in this category include the C1 motif which is used to bind diacylglycerol and tumor-promoting phorbol esters, the C2 motif used to bind calcium and anionic phospholipids and the PH domains which are used to bind bis or tris phosphatidylinositol phosphates (Hurley et al., 1997; Rebecchi and Scarlata, 1998; Rizo and Sudhof, 1998). In addition, binding of the lipid clamp often displaces an inhibitory domain from the active site, thus the concentration of specific lipid ligands in the membrane are key to regulation in this group of amphitropic proteins. The third category of membrane anchor is the amphipathic α -helix (AH). Rather than having a chemical binding site for a lipid monomer, AH motifs sense the physical properties of the membrane surface.

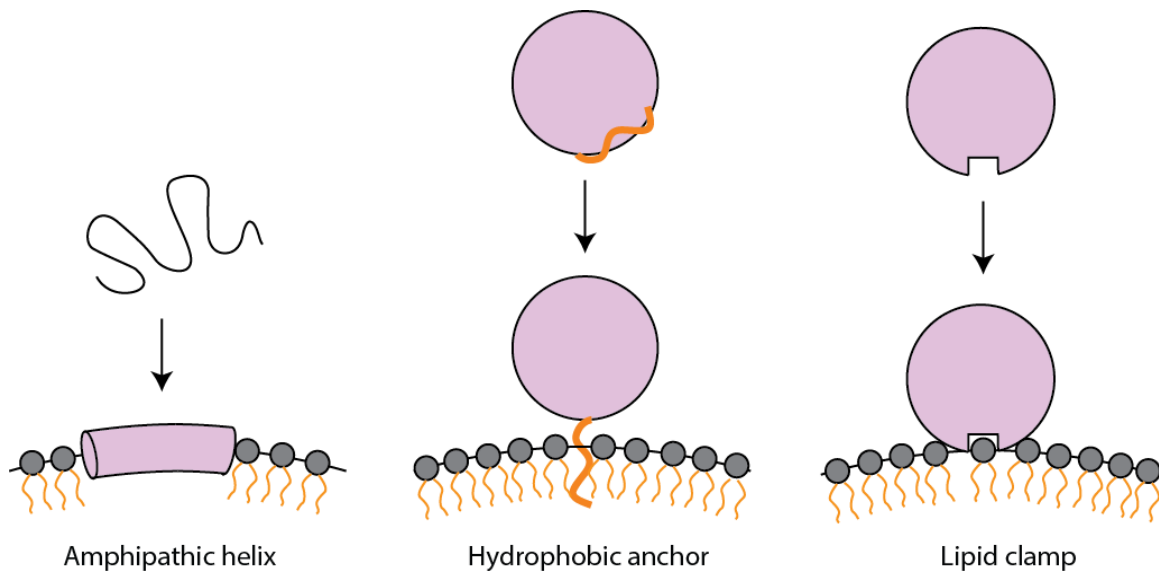


Figure 1.2. General strategies amphitropic proteins use to associate with membranes.

A protein may use an amphipathic helix to interact with membranes. This structure transforms from a disordered/partially disordered structure to a folded α -helix (shown as a cylinder) upon association with the membrane. Proteins may also use a hydrophobic anchor (which is often coupled with a polybasic motif). The hydrophobic anchor is usually hidden in the soluble form. Finally, proteins may use lipid clamps to bind specific lipid head groups.

1.2.1. *Polybasic / lipidated anchors and regulation by modulation of protein electrostatic and hydrophobic character*

McLaughlin and colleagues were among the first to highlight the importance of electrostatic and hydrophobic interactions in protein association with membranes. Using the amphitropic protein myristoylated alanine-rich protein kinase c substrate (MARCKS), they showed that the protein binds to the plasma membrane via hydrophobic insertion of its myristoyl chain as well as an electrostatic interaction between its polybasic region (PBR) with anionic phospholipid headgroups (Kim et al., 1994). They found that these two physical parameters work cooperatively, with insertion of the myristoyl tail into the membrane bringing the PBR closer to the bilayer and therefore increasing the chance for its interaction with anionic phospholipids. There is also evidence supporting the opposite process whereby the electrostatic attraction mediates insertion of the lipid tail (Buser et al., 1994).

These studies and others also show that regulation of protein targeting to membranes can involve not only modulation of the membrane electrostatic and hydrophobic character, but also modulation of these parameters on the protein. For example, the electrostatics of MARCKS and the non-receptor tyrosine kinase Src can be modified via the phosphorylation and dephosphorylation of serine residues within the PBR which in turn modifies its net charge, thereby regulating its cycling on and off the plasma membrane (Murray et al., 1998; Thelen et al., 1991). Hydrophobicity can be modulated by modifying the number of lipid anchors, for example reversible palmitoylation has been described for some amphitropic proteins of this class (Salaun et al., 2010).

MARCKS and Src are both peripheral proteins that associate with membrane leaflets via lipid tails and PBRs. What other amphiphilic motifs exist for localization onto membrane surfaces?

1.2.2. *Membrane-induced amphipathic helices*

Involving a similar synergism between electrostatic and hydrophobic driving forces for binding, many peripheral proteins use the amphipathic helix (AH) to reversibly bind membranes. Amphitropic amphipathic helices interconvert from an ensemble of

disordered structures in solution to a fully folded AH upon presentation of a suitable membrane for binding (Johnson and Cornell, 1999). I refer to these as membrane-induced amphipathic helices (m-AH). Not only do amphipathic helices serve as membrane anchors, they fulfill other functions as membrane de-stabilizers (Dathe and Wieprecht, 1999), as well as membrane curvature sensors (Hatzakis et al., 2009) or generators (Campelo et al., 2008; Farsad et al., 2001; Lee et al., 2005; Zimmerberg and Kozlov, 2006). In this case, the amphipathic character comes from the segregation of the hydrophobic and polar residues onto opposite sides of an alpha-helix (Drin and Antonny, 2010) (Figure 1.3). When fully folded and docked onto a membrane surface, the hydrophobic face is inserted into one leaflet of the bilayer whereas the polar face remains exposed to the aqueous environment – orienting the AH parallel with the membrane surface (Hristova et al., 1999). The insertion of the non-polar face into lipid packing defects is energetically favourable as it relieves the lipid packing stress in the membrane. In addition, there may also be a strip of positively charged residues at the interfacial zone which are ideally positioned to interact with negatively charged lipid headgroups, further stabilizing the AH on the membrane (Davidson et al., 1998; Johnson et al., 2003).

m-AHs can be characterized according to their hydrophobic moment, hydrophobicity and net charge (Cornell and Taneva, 2006; Drin and Antonny, 2010) and tampering with these protein parameters can change their membrane binding behaviour. The hydrophobic moment is a measure of the amphipathy of a helix. Increasing the hydrophobic moment of an AH increases its propensity to fold into an α -helix at the membrane surface. Hydrophobicity indicates its preference for membrane partitioning. Larger and bulkier residues in the m-AH hydrophobic face result in greater membrane partitioning. Finally, the magnitude of the net charge of the m-AH determines its reliance on electrostatics for binding to anionic membranes.

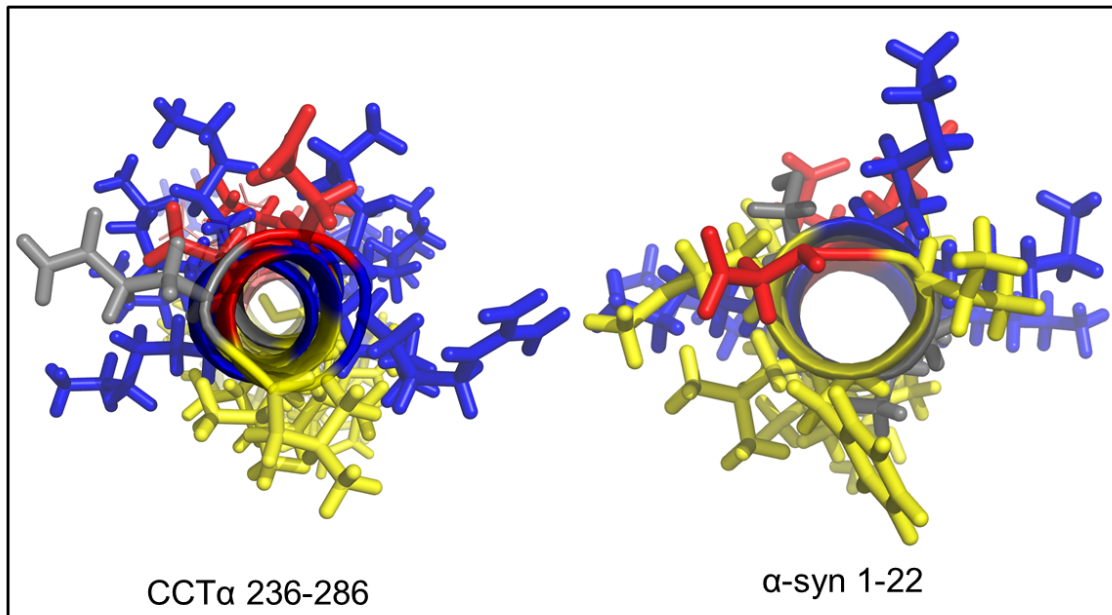


Figure 1.3. The m-AH of CCT α and α -syn have a polar and non-polar face.

View from the N-terminal of helix axis for CCT M + P residues 242 – 258 (using PDB 1peh) and α -syn residues 2-22 (using PDB 1xq8). Stick rendering for side-chains: blue represents (+) charged residues, red (-) charged, yellow hydrophobic residues and grey represents polar uncharged residues.

1.2.3. *Curvature sensing m-AH*

Defining the physical features of the m-AH that could augment interaction with curved membranes has been a topic that has received much attention recently (Antonny, 2011; Bhatia et al., 2010; Bigay and Antonny, 2012; Cui et al., 2011; Drin and Antonny, 2010; Hatzakis et al., 2009). There is consensus, however, that the m-AH recognizes exposed hydrocarbon from the membrane core that increases in area with increasing curvature (Antonny, 2011; Voth, 2013). Antonny and colleagues have proposed that it is the balance between the two major binding forces, electrostatics and hydrophobics, that determine the curvature sensing dependence of a protein (Antonny, 2011; Bigay and Antonny, 2012; Drin and Antonny, 2010). The weaker the electrostatic component of the interaction, the greater the reliance on hydrophobic interactions and the more responsive it will be to membrane curvature. Therefore, AHs that are weakly charged and/or presented with electrically neutral or repulsive membranes will rely on predominantly hydrophobic mechanisms for binding. On the other hand, AHs that are strongly positively charged and/or are presented with membranes with dense anionic surface charge will

bind membranes based on a predominantly electrostatically driven mechanism. Rather than being curvature sensitive, amphipathic helices in this scenario will likely be curvature inducing.

Different amphipathic helices are adapted to different degrees and types of membrane curvature. The amphipathic lipid-packing sensor (ALPS) motif is a well-described m-AH that is highly curvature-dependent, binding to vesicles of 60 nm in diameter (Antonny, 2011; Drin et al., 2007). The ALPS motif is found in proteins involved in vesicle trafficking such as Arf-GAP1, the golgin GMAP-210, the sterol transporter Osh4p and others. This m-AH has a strong hydrophobic face populated with bulky residues and a weak polar face rich in serine and threonine but lacking in basic residues. Mutations in the Arf-GAP1 ALPS that reduced the hydrophobic imbalance reduced curvature sensing (Drin et al., 2007). In contrast to the above two examples, DivIVA is a bacterial protein involved in initiating cell-division whose N-terminal amphipathic helix is suggested to bind negative curvatures at cell poles (Lenarcic et al., 2009). In this case, sensing of negative curvature is thought to arise due to the stabilization of DivIVA clusters by the bridging of opposing membrane surfaces.

1.3. Other protein motifs that can display membrane curvature sensing

Aside from curvature-sensing amphipathic helices, other motifs such as BAR domains or hydrophobic anchors have demonstrated membrane curvature sensing under certain conditions (Figure 1.4).

In the first case, the Bin-Amphiphysin-Rvs (BAR) domain is an example of how the protein geometry itself is attuned to membrane geometry. BAR domains can be found in amphiphysin and endophilin, two protein families involved in synaptic vesicle endocytosis and recycling (Peter et al., 2004). Positively charged arc-shaped structures made of dimerized coiled-coil α -helices, the classical BAR domains are shaped to favour interaction with positively curved membrane surfaces (Figure 1.4). It has been suggested that curved membranes act as templates upon which the curved monomers

can more easily assemble, effectively decreasing the critical concentration required for their oligomerization into the functional unit (Roux et al., 2010).

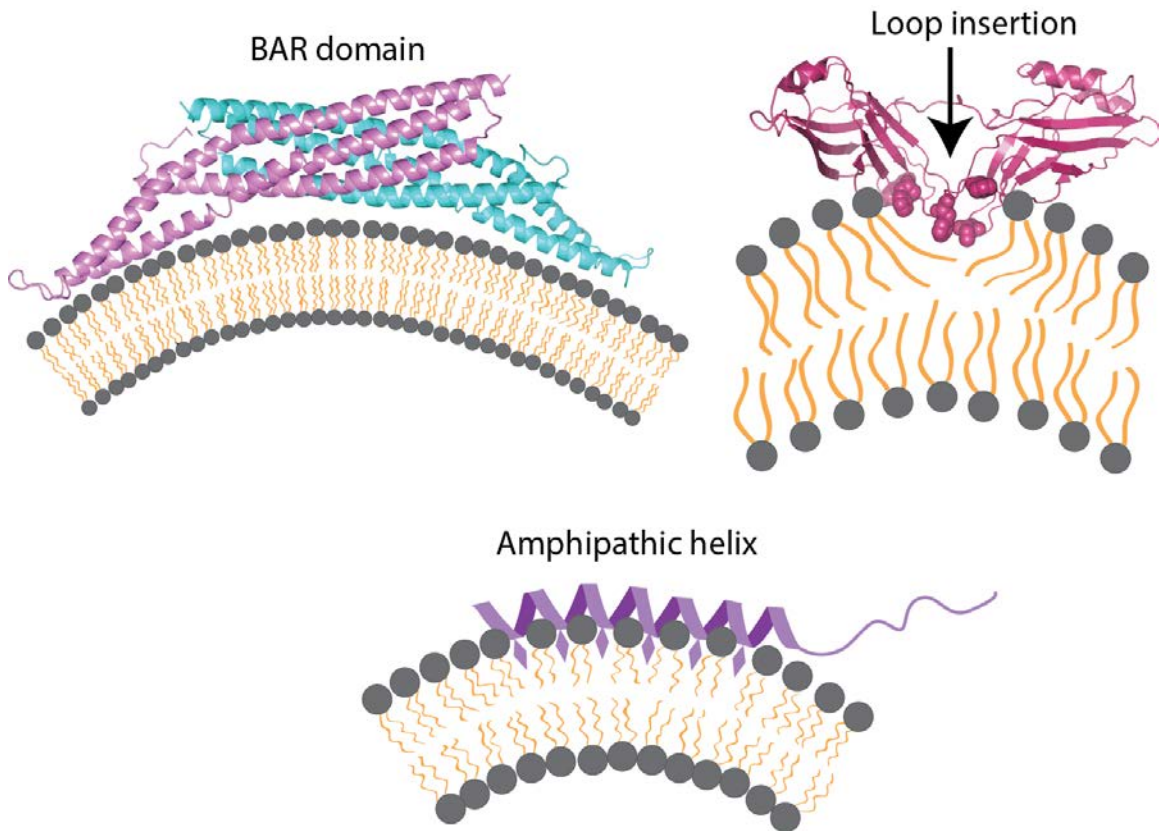


Figure 1.4. Examples of curvature sensing motifs found in proteins.

The BAR domain forms an arc-shaped dimer (shown as purple and teal monomers) and is found in proteins such as amphiphysin and endophilin, proteins which are involved in endocytosis and vesicle recycling (figure of BAR domain modified from McMahon and Gallop (2005)). Some proteins use hydrophobic loops to insert into hydrophobic patches in curved membrane surfaces. These include synaptotagmin, a protein involved in the calcium-induced exocytosis of synaptic vesicles (figure of synaptotagmin loop insertion modified from Martens and McMahon (2008) with the hydrophobic amino acids in synaptotagmin 3 are shown as spheres). Finally, the amphipathic helix inserts its hydrophobic face into the membrane (figure of the ALPS amphipathic helix modified from Bigay *et al.* (2005) with the hydrophobic amino acids inserted into the membrane represented as purple diamonds).

The second case provides a general model that any hydrophobic motif should be curvature sensitive. This is based on the idea that curved membranes have a higher density of lipid packing defects so proteins with hydrophobic anchors will be more concentrated on such membrane surfaces (Bhatia et al., 2010; Hatzakis et al., 2009). Hydrophobic anchors can be in the form of acylated proteins. Biochemically alkylated ovalbumin and glutathione S-transferase were shown to be curvature-sensitive (Hatzakis

et al., 2009). In addition, the lipidated accessory HIV-1 Nef protein involved in signalling and immune evasion binds smaller vesicles with a higher rate constant and association constant (K_a) compared to larger vesicles, though Nef also contains an m-AH which complicates the study (Gerlach et al., 2010). In addition to alkyl chains, hydrophobic anchors can consist of non-helical hydrophobic residues. For example, a protein functioning in the fusion of synaptic vesicles with the plasma membrane, Synaptotagmin, contains hydrophobic loops that impart membrane curvature sensitivity (Martens et al., 2007) (Figure 1.4).

1.4. Membrane curvature induction and sensing may be related

Although AHs, BAR domains and hydrophobic anchors are known to be curvature sensitive, there are also numerous proteins housing these motifs that can induce curvature. Examples of m-AH motifs that bind equally well to curved and flat membranes are the anti-microbial peptide, magainin (Wieprecht et al., 2000) and the honey bee venom peptide, melittin (Matsuzaki, 1998), both of which are known to form pores in membranes to aid in their translocation into liposomes. In contrast to the curvature-sensing m-AH, these m-AHs have strongly positively charged polar faces. These AHs act as wedges to push apart individual lipids of one leaflet as they bind, inducing curvature in the process (Taneva et al., 2012). Until my thesis work the m-AH of the protein CCT had only been characterized as a curvature inducer (Gehrig et al., 2008; Lagace and Ridgway, 2005; Taneva et al., 2012), rather than a sensor.

Interestingly, some peripheral proteins feature both curvature sensing and curvature inducing abilities (Baumgart et al., 2011; Bhatia et al., 2010; Richnau et al., 2004). The induction and curvature sensing ability of, for example, BAR domains, are not functions exclusive from one another. BAR domains may deform membranes to allow recruitment of more BARs in a positive-feedback cycle where curvature sensing is amplified to yield more curvature generation (Frost et al., 2009; Peter et al., 2004). Finally, recent studies have shown that local crowding of proteins is enough to bend membranes (Stachowiak et al., 2010). This suggests that proteins with hydrophobic

anchors that are concentrating in regions of high membrane curvature may also be deforming membranes.

From these studies, it is evident that some peripheral proteins can only sense membrane curvature, some can only generate curvature and others fulfill both functions. The physicochemical explanations behind the variety of protein-membrane interactions continue to be a focus of vigorous research.

Sections 1.1 to 1.3 provided an overview of how the interplay between electrostatic and hydrophobic interactions results in modulation of curvature sensing in m-AHs. Curvature-based interactions can be controlled by changes in membrane lipid composition, affecting the membrane surface negative charge density or hydrophobicity. Alternatively, or in concert with membrane-based changes, curvature sensing could be modulated by changing the protein's electrostatic character, for example by phosphorylation. In my thesis I, have conducted a simple probe of the hypothesis that reduction in protein electrostatic driving force towards anionic membranes can increase curvature dependence. I characterized and compared two proteins that bind membranes reversibly using very long m-AH motifs flanked by regions of variable negative charge: ***α*-synuclein (*α*-syn)** and **CTP: phosphocholine cytidyltransferase (CCT)**.

1.5. CTP:phosphocholine cytidyltransferase (CCT)

1.5.1. *CCT is the key regulatory enzyme in PC synthesis.*

CCT contains an m-AH and is an amphitropic enzyme (Figure 1.6) catalyzing the rate-limiting step in the synthesis of phosphatidylcholine (PC) (Kent, 2005). Phosphatidylcholine is the major phospholipid of most nucleated cells, making up 40-60% of membranes (van Meer et al., 2008). In addition to its membrane structural role PC is involved in processes such as formation of lipid droplets, serving as a substrate for signaling phospholipases that generate lipid second messengers, components of pulmonary surfactants and more (Li and Vance, 2008). PC biogenesis in eukaryotic cells can occur in two ways: via the ubiquitous CDP-choline pathway involving CCT or in restricted cell types via methylation of phosphatidylethanolamine (Kent, 1997). In the

Kennedy pathway, CCT catalyzes the transfer of cytidine from CTP onto phosphocholine to produce CDP-choline and pyrophosphate (Figure 1.5) (Cornell and Northwood, 2000). It is activated in its membrane bound form and inactivated in its soluble form in response to PC levels in the cell, maintaining phospholipid compositional balance.

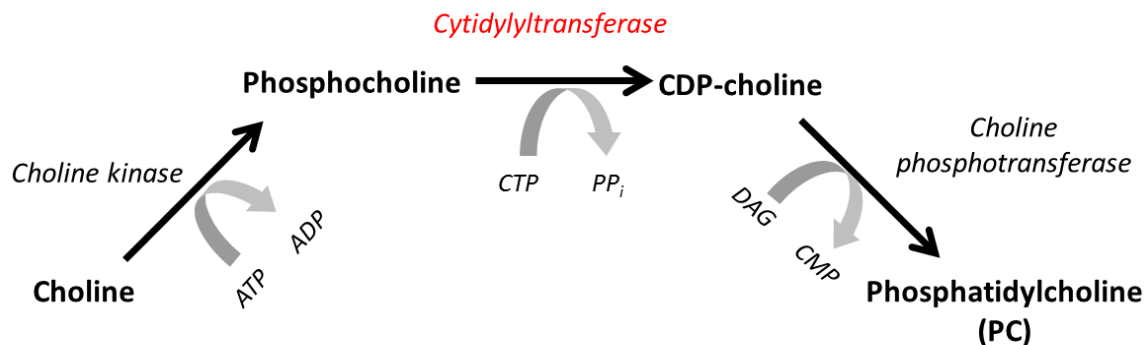


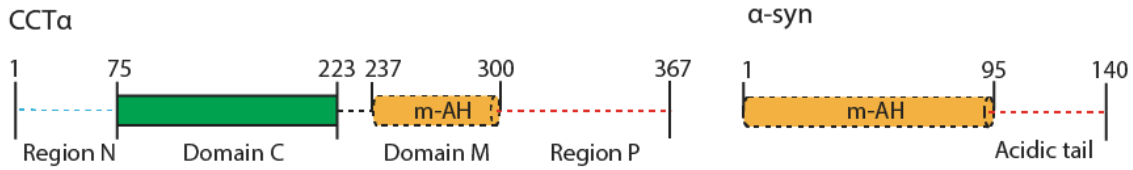
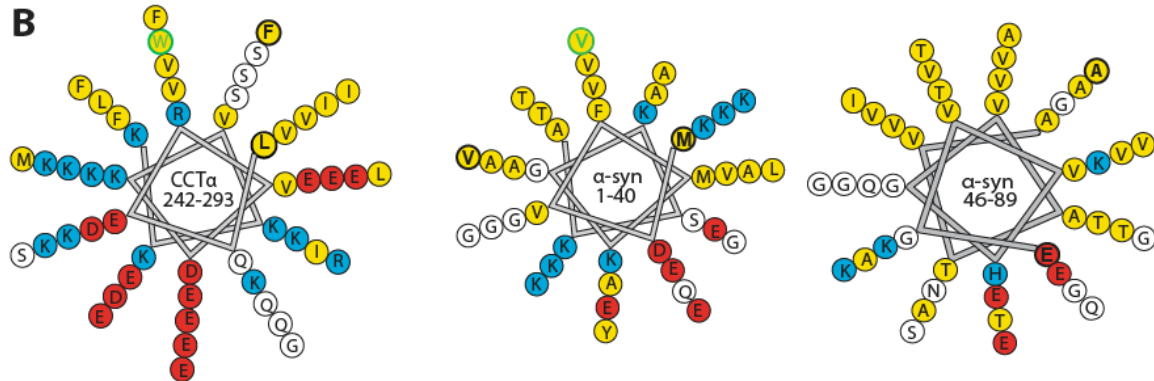
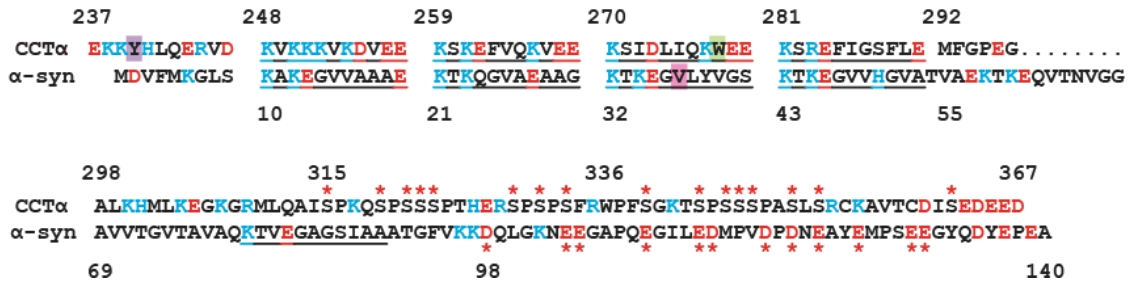
Figure 1.5. CCT is the rate limiting enzyme in the CDP-choline pathway of PC synthesis. CCT catalyzes the production of CDP choline, which then donates its headgroup in the synthesis of phosphatidylcholine.

In addition to its enzymatic function, there is growing evidence supporting the role of CCT in membrane remodelling, particularly of nuclear membranes, which I will discuss in a later section, as well as a function in the stabilization of lipid droplets (Krahmer et al., 2011). The lipid droplets of mammalian cells are surrounded by a membrane consisting of phosphatidylethanolamine (PE) and PC and dramatically change in volume under different metabolic states (from $\leq 300 - 900$ nm in diameter). It is thought that CCT binding to lipid droplets whose membranes are depleted in PC is the main mechanism preventing the fusion of lipid droplets with one another. In this case, the surfactant activity of the CCT m-AH may be stabilizing the curved droplets.

1.5.2. CCT genes, localization and domain organization.

There are two CCT genes in vertebrates referred to as CCT α and CCT β . CCT α is the most ubiquitously expressed and is predominantly found in the nucleus whereas the other isoform, CCT β , lacks a nuclear localization signal (NLS) and is therefore cytoplasmic (Lykidis et al., 1999). Both α and β isoforms are homodimers. While the

catalytic domain is highly conserved in sequence and fold, (Lee et al., 2009) the N- and C-termini are not, and appear to be disordered regions (Dennis et al., 2011; Ding et al., 2012). The CCT regulatory domain is C-terminal to the catalytic domain and is comprised of an m-AH (also known as domain M) followed by a carboxy-terminal phosphorylation region (region P; Fig. 1.6 A). The focus of this thesis is on the CCT α isoform, and in particular, the regulatory M and P domain (Figure 1.6).

A**B****C****Figure 1.6. Comparison of the M + P region of CCTα and α-synuclein.**

(A) CCTα contains a disordered N region (dashed blue line), a highly conserved catalytic domain (green), an m-AH in the M domain (yellow), followed by a disordered phosphorylation region (dashed red line). α-Syn contains a long m-AH (yellow) followed by a highly acidic tail (dashed red line). (B) 11-3 Helical wheel plots of the m-AH regions of CCTα and α-syn. Blue, basic residues; red, acidic; yellow, hydrophobic. The omitted segment between the two helices of α-syn (residues 41-45) is non-helical in several structural analyses (Bisaglia et al., 2005; Drescher et al., 2008; Georgieva et al., 2010). The starting and ending residues are bolded. Sites used to monitor membrane binding, W278 in CCT and V37 in α-syn, are highlighted green. (C) Sequence alignment of α-syn and CCTα M + P. Blue, basic residues; red, acidic residues. 11-mer motifs are underlined. Red asterisks above the CCT sequence indicate the 16 serines that are phosphorylated to some degree in cells. The residues Y240 and W278 in CCT, and V37 in α-syn are sites that were utilized to monitor membrane binding, and the red asterisks below the α-syn sequence indicate the 12 glutamates and aspartates that were mutated to serines to create a neutralized tail. These modifications will be described in more detail in Chapter 2 (see Table 2.1).

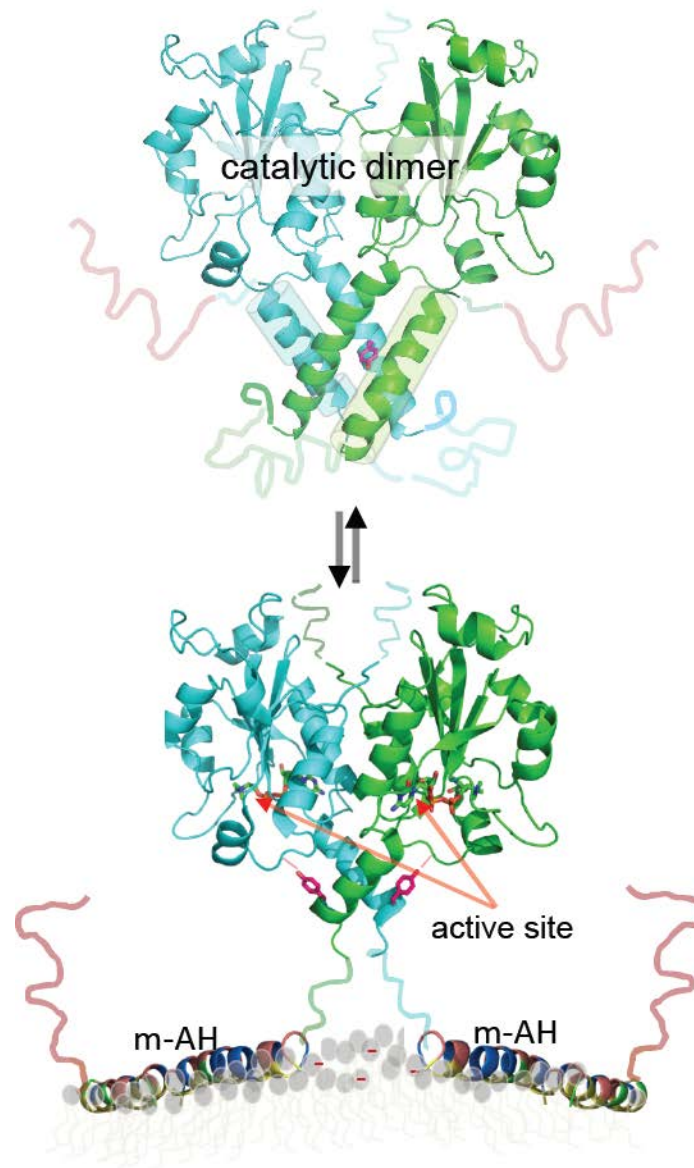
1.5.3. The CCT M domain amphipathic helix

Domain M houses the m-AH and contributes to the regulation of CCT activity and translocation onto membranes. CCT contains one of the longest m-AH studied and is rather poorly conserved across phyla (Ding et al., 2012). However, among the two mammalian isoforms this amphipathic helix is highly homologous (Dennis et al., 2011). Domain M transforms from a mostly disordered conformation in the CCT soluble form to a ~ 60 residue m-AH in response to increases in the content of anionic lipids (PS and PG among others) or lipids with a small head group relative to hydrophobic volume (diacylglycerol and PE), both of which are indications of a PC deficiency (Cornell and Taneva, 2006) (Figure 1.7). The binding of domain M relieves its auto-inhibitory interaction with the catalytic domain and induces an activating conformation at the active site (Cornell and Northwood, 2000; Ding et al., 2012; Friesen et al., 1999) (Figure 1.7).

Membrane binding of the CCT m-AH follows a two-step process: (1) membrane adsorption, driven by long-range electrostatic attraction between basic residues and acidic lipids; (2) folding into the stable m-AH and coincident intercalation of hydrophobic residues. The first step was captured when CCT bound to gel-phase negatively charged MLVs. Intercalation was observed upon MLV transition to liquid crystalline phase (Arnold et al., 1997).

The NMR structure of domain M peptides bound to membrane-mimicking SDS micelles revealed that the CCT m-AH has a ~120° hydrophobic wedge rich in aromatic residues and a polar face dominated by acidic residues with lysine residues arranged at the interfacial region (Figure 1.3 and 1.6 B) (Dunne et al., 1996). The neutralizing lysine to glutamine mutations reduced the electrostatic component of binding (Johnson et al., 2003). In addition, the three glutamates (residues 257, 268 and 279) in the polar face become protonated as the m-AH approaches an acidic membrane interface where the local pH is lower (Johnson et al., 2003). Protonation increases the net positive charge of the m-AH as well as its hydrophobicity, enhancing binding strength. Protonation is selective for anionic lipid surfaces, contributing to the binding selectivity for anionic lipids.

Soluble inactive state



Membrane-bound active state

Figure 1.7. CCT is an amphitropic protein that uses an m-AH to associate with membranes. CCT transitions from a soluble inactive state to a membrane-bound active state when the membrane displays properties reflecting PC-deficiency such as an increase in negative charge density and lipid packing defects (Figure modified from Huang *et al.* (2013)).

1.5.4. The CCT P region

C-terminal to domain M is the CCT phosphorylation (P) region, which is a proline rich, relatively non-conserved ~50 residue segment. This region remains highly unstructured even in the presence of lipids as shown by extreme sensitivity to proteases (Bogan et al., 2005). All 16 serine residues in this region are known to be phosphorylated to some extent after purification of CCT α , with an average of six phosphorylations/subunit (Bogan et al., 2005; Dennis et al., 2011; MacDonald and Kent, 1994) (Fig. 1.6 C). The kinases and phosphatases responsible for phosphorylating and dephosphorylating CCT *in vivo* remain unverified despite several candidates for cellular control of CCT function (Agassandian et al., 2005; Wieprecht et al., 1996).

The P region may play a role in fine-tuning CCT membrane affinity. There is evidence that increased phosphorylation status correlates with an accumulation of the soluble, inactive form of CCT (Kent, 1997). Phosphorylation reduces membrane-binding affinity (Arnold et al., 1997; Dennis et al., 2011); perhaps by introducing negative charges that counteract the attractive forces between positively charged lysines on domain M and negatively charged membrane surfaces. The role phosphorylation plays in fine-tuning the membrane curvature sensitivity of the CCT m-AH was unexplored at the onset of my thesis work, and is one of the main topics of focus in my thesis.

1.5.5. Curvature-related functions of CCT

The curvature inducing and/or sensing abilities of CCT along with its potential physiological function in the cell has been a focus of growing interest in recent years. The first instance suggesting CCT may be curvature sensitive was in an early work done in 1991, demonstrating CCT α binding to SUVs three orders of magnitude above MLVs (Cornell, 1991). Then in 2005, Lagace *et al.* presented evidence that CCT α can tubulate vesicles and may participate in the expansion of the nucleoplasmic reticulum (Lagace and Ridgway, 2005), an invaginated nuclear envelope membrane system that forms trans-nuclear tubules (Malhas et al., 2011). Gehrig *et al.* (2008) showed that domain M remodeling of the nuclear envelope into tubules is dependent upon the hydrophobicity and electrostatic nature of its m-AH. Mutations neutralizing interfacial lysines in the m-AH of full length CCT α reduced affinity for anionic membranes and reduced the ability to

form nuclear tubules whereas mutations strengthening the electrostatic attraction and hydrophobicity in the m-AH promoted tubulation (Gehrig et al., 2008; Johnson et al., 2003). In support of this work, Taneva *et al.* mapped the tubulation activity to the m-AH of domain M. Using transmission electron microscopy, they showed that domain M on its own is sufficient for curvature induction. They also found that tubulation involved growth from a bud, suggesting a cooperative process whereby CCT-induced local curvature serves as a target for subsequent binding of additional CCT (Taneva et al., 2012). Such experiments demonstrated that CCT curvature sensing initiates the tubulation process, providing the first evidence linking the role of curvature sensing and generation of CCT. Interestingly, this same work compared curvature induction of CCT with α -synuclein, a protein similar in structure and sequence to CCT M and P domain. Despite the similarities, it was found that α -synuclein is a weaker tubule inducer than CCT. There must therefore be significant differences in the relative electrostatic and hydrophobic driving forces that contribute to α -synuclein's membrane binding.

1.6. α -Synuclein (α -syn)

1.6.1. *α -Synuclein: Physiological function, folding and roles in disease*

α -Syn is both a curvature-inducing (Taneva et al., 2012; Varkey et al., 2010; Westphal and Chandra, 2013) and curvature sensing protein, famously known to be implicated in Parkinson's disease (Kjaer et al., 2009; Nuscher et al., 2004). It is localized to the pre-synaptic terminals (Iwai et al., 1995) of neurons where it binds reversibly to small synaptic vesicles of ~40nm in diameter. Its precise function in the cell is unclear, but there is growing evidence linking its function to synaptic vesicle recycling, neurotransmitter release and synaptic plasticity (Cheng et al., 2011).

Functional studies strongly suggest α -synuclein's involvement in processes related to dopamine homeostasis. Synuclein is a negative regulator of tyrosine hydroxylase, an enzyme in the dopamine biosynthetic pathway (Leong et al., 2009). After synthesis in the cytoplasm, dopamine (which is prone to oxidation into reactive species) is packaged into low pH synaptic vesicles where it is protected from oxidation.

Synuclein expression may result in an increase in cytosolic dopamine which may bind with synuclein, preventing its conversion into fibrils and therefore promoting the soluble oligomeric state, a state which is thought to be more toxic than the fibrillar state (Conway et al., 2001).

Recently, it was found that α -synuclein is implicated in the regulation of actin dynamics, and therefore involved in the modulation of traffic to and from synaptic membranes. It has been proposed that it directly binds actin, sequestering the pool of available actin for polymerization and fine-tuning formation of actin tracks in the cell (Sousa et al., 2009). A Parkinson's related mutation of α -synuclein, Ala30Pro, was incapable of binding actin monomers and rather bound actin filaments, disordering the dynamics of actin organization by creating actin-rich foci.

Synuclein has also been suggested to be involved in the proper assembly of SNARE proteins in conjunction with a SNARE chaperone, CSP α (Chandra et al., 2005). In this manner, α -synuclein may help to maintain normal levels of SNARE complexes, thereby suppressing synaptic degeneration associated with CSP α depletion (Chandra et al., 2005). More recently, Burre *et al.* (2010) showed evidence that synuclein may act as a non-classical chaperone by simultaneously interacting with phospholipids (via its m-AH) and a protein of the SNARE complex, synaptobrevin-2 (via its acidic C-terminal tail) to promote SNARE-complex assembly. They observed that disruption of SNARE complex assembly can be rescued by synuclein on a transgene (Burre et al., 2010). Their work suggests that synuclein is an important player in preventing age-dependent neurodegeneration. Alternatively, it has been proposed that synuclein may negatively regulate docking and priming of synaptic vesicles in exocytosis of neurotransmitters, regulating the reserve pool of synaptic vesicles (Cooper, 2008). To date, there is vigorous ongoing research into the function of synuclein in the cell, with much evidence correlating its function to its curvature sensing ability.

The folding pathways of synuclein are very complex. Its misfolding into fibrillar oligomers and subsequent aggregation into proteinacious deposits is considered a hallmark of Parkinson's Disease (Auluck et al., 2010; Bussell and Eliezer, 2003; Conway et al., 1998; Fink, 2006; Jellinger, 2012; Uversky et al., 2001; Vilar et al., 2008; Volles and Lansbury, 2003; Volles et al., 2001). It is thought that fibril formation may actually be

a protective pathway that can sequester toxic protofibrils and thereby prevent the toxic effects of pre-fibrillar oligomers while maintaining pools of normal, functioning synucleins (Beyer and Ariza, 2008). Protofibrils may appear spherical or annular in their morphologies and disappear as they are converted to fibrils (Ding et al., 2002; Fink, 2006; Uversky et al., 2001). There are various studies demonstrating how these toxic protofibrils may form. For example, in one scenario where lipid is absent, synuclein will slowly oligomerize, converting into long amyloid fibrils made of stable stacks of beta strands (Fink, 2006; Vilar et al., 2008). Another scenario described that the presence of small amounts of anionic vesicles causes α -synuclein to concentrate onto the limited vesicle surface. In this case, the crowding onto the membrane accelerates fibrillization via a poorly understood mechanism (Aisenbrey et al., 2008; Lee et al., 2002; Zhu and Fink, 2003). Finally, oxidized dopamine promotes the formation of toxic α -synuclein oligomers (Choi et al., 2013).

1.6.2. α -Synuclein: Domain structure and similarity to the CCT tail region

Synuclein and the CCT tail region share many similarities in sequence and structure. Like CCT, α -syn contains a long ~80-90 residue m-AH followed by a highly negatively charged region (Fig. 1.6 A). In solution, it is considered to be a classic example of an intrinsically disordered monomeric protein (Weinreb et al., 1996), though there is recent controversial work suggesting that it may be a helically folded tetramer *in vivo* (Bartels et al., 2011). Synuclein and CCT domain M share a novel 11-mer sequence motif (Taneva et al., 2012)(Figure 1.6 C). This 11-mer tandem repeat is repeated 4 times in CCT and 7 times in α -syn. In addition to the conserved KTKEGV imperfect repeats, synuclein's m-AH also contains a region called the non-amyloid- β component (residues 61-95) (Bisaglia et al., 2006), which is required for its fibrillization potential (Bisaglia et al., 2006).

Like CCT, the m-AH in α -syn transitions from a disordered structure to a fully folded helix when presented with membranes enriched in acidic lipids or packing defects (Davidson et al., 1998; Nuscher et al., 2004). Its membrane binding is therefore similarly driven by a mixture of electrostatic attraction to anionic lipids and a hydrophobic component which favours binding to highly curved vesicles (Ding et al., 2012; Middleton

and Rhoades, 2010; Pranke et al., 2011). In the presence of detergent micelles, α -syn displays a broken helix conformation, with a short interruption at residues 41-44 (Georgieva et al., 2008), however vesicle-associated α -syn is one continuous unbroken helix (Georgieva et al., 2008; Trexler and Rhoades, 2009). The m-AH is also followed by an unstructured, highly acidic tail (15 aspartates/glutamates) which is similar to the phosphorylated state of the CCT tail (Figure 1.6 C)(Taneva et al., 2012). The negative charges on the C-terminal tail are thought to mediate interactions with other proteins (Jensen et al., 1999; Uversky et al., 2001), metal ions (Brown, 2007) or various cellular ligands such as dopamine (Eliezer et al., 2001; Leong et al., 2009). The C-terminal region of α -syn can be phosphorylated at Tyr 125, 133, and 136, and on Ser 129 (Hejjaoui et al., 2012; Recchia et al., 2004), further increasing the charge of its tail. Phosphorylation at Ser 129 may be fibril-promoting and implicated in the pathogenesis of neurodegenerative disorders (Paleologou et al., 2008).

1.6.3. Curvature sensing of synuclein

What is the origin of synuclein's curvature sensing ability? It has been suggested that synuclein has an unbalanced AH with a weakly hydrophobic face. Mutations enhancing the hydrophobic face of α -synuclein abolished curvature sensing (Pranke et al., 2011). It was argued that the under-developed hydrophobic face of α -syn dictated its dependence on membrane hydrophobicity (packing defects). Synuclein thus uses its charged polar face to compensate for the meagre contribution of its hydrophobic face, and this explains its requirement for anionic lipids. This specific chemistry of curvature sensing may make synuclein ideally suited to interact with secretory and endocytic vesicles having high anionic lipid content and highly curved surfaces, properties characteristic of membranes in the late secretory pathway.

α -Synuclein's curvature sensing ability may be crucial for its targeting to small synaptic vesicles which have a mean diameter of ~40nm (Zhang et al., 1998). The lipid composition of synaptic vesicles is estimated to be primarily ~39% PC, 45% PE, 14% PS, 2% PI with the proportion of acidic lipids approximately ~16% (Liu et al., 2011) . Localization onto these small vesicles may be important for its potential function as, for example, a chaperone in SNARE-complex assembly (Burre et al., 2010).

1.6.4. Differences between α -synuclein and CCT

Though their m-AH motifs are very similar, the m-AH of CCT and α -syn differ in the hydrophobicity of their non-polar faces. Whereas the non-polar face of the CCT m-AH is rich in bulky and aromatic amino acids, that of α -syn features short aliphatic residues such as valine, alanine, and even glycine (Fig 1.6 B; helical wheel plot). The hydrophobic face of CCT is also much narrower ($\sim 120^\circ$) compared to synuclein (180°) (Cornell and Taneva, 2006). These differences lead to the prediction that CCT which has a more strongly hydrophobic face would insert more deeply into the bilayer than α -syn, and that the two proteins might show differences in curvature sensitivity. A goal of my comparative studies on the m-AH and acidic tail regions of CCT and α -syn was to clarify the evolutionary advantages of membrane binding that can be modulated by not only the electrostatic character of the lipid but the protein's electrostatic nature as well.

1.7. Overview of research objectives

The goal of this thesis was to further explore the curvature sensing ability of the m-AH segments of CCT and α -synuclein, as well as to compare the effect of electrostatic modulation in regions flanking the m-AH on the curvature sensing ability of both proteins. The two major questions that this thesis aims to answer are:

- i. How does changing peptide electrostatic character affect curvature sensing of the CCT vs. synuclein m-AH?
- ii. How does changing the membrane electrostatic properties affect curvature sensing of the CCT vs. synuclein m-AH?

To address these questions a phosphorylation mimicking mutant for CCT as well as a synuclein mutant with a neutralized tail were generated to obtain CCT and synuclein protein pairs with and without negatively charged tails. I then used circular dichroism and fluorescence methods to observe membrane binding of the proteins under the following conditions:

- a) CCT and synuclein pairs were titrated with vesicles varying in curvature (size) to characterize membrane curvature selectivity

- b) CCT and synuclein peptide pairs were titrated with vesicles varying in charge density and in the presence of varying ionic strength to test the effect of varying electrostatic character on curvature sensing ability

Chapter 2. Experimental Procedures

2.1. Materials

Ampicillin, chloramphenicol, sodium dodecyl sulphate (SDS) and β -octylglucoside (OG) were from Sigma-Aldrich. RosettaTM Competent Cells were from Novagen. Ni-NTA agaros beads were from Qiagen and Thrombin proteases were from Amersham Biosciences. Amicon Ultra-4 centrifugal filters were from Millipore. All vesicles used in these experiments were composed of Egg PC/egg PG which were purchased from Avanti Polar Lipids. Polycarbonate membrane pores were from Avestin. Spectra/Por 7 dialysis membranes (10 kD MWCO) were purchased from Spectrum Labs Inc. Isopropylthio- β -galactoside (IPTG) and the fluorescent dye *N,N'*-Dimethyl-*N*-(Iodoacetyl)-*N'*-(7-Nitrobenz-2-Oxa-1,3-Diazol-4-yl) Ethylenediamine (iodoacetyl NBD amide) were purchased from Invitrogen.

2.2. Cloning

The pET-14b vector for the CCT M+P and α -syn proteins have an N-terminal His₆-tag sequence followed by a thrombin cleavage site and three cloning sites with an IPTG-inducible T7 RNA polymerase promoter. The plasmids were propagated in RosettaTM cells, a derivative of BL21 (DE3) *E. coli* cells specialized for expression of eukaryotic proteins containing codons not usually used in *E. coli*.

2.2.1. *Preparation of plasmids for transformation*

Several sets of CCT M+P and α -syn proteins were used in my thesis work. The unphosphorylated CCT (UP) proteins encompassed residues 237-367 of rat CCT α which include the M domain and the P region (Figure 1.6 A). The phosphomimic CCT (PM) protein had 16 serine to glutamate substitutions between residues 315 - 367 at the

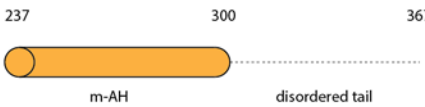
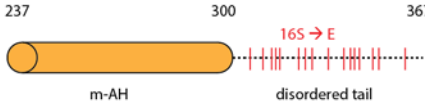

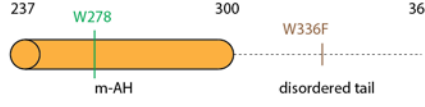
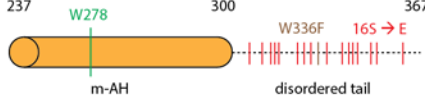
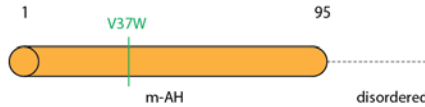

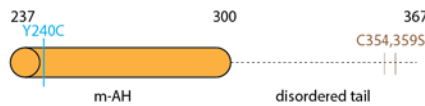
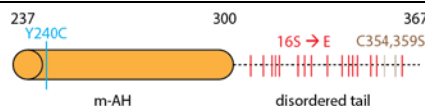
positions denoted in Figure 1.6 C and listed in Table 2.1. I used wild-type human α -syn as well as an α -syn construct where 12 acidic glutamates and aspartates between residues 98-140 were mutated to serines (α -syn12S) as shown in Figure 1.6 C and listed in Table 2.1. The construction of pET14b plasmids containing wild-type and PM versions of the CCT M+P domains and wild-type α -syn was developed by Joseph Lee and is described in Taneva *et al.* (2012). pET14b α -syn12S was prepared by gene synthesis. Double-stranded DNA encoding α -syn (with AGC mutations to create serine at the 12 sites denoted in Figure 1.6 C and listed in Table 2.1) was synthesized (Eurofin Operon) with 5' Nde1 and 3' Xho1 restriction sites. The digested synthetic gene was ligated into the Nde1/Xho1 sites of similarly digested pET14b.

For tryptophan fluorescence analysis single Trp variants were generated within the m-AH regions of CCT and α -syn. CCT has a native Trp at position 278 in the hydrophobic face of its m-AH (see Figure 1.6 B). A second Trp at position 336 in the P region was replaced with a Phe using QuikChange site-directed mutagenesis with pET14b-CCT M+P and pET-14b-CCT M+P (PM) as templates and mutagenic primers complementary to the targeted sequence. Since α -syn has no native Trp, a Trp was engineered at position 37 (replacing Val) in the hydrophobic face of its m-AH (see Figure 1.6 B) using QuikChange mutagenesis, mutagenic primers, and pET14b- α -Syn or pET14b- α -syn12S as templates. The pET14b plasmids containing the CCT M+P (UP), (PM) and α -syn tryptophan constructs were prepared by Joseph Lee (Huang *et al.*, 2013), and Jaeyong Lee prepared the α -syn12S Trp mutant in pET14b.

For NBD fluorescence analysis, single-cysteine variants of CCT M+P in pET14b were generated by Ziwei Ding. He replaced the two naturally occurring cysteines located in the P region (positions 354 and 359 in full-length CCT α) with serines, and engineered a cysteine in the hydrophobic face of domain M at position 240 of full-length CCT α in place of a tyrosine. These mutations were generated by QuikChange using pET14b-CCT M+P (UP) or (PM) as templates.

All CCT M+P and α -syn proteins contain a linker (Gly-Ser-His-Met), N-terminal to the thrombin cleavage site. The fidelity of all proteins generated by QuikChange mutagenesis was checked by sequencing of both strands. All proteins used in my thesis are listed in Table 2.1.

Table 2.1. CCT M+P and α -syn proteins used in vesicle binding experiments

Method	Proteins	Simplified diagram	Mutations
Circular dichroism	CCT M + P (UP)		CCT α 237 - 367
	CCT M + P (PM)		CCT α 237 - 367 S(315, 319, 321, 322, 323, 329, 331, 333, 339, 343, 345, 346, 347, 350, 352, 362)E
	α -syn		α -syn 1 - 140
Trp Fluorescence	CCT M + P (UP) W278		CCT α 237 - 367 W336F
	CCT M + P (PM) W278		CCT α 237 - 367 S(315, 319, 321, 322, 323, 329, 331, 333, 339, 343, 345, 346, 347, 350, 352, 362)E W336F
	α -syn V37W		α -syn 1 - 140 V37W
	α -syn 12S V37W		α -syn 1 - 140 D(98, 115, 119, 121)S E(104, 105, 110, 114, 123, 126, 130, 131)S V37W
NBD Fluorescence	CCT M + P (UP) Y240C		CCT α 237 - 367 Y240C C(354,359S)
	CCT M + P (PM) Y240C		CCT α 237 - 367 S(315, 319, 321, 322, 323, 329, 331, 333, 339, 343, 345, 346, 347, 350, 352, 362)E C(354,359S) Y240C

2.3. Protein overexpression

The pET14b vector enabled IPTG-inducible expression of CCT M+P and α -syn proteins in *E. coli* Rosetta strain as His₆-tagged proteins with thrombin cut sites. Expression optimization of the majority of the His₆-tagged CCT M + P and α -syn proteins was previously developed by Joseph Lee (2011) . I determined optimal expression conditions for the new proteins, CCT M + P (UP) and (PM) Y240C (used in NBD fluorescence experiments) as well as α -syn12S V37W (used in Trp fluorescence experiments).

2.3.1. Expression conditions

Expression times and temperatures of all CCT M+P and α -syn proteins were varied to optimize for the IPTG induction of soluble protein (Figure 2.1). Induction conditions are listed in Table 2.2. The soluble form of the CCT M+P proteins overexpressed well within 2 h of IPTG induction (at 20 °C) whereas α -syn required a 3 h induction (at 37 °C) for significant soluble protein to be observed. Joseph Lee observed that longer induction times caused protein aggregation. The His₆-tagged CCT M+P proteins are ~18 kDa, with the CCT (PM) protein migrating at a slower rate due to its highly acidic tail sequence. The His₆-tagged α -syn proteins are ~16.6 kDa.

Table 2.2. Induction times and temperatures for expression of CCT and α -syn

Proteins	Induction	
	Time (h)	Temperature (°C)
CCT M + P (UP)	2	20
CCT M + P (PM)	2	20
CCT M + P (UP) W278	2	20
CCT M + P (PM) W278	2	20
CCT M + P (UP) Y240C	2	20
CCT M + P (PM) Y240C	2	20
α -syn	3	37
α -syn V37W	3	37
α -syn12S V37W	3	37

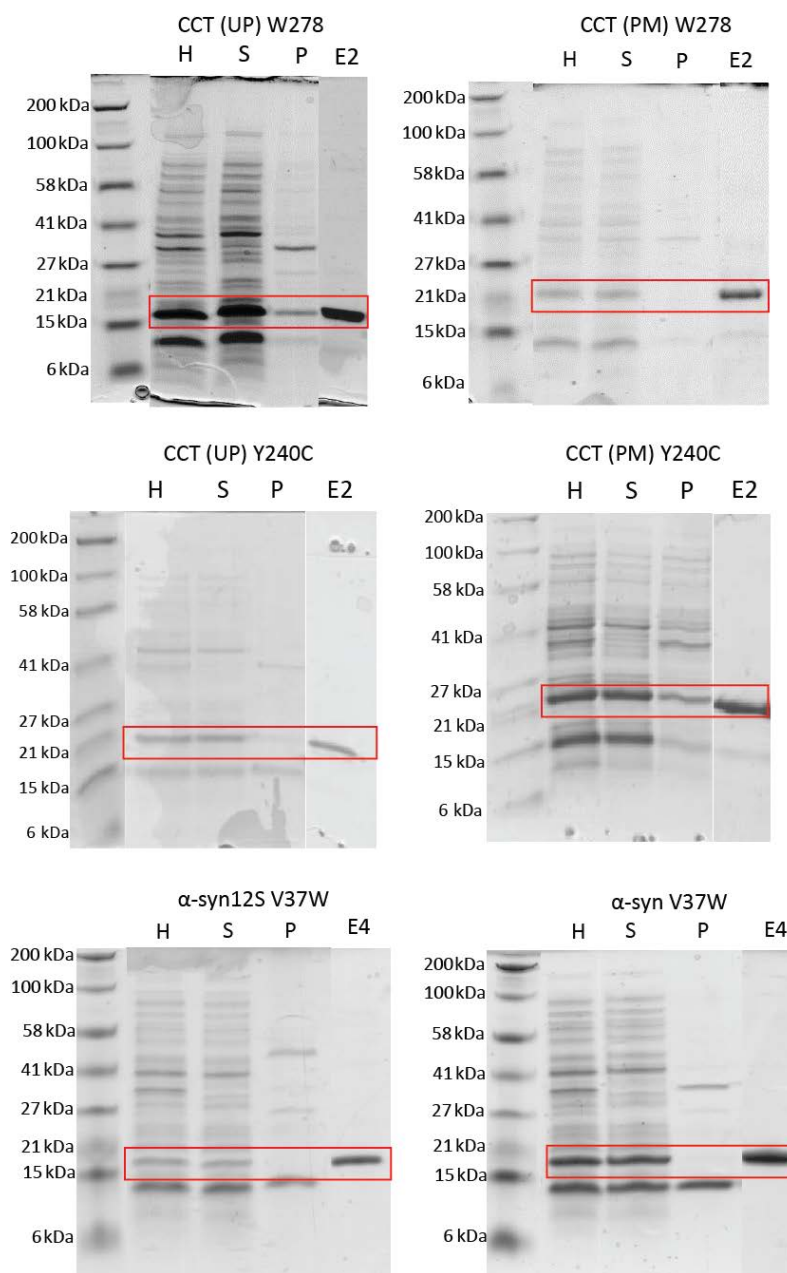


Figure 2.1. Overexpression and purification of His₆-tagged CCT M+P and α-syn proteins. 10% tricine gels showing the homogenate (H), supernatant (S) and pellet (P) of each protein. The elution fraction (E) of the purified protein that was used in subsequent experiments is shown in the final lane. The molecular weight of the His₆-tagged CCT M+P proteins is ~18 kDa and α-syn is ~16.6 kDa. Proteins are in red boxes.

2.3.2. General large scale overexpression

All liquid media was composed of LB with 100 µg/mL ampicillin and 34 µg/mL chloramphenicol, compatible with the pET14b and Rosetta cell resistance markers, respectively. Starter cultures (3 mL) were prepared by inoculation of LB with glycerol stocks of Rosetta cells transformed with the pET14b constructs containing CCT or α -synuclein coding sequences. After a 12 h incubation at 37 °C (with shaking), the 3 mL starter was transferred to a 30 mL liquid culture and incubated under the same conditions overnight. The next day, the 30 mL culture was transferred to a 1 L liquid culture and allowed to grow until an optical density (Abs_{600nm}) in the range of 0.6 – 0.8 was reached. Overexpression was then induced with concentrations of IPTG at the induction times and temperatures specified in Table 2.2. After the induction period, the 1 L liquid culture was centrifuged at 3,000 × g for 10 min, the supernatant was decanted and the cell pellet stored at -80 °C until purification.

2.4. Protein purification

All protein purification and His₆-tag cleavage protocols used were developed by Joseph Lee. The protocols were adapted from published procedures for purification of His₆-tagged CCTs (Dennis et al., 2011; Taneva et al., 2012). Buffers used in cell lysis, purification and thrombin digestion protocols contain the reducing agent DTT to prevent formation of potentially cross-linking disulfide bonds from the cysteines in the tail region of CCT α and the detergent OG was added to reduce aggregation of proteins.

2.4.1. Cell lysis

The 1 L frozen cell pellets were resuspended in 100 mL of lysis buffer composed of PBS pH 7.4, 2 mM DTT, 25 mM OG, 200 µg/mL of lysozyme, 10 µg/mL of DNaseI and protease inhibitors (2.5 µg/mL leupeptin, 2 µg/mL chymostatin, 1 µg/mL antipain, 2 µg/mL pepstatin, 10 µg/mL p-amino-benzadine, 10 µg/mL benzamidine and 0.5 mM PMSF). The sample was sonicated on ice using a Fisher Sonic Dismembrator Model 300 for 4 × 15 sec (with 15 sec pauses in between) with output set at 30%. The

homogenate was then separated into supernatant and pellet fractions by centrifugation at 23,000 × g for 30 min at 4 °C.

2.4.2. Purification

The isolated supernatant containing the majority of the His₆-tagged protein was slowly mixed with 10x binding buffer (50 mM NaPi, 5 M NaCl, 150 mM imidazole, pH 8.0) in a 1:10 ratio of 10x binding buffer to supernatant. Binding buffer had high ionic strength to prevent non-specific binding of other proteins with the resin. A 50% slurry of Ni-NTA Agarose beads was mixed with the sample in a 1:25 Ni-NTA slurry to sample ratio and rotated at 4 °C for 2 h for complete binding of His₆-tagged protein with Ni beads. Beads and supernatant mixture were then poured into a 1 cm × 10 cm stop-cocked column and allowed to settle at 4 °C before the flow-through was collected. The column containing the His₆-tagged proteins bound to the Ni beads was washed first with wash buffer 1 (50 mM NaPi, 0.5 M NaCl, 25 mM imidazole, 25 mM OG, 2 mM DTT, pH 8.0) then with wash buffer 2 (50 mM NaPi, 100 mM NaCl, 25 mM imidazole, 25 mM OG, 2 mM DTT, pH 8.0). His₆-tagged proteins were then eluted with 50 mM NaPi, 100 mM NaCl, 350 mM imidazole, 25 mM OG, 2mM DTT, pH 8.0 and collected into 8 × 2 mL fractions. Elution fractions were electrophoresed using 10% tricine gels to determine which elution fraction contained the most protein (Figure 2.2). An Amicon Ultra-4 (10,000 MWCO) ultrafiltration device was then used to reduce imidazole concentration in the buffer of the peak fraction to 10 – 20 mM by diluting the sample with PBS/ 2 mM DTT/ 25 mM OG. The filtered protein (in a final buffer of PBS, 2 mM NaP_i, 3 mM NaCl, 11 mM imidazole, 25 mM OG, 2 mM DTT and pH 7.4) was stored at -80 °C until the next step.

2.4.3. Thrombin Digestion

Purified and filtered proteins were diluted 4x with PBS/ 2 mM DTT/ pH 7.4 to reduce OG from 25 mM to 6.25 mM and allow optimal thrombin protease activity. 1 unit of thrombin per 50 µg of protein was added to the sample and digestion was complete after incubation at room temperature for 7 h on rotation (Figure 2.2). Protease inhibitors (final concentration of 10 µg/mL benzamidine, 2 µg/mL chymostatin, 1µg/mL antipain and 2.5 µg/mL leupeptin) were added and the OG concentration was again reduced to 0.1 mM using Amicon ultrafiltration and PBS/ 2 mM DTT/ pH 7.4 as the diluting buffer,

removing cleaved His₆-tags and concentrating the proteins in the process. All proteins after thrombin digestion carry a Gly-Ser-His-Met linker peptide sequence at their N-termini.

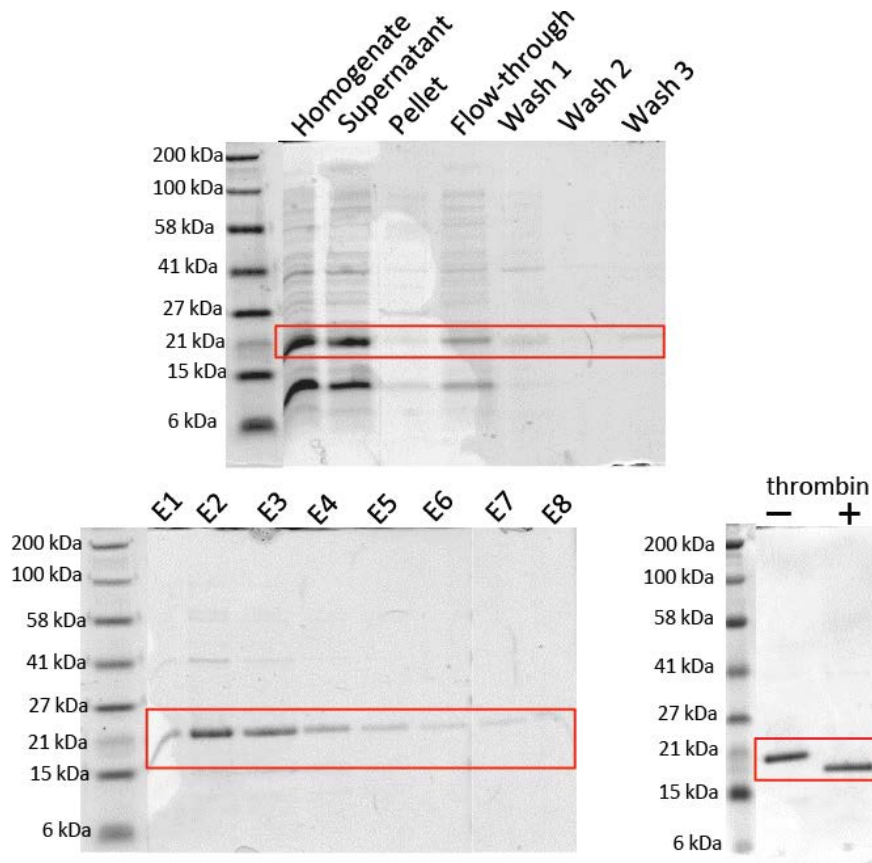


Figure 2.2. Purification and thrombin cleavage of His₆-tag.
 A set of 10% tricine gels illustrating the purification and His₆-tag cleavage of CCT (PM) W278. Top gel shows homogenate, supernatant and pellet fractions collected after cell lysis. The Flow-through, Wash 1, Wash 2 and Wash 3 from the purification procedure and the eight elution fractions (E) collected are shown (top and bottom left gels). Bottom right gel shows the protein before and after thrombin cleavage of His₆-tag. Faster migration of protein band after thrombin is added indicates His₆-tag is removed. The molecular weight of the CCT (PM) W278 protein is ~18 kDa and after thrombin cleavage is ~16 kDa. Red boxes highlight the position of CCT on the gel.

2.4.4. Protein quantification methods

The concentration of the final protein sample was determined using both the Bradford method and Nanodrop readings.

In the Bradford method (Bradford, 1976), I used BSA standards (ranging from 0 – 5 ug BSA) with sample volumes adjusted to 20 μ L using dH₂O. 200 μ L of Bradford Dye Reagent (0.005% w/v Coomassie Brilliant Blue R, 5% v/v ETOH, 10% v/v H₃PO₄) was quickly added and followed by immediate vigorous vortexing. Samples and standards were incubated with shaking for 15 min at 37 °C in a water bath and the absorbance at 595 nm of each sample was measured with a Beckman DU 640 Spectrophotometer.

The Nanodrop ND-1000 Spectrophotometer was used to measure the absorbance at 280 nm of 2 μ L samples. The final concentration was calculated by the program internal to the instrument and was based on the protein's extinction coefficient and molecular weight as listed in Table 2.3.

Table 2.3. Protein physical parameters

Proteins ¹	Molecular weight ² (kDa)	Extinction coefficient ² (M ⁻¹ cm ⁻¹)
CCT M + P (UP)	15.36	12,490
CCT M + P (PM)	16.03	12,490
CCT M + P (UP) W278	15.32	6,990
CCT M + P (PM) W278	15.99	6,990
CCT M + P (UP) Y240C	15.26	11,000
CCT M + P (PM) Y240C	15.94	11,000
α -syn	14.87	5,960
α -syn V37W	14.96	11,460
α -syn12S V37W	14.51	11,460

¹His-tags were removed but N-terminal Gly-Ser-His-Met linker contributed to the mass.

²The parameters were calculated using the protein sequences and the ExPASy ProtParam tool (<http://web.expasy.org/protparam/>).

2.5. Phospholipid vesicle preparation

2.5.1. Preparation of single lamellar vesicles (SUVs) and extruded vesicles (LUVs)

A suspension of multilamellar vesicles were prepared by aliquoting appropriate volumes of lipid chloroform stocks into a round bottom flask, evaporating the chloroform

using a rotary evaporator, and re-suspending the lipid film with the appropriate volume of ddH₂O. All steps were carried out under vacuum or Argon gas to prevent oxidation of lipids. The concentration of the chloroform stocks were determined by phosphorus assay (Bartlett, 1959).

To prepare SUVs, this MLV suspension was sonicated for 10mins on ice using a Branson sonifier 450 set at 30% duty cycle until the solution was clear. The sample was then centrifuged for 5 min at 12, 500 × g at 4 °C to pellet any remaining MLVs. The supernatant containing the SUVs was removed and kept under Argon gas and on ice or at 4 °C while being used in experiments or stored. SUVs were used for up to 2 days under these storage conditions.

To prepare LUVs, 0.5 – 1 µL of ³H DPPC was first added to the chloroform lipid mixture and a suspension of MLVs were prepared as described. An Avestin hand-held extruder fitted with two polycarbonate membranes of the desired pore size was rinsed by passing ddH₂O through the filters 12x. The ddH₂O was removed and the suspension of MLVs was added and extruded through the filters 21 times. The final LUVs were stored under Argon gas on ice and used for experiments the same day. To adjust for the potential loss of lipid in the extrusion process, the final concentration of the LUVs was determined by comparing the average counts per minute (cpm) of 3 × 5 µL samples each of pre-extruded and post-extruded ³H-DPPC doped vesicles.

2.5.2. Vesicle sizing

Vesicle size was determined by dynamic light scattering (DLS) and transmission electron microscopy (TEM). DLS measurements and analyses were greatly assisted by Dr. Barbara Frisken and her students, Gabriel Espinosa and Rasoul Narimani. TEM measurements were assisted by Dr. Svetla Taneva.

2.5.2.1. Vesicle sizing using dynamic light scattering (DLS)

The principle of dynamic light scattering is based on the light scattering behavior of particles in solution diffusing in Brownian motion. A laser is shone on the sample, generating a scattering intensity which varies with time as the particles fluctuate in their position due to diffusion (Burn, 1988; McMahon and Gallop, 2005). An autocorrelation of

these intensities in which the signals from these particles are compared over short intervals of time provides information on the size of the particles. Over time, the signals will no longer correlate with the initial state of the sample, and an exponential decay in the autocorrelation will be observed. A smaller particle diffuses more rapidly in solution resulting in a shorter time to observe an exponential decay in the autocorrelation whereas a larger particle moves more slowly and will therefore change its position and scattering intensity over a longer period of time. The hydrodynamic radius, r_h , is computed using the Stokes-Einstein equation and the polydispersity of the sample is computed using the cumulant method (McMahon and Gallop, 2005). The polydispersity index is an indication of the variance/distribution of vesicle sizes measured, with larger numbers indicating broader size distributions. 1,500 μL samples of 0.1 mM vesicles in filtered ddH₂O were prepared for the measurements. Autocorrelation plots are shown in Fig. 2.3. The summary of results is listed in Table 2.4.

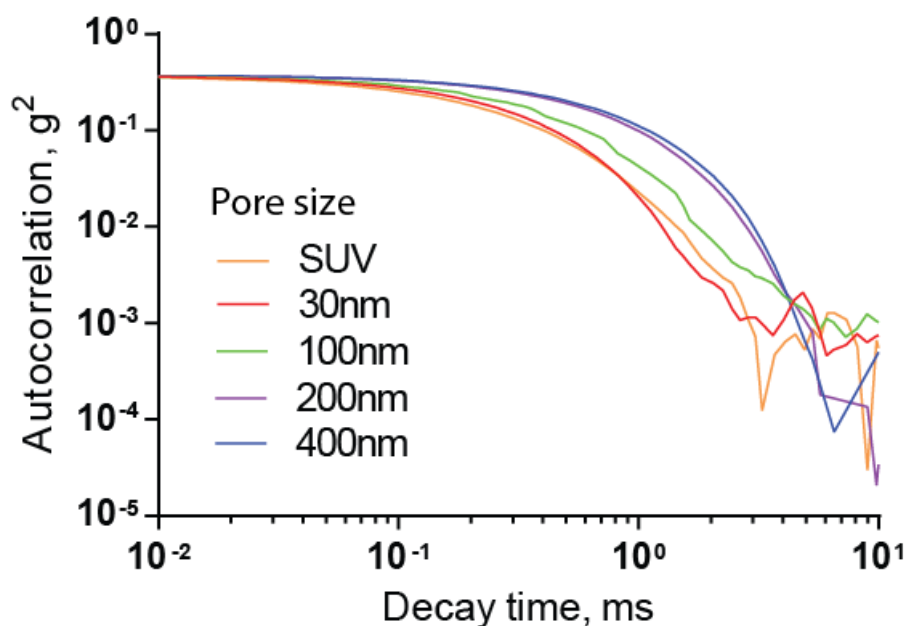


Figure 2.3. The hydrodynamic radius of sonicated and extruded vesicles were measured using DLS.

Logarithmic plots showing exponential decay rates of autocorrelation functions for each vesicle size. Vesicles were 30 mol% PG.

2.5.2.2. Vesicle sizing using transmission electron microscopy (TEM)

The size measurements of vesicles in TEM images were used to support some of the data collected from the DLS measurements. In TEM, a beam of electrons is transmitted through a thin specimen, interacting with the thickness and composition of the material. The pattern of occlusion and absorption of the electrons that interact with the sample is used to create a high resolution image. Regions of the material that are denser in electrons can be differentiated from regions poorer in electrons due to their differing electron scattering properties. I prepared 1.5 mM samples of SUVs and 100 nm LUVs for TEM. The vesicles were absorbed onto a copper grid for 30 min, followed by negative staining using uranyl acetate (2 wt. %) to enhance contrast. Images were digitally captured using a Hitachi H-8000 STEM electron microscope (Taneva et al., 2012). After images were collected, the long and short axes of the vesicles from a sample size of 250 vesicles were measured using tools from Adobe Photoshop. Sample TEM images of the vesicles are provided in Fig. 2.4 and the results are listed in Table 2.4.

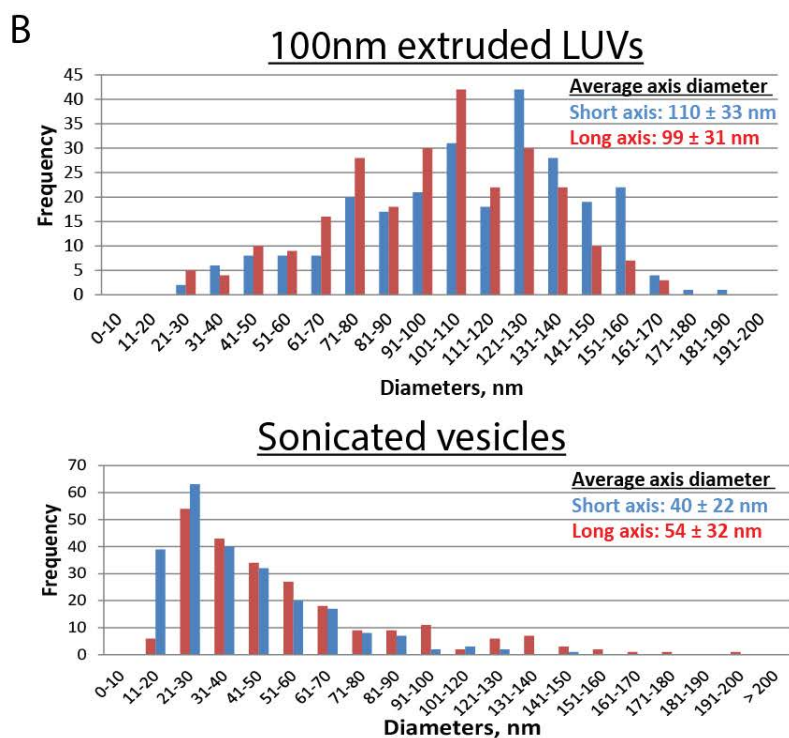
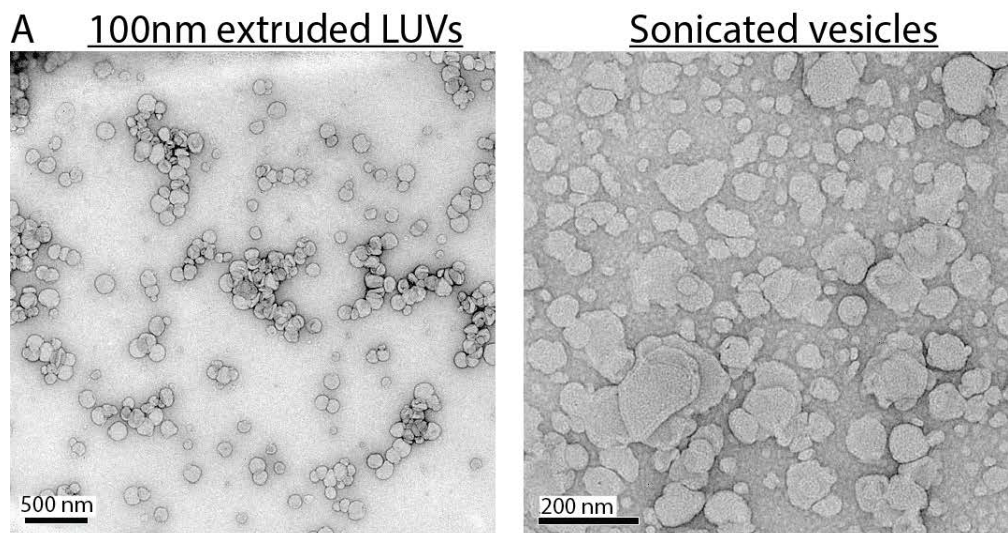


Figure 2.4. The sizes of SUV and 100 nm extruded vesicles were measured using TEM. (A) Sample TEM images of 100 nm extruded and sonicated 30 mol% PG vesicles negatively stained with uranyl acetate from which the diameters of a population of vesicles were measured. (B) The long and short axis of the vesicle diameters were measured and a chart describing the distribution of vesicles was plotted. Average diameters \pm standard deviation is reported for each set. A sample size of 250 vesicles were measured.

Table 2.4. Summary of results for DLS and TEM vesicle sizing measurements.

Pore diameter	DLS		TEM		Size reported (nm)
	Diameter (nm)	Polydispersity Index	Long axis diameter (nm)	Short axis diameter (nm)	
SUV	47	0.58	54 ± 32	40 ± 22	47
30 nm	85	0.10			85
100 nm	112	0.02	110 ± 33	99 ± 32	112
200 nm	144	0.02			144
400 nm	155	0.09			274 ± 74*

*The literature value for vesicles extruded using the 400 nm pore size were reported in my thesis: (Brewer et al., 1998; Frederick et al., 2009; Matsuzaki et al., 2000; Mayer et al., 1986)

2.6. Membrane binding analyses

Membrane binding analyses were performed using circular dichroism (CD) as well as tryptophan and NBD dye fluorescence. From the raw data collected using these methods, membrane binding curves were generated and partition coefficients calculated where possible for each of these methods.

2.6.1. Circular Dichroism and deconvolution

2.6.1.1. Theory

Circular dichroism uses light in which the electric field vector is rotating about its direction of propagation with a constant magnitude (Kelly et al., 2005). Left and right circularly polarized light of a specific wavelength are alternately passed through an optically active medium. When this circularly polarized light passes through the medium, the left and right polarized light are absorbed to a different extent. The resulting difference in absorbance can be corrected for concentration and reported as molar ellipticity to yield the CD spectrum of the sample. Secondary protein structures have distinct far-UV CD spectra which can provide information about the fraction of alpha-helix, beta-sheet, beta-turn or random coil conformations in the molecule (Kelly et al., 2005).

2.6.1.2. Sample preparation and data collection

For circular dichroism measurements, the CCT M+P (UP), CCT M+P (PM) and α -syn constructs were used (refer to Table 2.1 for details).

The proteins (5 μ M) in dilute PBS (ionic strength 15 mM) were mixed with varying concentrations of lipid vesicles at 25 °C and incubated for 5 min. The buffer contained low salt concentration to reduce interference from light scattering. CD spectra were recorded by a Jasco-J-810 spectropolarimeter in a 0.1 cm path-length cuvette at a scanning rate of 100 nm/min and a band width of 1 nm. Two scans were averaged per spectrum. All spectra were smoothed, corrected for the corresponding background (buffer +/- vesicles) and converted to molar ellipticity deg.cm²/dmol using the molecular masses listed in Table 2.3. The content of secondary structure was determined using the CDPro package and protein reference set #7, which includes 43 soluble proteins whose structures have been solved and 5 denatured proteins (Sreerama and Woody, 2000). The reported fractions of secondary structure are the average \pm SD determined by SELCON, CONTINLL, and CDSSTR included in the package. The fraction of secondary structure was plotted vs. log [accessible lipid] which is 60% of total lipid for SUVs and 50% for LUVs. The resulting curves were fitted using either GraphPad Prism 5 sigmoidal dose-response with variable slope.

2.6.2. Fluorescence

2.6.2.1. Theory

In fluorescence spectroscopy, a fluorophore is irradiated with UV light of a certain wavelength. The electrons absorb the energy from the photons and are excited from their ground state to various vibrational levels in excited electronic energy states. Collisions or various conformational changes cause the electrons of the fluorophore to relax back to the lowest vibrational level of the first excited state, called non-radiative relaxation. Electrons returning from the first excited state to the vibrational levels of the ground state can emit the excess energy in the form of a photon; this is a radiative transition known as fluorescence (Bigay et al., 2005). Electrons can relax to the ground state vibrational levels via other routes as well, which will reduce the quantum yield of the sample. Environmental factors affecting fluorescence spectra and quantum yields

are solvent polarity, presence of quenching species, pH of the medium and temperature. Polar solvents stabilize the excited state of the fluorophore by re-orienting their dipoles around the excited fluorophore's dipole (solvent relaxation), lowering the energy level of the excited state which results in a lower energy, red-shifted emission (Bigay et al., 2005). In my experiments, I used a native tryptophan or a conjugated external fluorophore (NBD) to probe the microenvironment of my proteins. The wavelengths of their emission maxima blue-shift which corresponds to a translocation from the polar aqueous environment to the non-polar membrane medium.

2.6.2.2. Tryptophan fluorescence: Sample preparation and data collection

For tryptophan fluorescence measurements, the CCT M + P (UP) W278, CCT M + P (PM) W278, α -syn V37W and α -syn12S V37W proteins were used (refer to Table 2.1. for details).

The proteins (1 μ M) in dilute PBS (ionic strength, 115 mM unless noted) were mixed with a range of vesicle concentrations and incubated for ~5 min at 20 °C. Samples were placed in a 10 mm path-length quartz cuvette and spectra were recorded using a Varian Cary Eclipse Spectrofluorometer with excitation at 280 nm and an emission scan from 300 – 400 nm. Excitation and emission slits were set to 10 and 5 nm, respectively; PMT voltage was 925 V. Six scans were averaged and the resulting spectra were smoothed and corrected for the corresponding background (buffer +/- vesicles). The average wavelength of maximum intensity for unbound CCT and α -syn was 350 nm. In the presence of saturating lipids, this wavelength of emission maxima blue-shifted to 325 nm. I plotted fluorescence ratio (Intensity (I) at 325 nm / 350 nm) for each spectra vs. log [accessible lipid].

2.6.3. NBD fluorescence

For NBD fluorescence, the cysteine mutants CCT M + P (UP) Y240C and CCT M + P (PM) Y240C were used (refer to Table 2.1. for details).

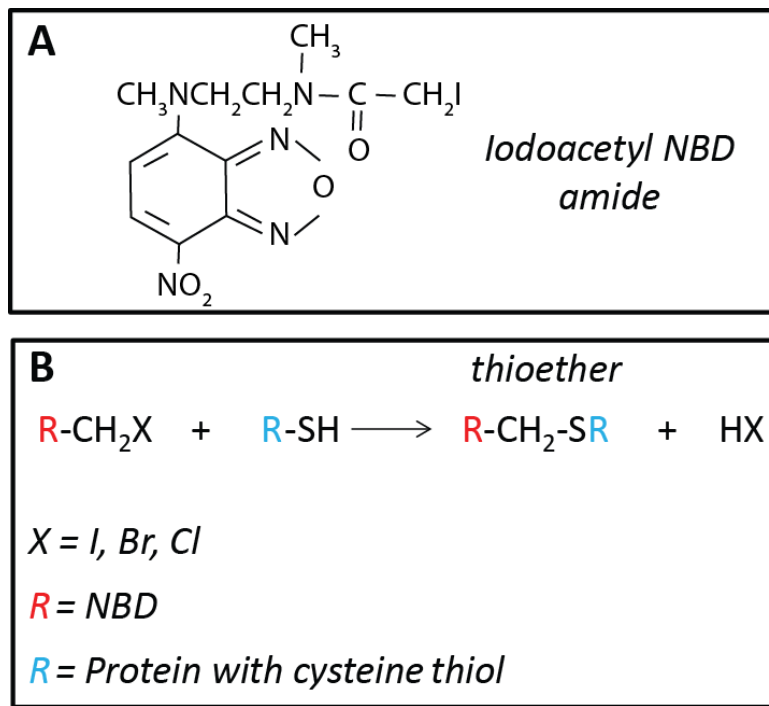


Figure 2.5. Labelling of protein with NBD fluorophore.

(A) Structure of the iodoacetyl NBD amide. (B) General reaction scheme showing the haloacetyl amide NBD reacting with a protein's cysteine group to form a thioether bond.

2.6.3.1. NBD labeling procedure

NBD was conjugated via a stable thioether bond to the engineered cysteine at residue 240 (Y240C) (Figure 2.5). The protein buffer was adjusted to PBS, 1mM DTT, 0.14 M NaCl, pH 7.4. An increase in OG concentration to 6 mM and the ionic strength to ~ 300 mM was found to reduce aggregation propensity. The His₆-tag was completely cleaved with 1 unit of thrombin per 50 ug of protein at room temperature for 1 h on rotation. Iodoacetyl NBD amide was prepared in DMSO at ~20 mM, based on absorbance at 480 nm. The NBD was added to the digested proteins to a final concentration of 2 mM and 2-fold molar excess over the sum of the CCT Y240C constructs plus DTT. DMSO was < 5% volume. After 1 h at room temperature in the dark, OG, free NBD and NBD-DTT conjugates as well as His₆-tags were removed via dialysis at room temperature in the dark for 4 h (with a buffer change every 2 h) and then overnight in the dark. The dialysis buffer was PBS, 0.14 M NaCl, pH 7.4. The stoichiometry of labeling was ~1:1 (NBD / protein molar ratio), measured via absorbance at 480 nm and 280 nm, respectively. Protein concentration was verified with the Bradford assay (Bradford, 1976) and labeling was confirmed by visualization of fluorescent bands

separated by 10% tricine gels using a Typhoon Variable Mode Imager (Amersham Biosciences) with green laser (532 nm) irradiation. The NBD-labelled peptides were stored in the dark at -80 °C.

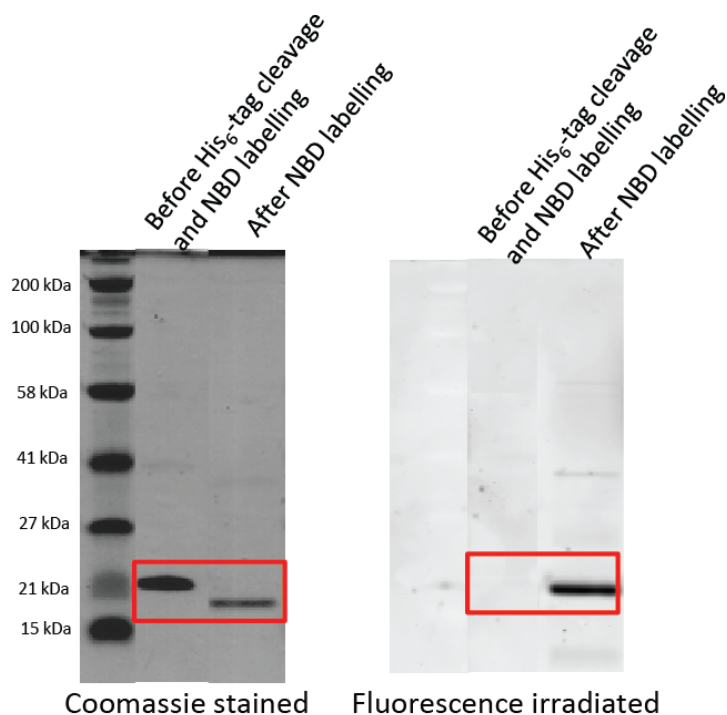


Figure 2.6. NBD labelling was confirmed by fluorescence imaging of CCT band on gel. Example of 10% tricine gel showing CCT (PM) Y240C before and after NBD labelling procedure. Left-hand gel is Coomassie-stained and right-hand gel is the same gel fluorescently irradiated.

2.6.3.2. Sample preparation and data collection

The proteins (0.1 μM) were diluted and mixed with lipids, and spectra were recorded, smoothed and corrected as described section 2.6.2.2 with different spectrofluorometer settings. For NBD fluorescence, excitation was at 478 nm and the emission scan was from 500 – 650 nm. Excitation and emission slits were set to 10 nm. The average wavelength of maximum intensity for unbound CCT was 550 nm. In the presence of saturating lipids, this peak blue-shifted to 533 nm. I plotted fluorescence intensity at 533 nm for each spectra vs. \log [accessible lipids].

2.6.4. Procedure for constructing binding curves and obtaining partition coefficients (K_p)

To obtain partition coefficients, the plots of secondary structure or fluorescence signals vs. log [accessible lipid] generated from circular dichroism, tryptophan fluorescence and NBD fluorescence were normalized to create binding curves using equation 1 as described in Table 2.5.:

Table 2.5. Equations used to normalize binding curves

Method	% Bound equation	
Circular Dichroism	$\% \text{ bound} = \frac{X - X_0}{X_{100} - X_0}$ (equation 1)	where X = fraction of α -helical Structure
Trp Fluorescence		where X = $I_{325 \text{ nm}} / I_{350 \text{ nm}}$
NBD Fluorescence		where X = Intensity at 533 nm

The plots of percent bound vs. [accessible lipid] were fit to the equation:

$$\% \text{ bound} = \frac{K_p[L]}{1 + K_p[L]} \quad (\text{equation 2})$$

Where [L] is the accessible lipid concentration and K_p is the apparent molar partition coefficient. The resulting EC_{50} were used to calculate the K_p values using the equation $K_p = 1/EC_{50}$. The hyperbolic curves were then transformed onto a log scale for visualization purposes.

2.6.5. Assessment of the reliability of K_p values

As discussed elsewhere (Buser and McLaughlin, 1998; Mesmin et al., 2007; Murray et al., 1998) partitioning analyses require that the membrane surface area is not limiting. If the membrane surface is limiting when lipid concentrations are at K_p then the population of proteins may have insufficient membrane surface for complete stabilization of their fully folded m-AH in the membrane leaflet. It is estimated that one CCT m-AH requires ~25 lipids for solvation on the membrane (Taneva et al., 2012). I used the

following equation to estimate the excess lipid available when 50% of the protein is bound:

$$[\text{excess lipid}] = [\text{EC}_{50}] - 25 [0.5 (P_t)] \quad (\text{equation 3})$$

where P_t is the total protein concentration and EC_{50} , the accessible lipid at 50% bound, is obtained from the binding curve. If there was no excess residual lipid at EC_{50} , the K_p values were deemed to be underestimated, as there is not enough membrane surface available. Unless noted, I have reported apparent K_p values representing systems where there was excess lipid at EC_{50} .

Chapter 3. Results: Comparison of the curvature dependence of CCT and α -synuclein and the role of their negatively charged tails

In this chapter, I present the results of the binding analyses of CCT and α -syn m-AHs to vesicles with variable curvature. In the course of my thesis work, I faced the recurring challenge of characterizing the membrane binding behavior of m-AHs that bind very strongly to lipid membranes, a problem described in section 2.6.5 as well as in the following sections. In these systems, membrane surface is limiting at low lipid concentrations, and there is a risk that the proteins may not be fully solvated by the membrane lipids even at the lipid concentration corresponding to the K_d . This is the primary reason why I have repeated my membrane binding measurements using different techniques: first using circular dichroism then using native Trp and NBD fluorescence. As a result, I have obtained a comprehensive set of reproducible data with trends that all correlate qualitatively. In this chapter, I will relate the challenges I faced using each method and, ultimately, the results that I felt were most reliable.

3.1. Curvature-sensitivity of the m-AH is modulated by the charge of its flanking region.

3.1.1. *Curvature dependent binding as probed by circular dichroism*

I used bacterially-expressed, non-phosphorylated α -syn and CCT regulatory domains. The CCT constructs were composed of the M and P regions in unphosphorylated (CCT (UP)) and phosphomimic (CCT (PM)) forms. CCT (PM) is a variant with all 16 phosphoserine sites substituted with glutamates. It has been studied in the context of the full-length enzyme, showing reduced membrane partitioning (Wang and Kent, 1995), similarly to hyper-phosphorylated CCT (Watkins and Kent, 1991).

Initially, I examined the vesicle size-dependence of the interaction of CCT M+P proteins and α -syn using circular dichroism (CD) to monitor changes in secondary structure coincident with binding. CCT (UP), CCT (PM) or α -syn were titrated with SUVs and LUVs of known diameters composed of 30 mol% egg PG, whose diameters were determined by light scattering and TEM (see Section 2.5. and Table 2.4). The balance of the lipid was egg PC in these and all other vesicles. 30 mol% anionic lipid represents the high end of physiological anionic lipid content (Dowhan, 1997). Representative titrations with sonicated 47 nm vesicles and extruded vesicles of 112 nm and 274 nm diameter are shown in Figure 3.1 for CCT (UP), CCT (PM) and α -syn.

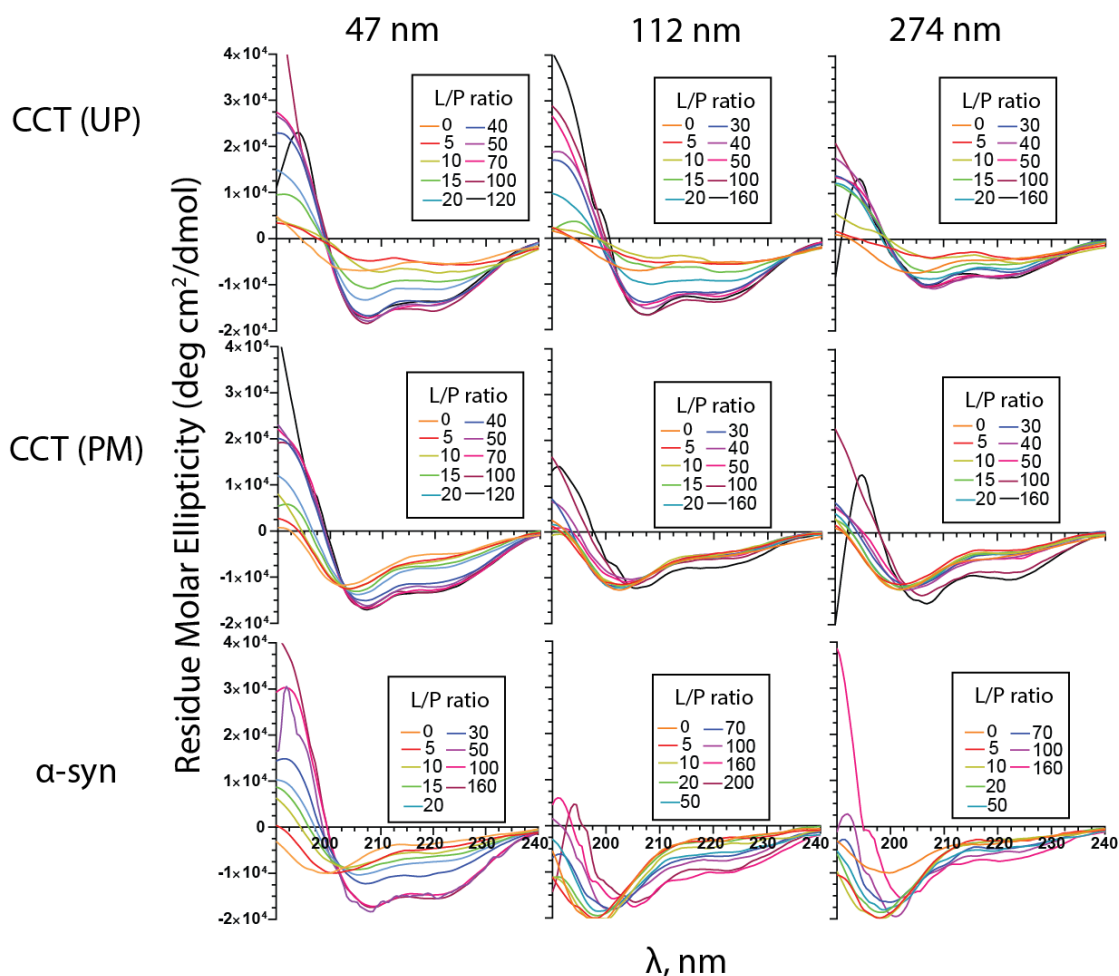


Figure 3.1. Curvature dependence of CCT and α -syn as probed by CD.

CD spectral set from one trial of 5 μ M CCT (UP), CCT (PM) and α -syn titrated with 30 mol% vesicles of varying diameter and 15 mM ionic strength. The Y-axis was plotted as residue molar ellipticity which reports the molar ellipticity for the individual amino acid residues (calculated by the molar ellipticity divided by the number of amino acids in the protein). Another trial was repeated with similar results.

Deconvolution of CD spectra indicated that the m-AH regions of the CCTs and α -syn transform from a mixture of predominantly disordered and beta strand conformations into nearly fully folded helical conformations in the presence of vesicles (Figure 3.2). The deconvolution results showed that the m-AH regions in CCT and α -syn comprise ~0.44 and 0.67 of the total protein sequences, respectively. In the absence of lipids, the ensemble of the CCT M+P proteins featured ~ 50% unordered conformations, and ordered content comprised of ~10% helical, 15% turns, and ~25% β -strand. On the other hand, the ensemble for α -synuclein featured ~80% unordered content and almost no helical structure in the absence of lipid. As lipid was titrated, the m-AH of CCT transformed into helical structure at the cost of disordered and β -strand structure, while the fraction of turns remained constant. In the case of α -synuclein, there was a direct correlation between decrease in disordered structure and increase in helical structure upon addition of lipid, while the fraction of turns and β -strand remained very low and constant. The fraction of helical content was used to create binding curves (Figure 3.3).

The plots of percent bound protein vs. log [accessible lipid] (Figure 3.3) indicated a binding affinity rank order of CCT (UP) > CCT (PM) > α -syn, in keeping with previous analyses (Taneva et al., 2012), and in agreement with the notion that repulsive charge adjacent to the m-AH can weaken affinity (Arnold et al., 1997; Dennis et al., 2011). CCT (PM) and α -syn showed a significant difference in binding to large vs. small vesicles, whereas the CCT (UP) showed very little selectivity for size (Figure 3.3). Thus it appeared that the m-AH segments flanked by acidic tails are curvature sensitive, but the m-AH segments flanked by a neutral tail are not.

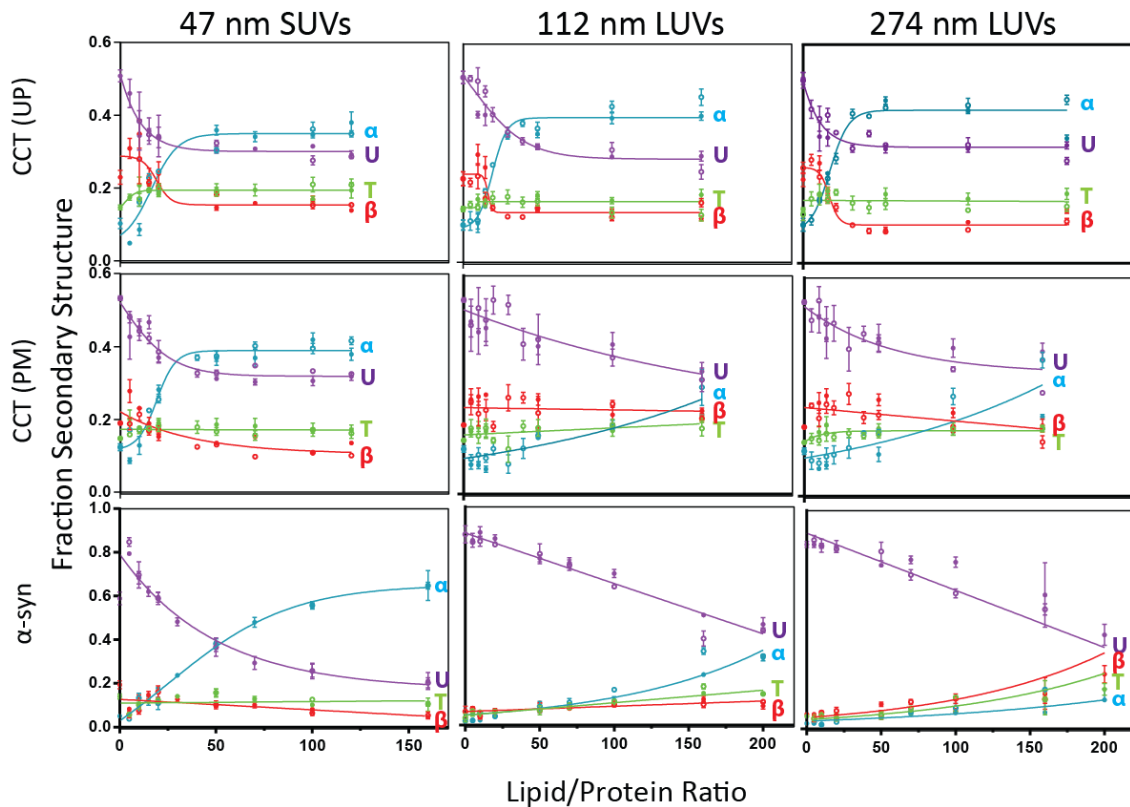


Figure 3.2. Deconvolution of CD spectra show a transition from unordered structure to alpha-helix with increasing lipid concentration.

Spectra were deconvoluted to generate fractional secondary structure; α -helical (blue), unordered (purple), turn (green) and beta strand (red) structure. The open and closed symbols represent two independent trials. Error bars represent means \pm S.D. of the fractional secondary structure content deconvoluted using the three programs, SELCON, CONTINLL, and CDSSTR, within the CDPro package (<http://lamar.colostate.edu/~sreeram/CDPro/main.html>). Proteins are 5 μ M and vesicles were composed of 30 mol% PG.

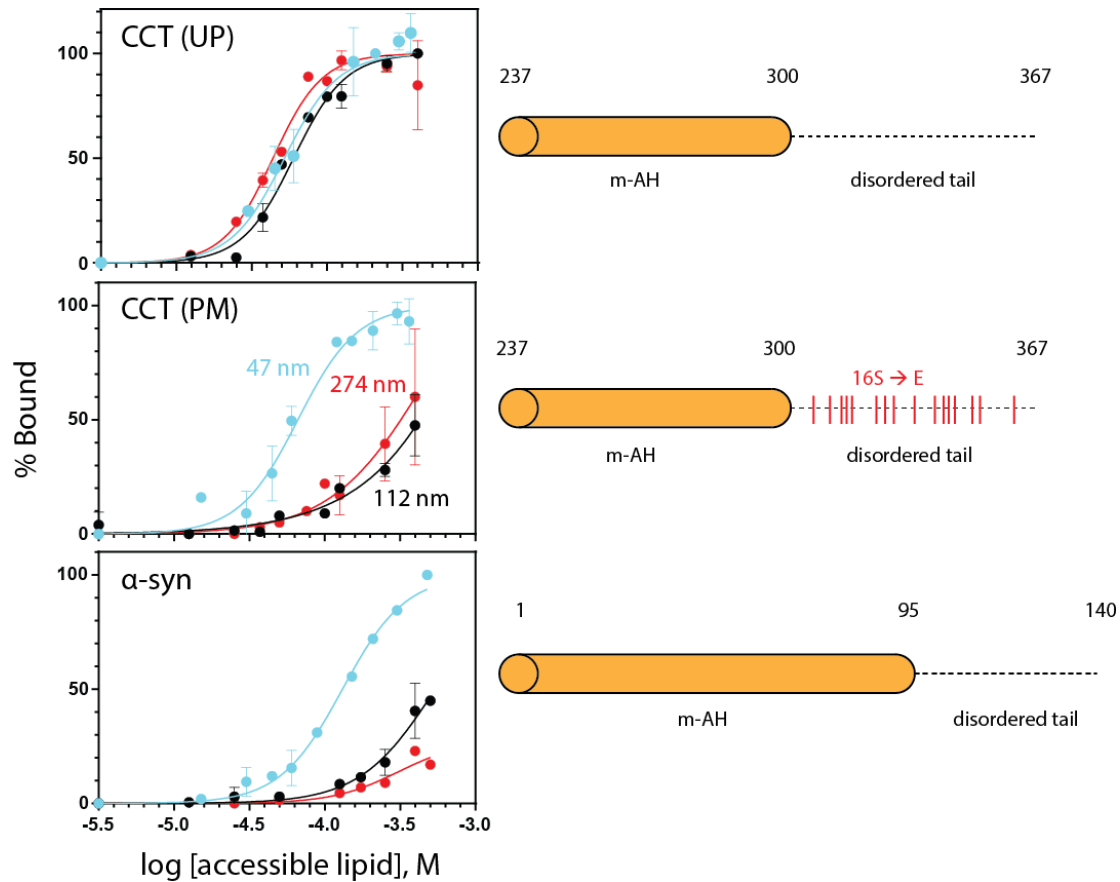


Figure 3.3. CCT (PM) and α -syn are more curvature dependent than CCT (UP).

The percent bound value was based on the fraction of helical structure in the absence of lipid (0% bound) and at saturating lipid (100% bound) which was obtained from the deconvoluted CD data in Figure 3.2. 5 μ M proteins were titrated with 47 nm (light blue), 112 nm (black) or 274 nm (dark blue) vesicles composed of 30 mol% PG in 15 mM ionic strength buffer. Error bars represent the S.D. from two independent trials. Curves were fitted using GraphPad Prism sigmoidal-dose response (variable slope). The schematic of each protein is shown beside the correlated binding curves.

3.1.2. Curvature dependent binding as probed by Trp fluorescence

Though the CD data supported my hypothesis, there were several drawbacks to this method that forced me to seek more sensitive assays to follow membrane binding. Firstly, the CD data were acquired at low (non-physiological) ionic strength to reduce light scattering from salt content. In addition, light scattering was observed at high concentrations of large vesicles, therefore partitioning coefficient (K_p) values could not be determined in cases where binding was weak and higher concentrations of lipid must be reached to observe saturation of binding. Furthermore, as discussed in section 2.6.5,

I was concerned that the results for the strongly binding CCT (UP) may have been complicated by limited membrane surface at low lipid concentrations.

To circumvent these problems and to obtain reliable partitioning coefficients, I monitored membrane binding by using native Trp fluorescence, a more sensitive method that would enable the use of protein concentrations that were ~ 5-fold lower than those needed for the CD analyses. The CCT M+P proteins have a native tryptophan at position 278 in the middle of the m-AH (Table 2.1). The translocation of the Trp from aqueous to membrane-bound results in the Trp emission maxima blue-shifting ~25 nm upon titration of lipid, allowing for observation of membrane binding. The blue-shifting is due to reduced energetic transitions when the Trp engages in dipole interactions with the polar solvent as compared to when the Trp is buried in the membrane, which shields these interactions. The Trp method was more sensitive than the CD method, requiring less protein (1 μ M) to detect a signal. Furthermore, I was able to reach physiological salt concentrations as well as high vesicle concentrations without problems from light scattering. This allowed me to obtain partition coefficients for weakly binding proteins that I could not calculate from CD measurements.

Figure 3.4 shows representative spectra of titrations of CCT (UP) and (PM) with vesicles varying in size and curvature (30 mol% PG). To address any fluorescence emission contributions from tyrosine 240 located on the M domain, I monitored membrane binding via fluorescence intensity at the wavelength of saturating lipid concentrations (~325 nm) over initial intensity in the absence of lipids (~350 nm) (Table 2.5). Two excitation wavelengths were also used: 280 nm and 290 nm excitation (where contributions from tyrosine are less significant)(Ladokhin et al., 2000), however only the results from the 280nm excitation are reported as there were no significant differences in the resulting binding curves. The plots of fluorescence ratio as well as the corresponding sets of normalized binding curves for the CCTs with 30 mol% PG vesicles are shown in Figure 3.5. Partition coefficients were calculated from these curves.

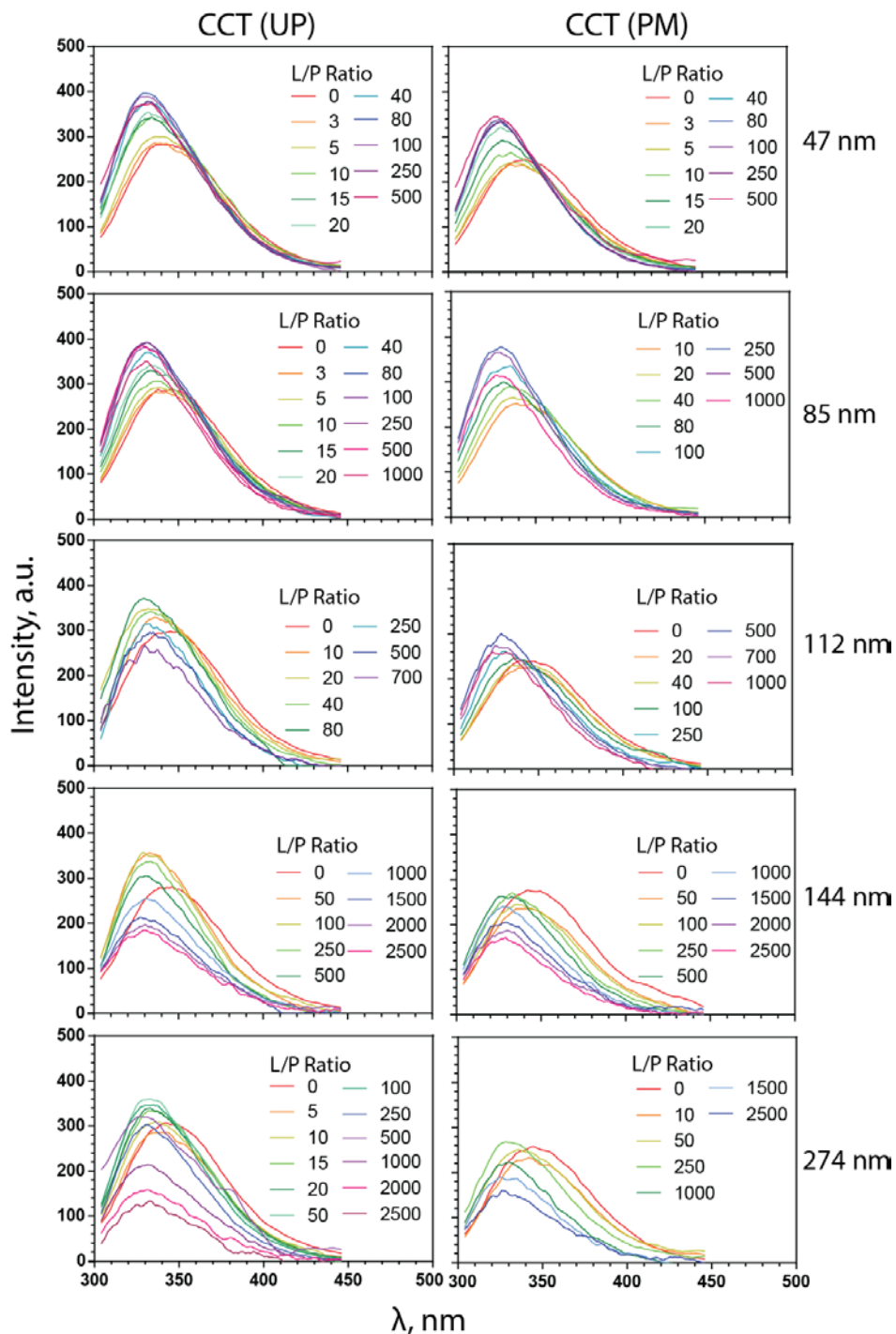


Figure 3.4. The fluorescence of the native Trp in CCT shows a blue-shift and increase in intensity upon titration with vesicles of varying sizes. CCT (UP) and CCT (PM) (1 μ M) with 47, 85, 112, 144 and 274 nm vesicles (30 mol% PG, ionic strength 115 mM). With the larger vesicle sizes (i.e. \geq 112 nm), the spectral intensities are significantly dampened with increasing vesicles due to increased scattering from larger particles. Spectra were smoothed and background-corrected, as described in the methods. The experiments were repeated with similar results.

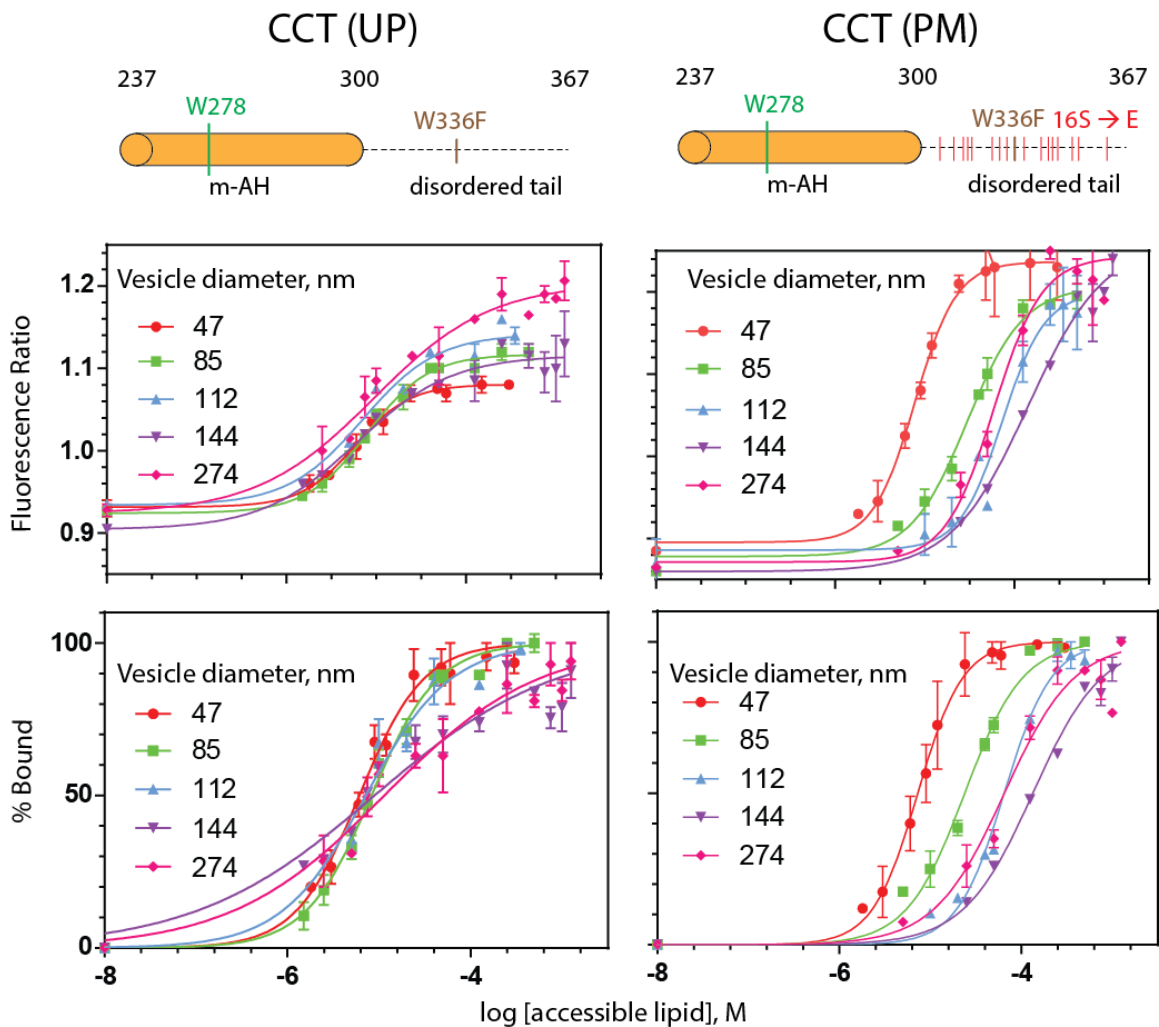


Figure 3.5. Binding curves from Trp fluorescence show that CCT (PM) is more curvature sensitive than CCT (UP).

Corresponding lipid binding curves from Trp fluorescence for the spectral sets in Figure 3.4. 0% bound is set to the fluorescence ratio in the absence of lipid and 100% bound is set to the fluorescence ratio at saturating lipid concentrations. Protein concentration is 1 μ M, vesicles were composed of 30 mol% PG and the ionic strength was 115 mM. Error bars represent the \pm S.D. from two independent trials. Curves were fitted using GraphPad Prism sigmoidal-dose response (variable slope). Lipid / Protein ratio varies from 5 to 2500 within the set of binding curves. The associated simple schematic of each protein is shown above its binding curves.

The results for trials with 30 mol% PG (Figure 3.5) revealed a difference in the curvature sensing of CCT (UP) vs. CCT (PM) in qualitative agreement with the trends observed from the CD measurements (Figure 3.3). Partitioning of CCT (UP) was independent of size, whereas CCT (PM) partitioning increased an order of magnitude from large to smaller vesicles. The results from Trp fluorescence suggested that

introducing negative charges in the region flanking the m-AH weakened binding to vesicles ≥ 112 nm by ~ 10 -fold but strong binding was maintained to 85 nm and even stronger binding to 47 nm vesicles. However, calculations using equation (3) revealed that under conditions of strong binding such as when CCT (UP) proteins bind with vesicles composed of 30 mol% PG, there was no excess lipid at K_p . For example with CCT (UP) and 85-nm vesicles (30 mol% PG), K_p from Trp fluorescence was calculated to be $163,000 \text{ M}^{-1}$ which correlates with an EC_{50} value of $6 \mu\text{M}$. Equation (3) estimates that there is no excess lipid:

$$[\text{excess lipid}] = [EC_{50}] - 25 [0.5 (P_t)]$$

$$[\text{excess lipid}] = (1 \mu\text{M}) - 25 (0.5 \cdot 1 \mu\text{M}) = - 6.5 \mu\text{M}$$

I was therefore uncertain whether my results reflected the curvature independent behaviour of CCT (UP) or whether this method was incapable of capturing the upper limits of partitioning strength. I therefore chose an even more sensitive method of monitoring binding by using an extrinsic fluorescence probe, NBD. This method allowed me to work with 10-fold lower ($0.1 \mu\text{M}$) protein concentrations.

3.1.3. Curvature dependent partitioning as probed by NBD fluorescence

NBD was conjugated via a stable thioether bond to an engineered cysteine at residue 240 (Y240C), near the N-terminal of the CCT m-AH. Since NBD has a structure similar to tryptophan, it should not interfere significantly with membrane binding. The NBD fluorophore was also used to monitor membrane binding of α -synuclein (Pranke et al., 2011). NBD absorbs and emits in the visible spectrum where light scattering interference by large vesicles is small. It can blueshift ~ 15 nm and show enhanced quantum yield when relocated to a hydrophobic environment (Rapaport and Shai, 1991; Shai, 1999).

Figure 3.6 shows representative spectra of titrations of CCT (UP) and (PM) with vesicles varying in size and curvature (30mol% PG). In this case, I monitored membrane binding via the increase in intensity at ~ 533 nm, which is the emission wavelength representing the fully bound NBD-labelled proteins. These plots along with their

corresponding normalized binding curves for the CCTs with 30mol% PG vesicles are shown in Figure 3.7 with apparent K_p values extracted from the accessible lipid concentration at 50% bound peptide (Figure 3.8 A Table 3.1). From calculations using equation (3), there was excess lipid when 50% of the CCT (UP) was bound to 30 mol% vesicles, thus providing more reliable K_p values. In agreement with the CD and Trp fluorescence results, I observed curvature independent binding for CCT (UP) with vesicles between 85 – 144 nm in diameter whereas CCT (PM) membrane binding decreased ≥ 10 -fold from small to larger vesicles.

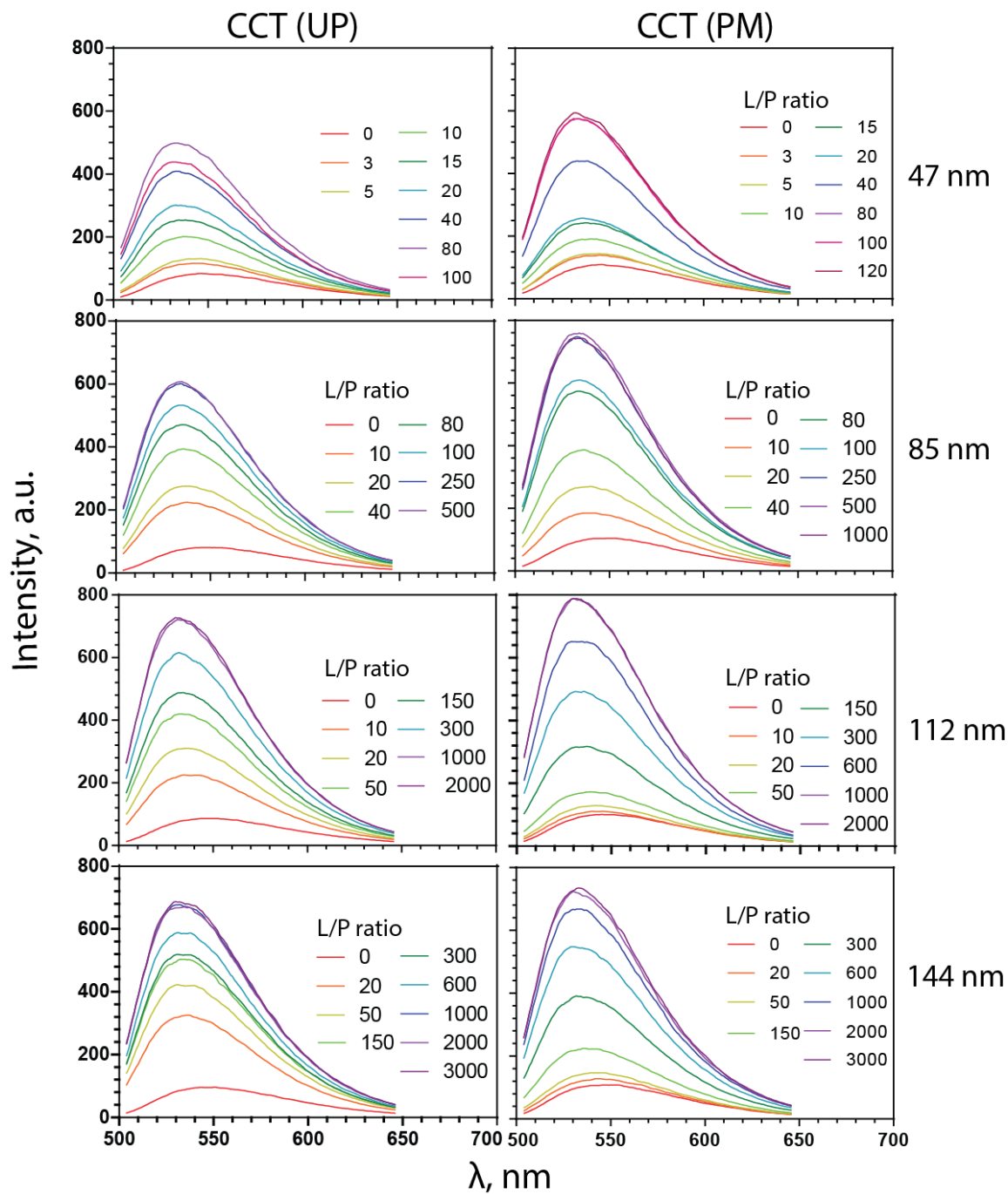


Figure 3.6. The fluorescence emission maxima of the NBD labeled CCT shows a blue-shift and increase in intensity upon titration with 30% PG vesicles of varying sizes. CCT (UP) and CCT (PM) (0.1 μM) with 47, 85, 112 and 144 nm diameter vesicles (30 mol% PG, ionic strength 115 mM). Spectra were smoothed and background-subtracted. Each set was repeated with similar results.

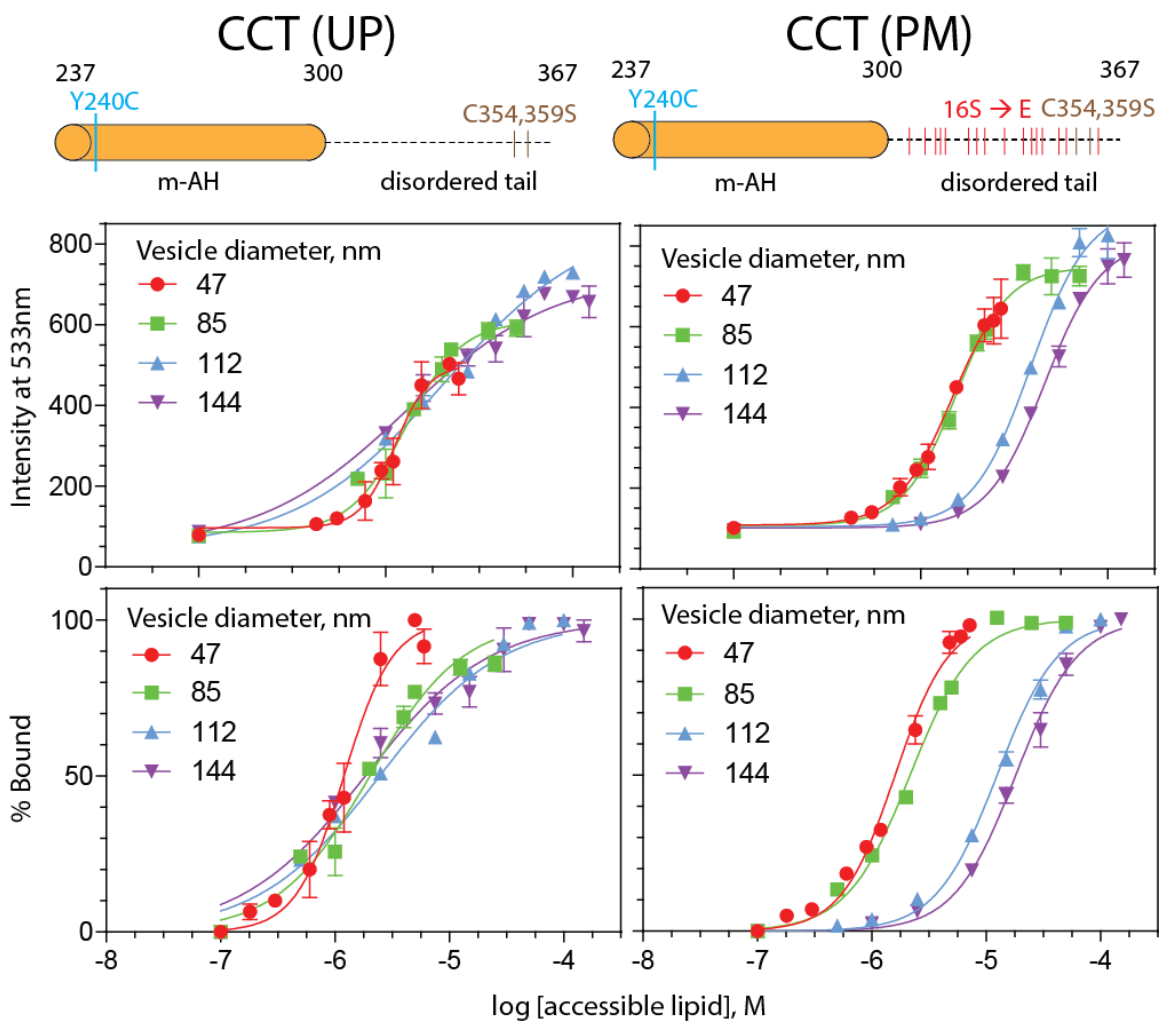


Figure 3.7. Binding curves from NBD fluorescence show that CCT (PM) is more curvature sensitive than CCT (UP).

Corresponding lipid binding curves from NBD fluorescence for the spectral sets in Figure 3.6. 0% bound is set to the fluorescence ratio in the absence of lipid and 100% bound is set to the fluorescence ratio at saturating lipid concentrations. Proteins were 5 μ M, vesicles were composed of 30 mol% PG and the ionic strength was 115 mM. Error bars represent the \pm S.D. from two independent trials. Curves were fitted using GraphPad Prism sigmoidal-dose response (variable slope). Lipid / Protein ratio varies from 5 to 2500 within the set of binding curves. The associated simple schematic of each protein is shown on above its curves.

Results from CD, Trp fluorescence and NBD fluorescence supported the notion that curvature dependence is augmented by a negatively charged tail flanking the m-AH. Regardless of whether the reporter was located at the N-terminal (NBD labelling at position 240 of CCT m-AH) or middle of the CCT m-AH (Trp at position 278 of the CCT

m-AH), a similar trend of curvature sensing was observed with CCT (PM) variant and lack of curvature sensing with CCT (UP).

3.2. The curvature sensitivity of CCT (UP) is influenced by the membrane charge.

Vesicles with 30% anionic lipid have a strong electrostatic surface potential which could mask the impact of changes in curvature-induced membrane hydrophobicity. This might explain the apparent curvature insensitivity of CCT (UP). If strong electrostatic interaction is the basis for the curvature-independent binding, then reduction in membrane charge should generate curvature dependent binding.

Using NBD fluorescence, I measured the partitioning into vesicles composed of 22.5% or 15% PG to show that this is indeed the case. As anionic lipid is decreased, the binding of CCT (UP) became more curvature dependent (Figure 3.8). CCT (UP) binding was > 10-fold weaker towards the flatter, larger vesicles than the smaller curved vesicles. With vesicles containing 15% PG the size dependence for binding was nearly the same for both CCT proteins (Figure 3.8 B and C). These results indicate that membrane charge is a factor influencing curvature dependence for the CCT with an uncharged tail.

On the other hand, the partitioning of CCT (PM), with its electrically repulsive tail, showed curvature dependence regardless of the membrane charge. The effect of increasing membrane charge on the partitioning of CCT (PM) was more muted than the effect on CCT (UP), and this was especially apparent with the larger vesicles.

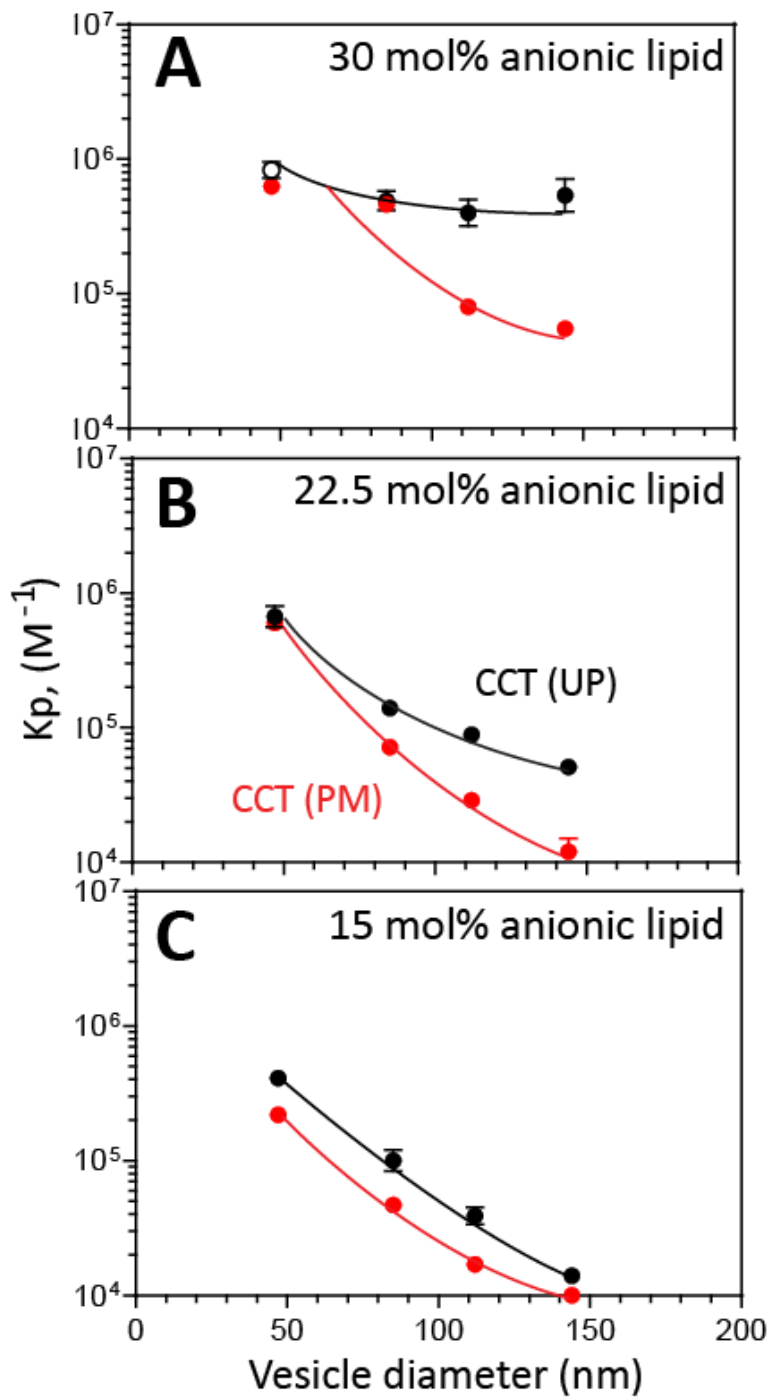


Figure 3.8. Curvature sensing of CCT can be modulated by protein and/or membrane electrostatic properties.

K_p values were determined from binding curves shown in Figure 3.7(NBD fluorescence). $K_p = 1/EC_{50}$. Each data point is the average partition coefficient, $K_p \pm 95\%$ confidence interval for two independent binding analyses. Curves are to facilitate viewing only. The data points in the open black and red circles represent K_p values that are likely underestimated, as there was no excess lipid present at EC_{50} (see Experimental Procedures and Table 3.1).

Table 3.1. Summary of K_p values for CCT (UP) and (PM) using NBD fluorescence: Effect of varying anionic lipid and size of vesicles.

Apparent partition coefficients were the log [accessible lipid] when the protein is 50% bound (EC_{50}) as derived from binding curves and equation (2). Curves were fitted using GraphPad Prism 5.0. Errors are \pm 95% confidence interval for two independent binding analyses; R^2 values are taken from curve fits. K_p estimations were based on $1 / [\text{excess lipid}]$ as described in equation (3) of section 2.6.5.

Mol% PG	Vesicle diameter, nm	CCT (UP)			CCT (PM)		
		Apparent K_p	R^2	K_p estimations	Apparent K_p	R^2	K_p estimations
			$\times 10^3, M^{-1}$			$\times 10^3, M^{-1}$	
30	47	830 \pm 120	0.960	No excess lipid	630 \pm 50	0.988	2900
	85	490 \pm 90	0.968	1300	460 \pm 40	0.993	1100
	112	400 \pm 100	0.975	820	80 \pm 8	0.992	89
	144	540 \pm 170	0.962	1700	55 \pm 5	0.992	60
22.5	47	670 \pm 130	0.968	4100	600 \pm 63	0.985	2300
	85	140 \pm 20	0.982	170	72 \pm 6	0.986	80
	112	89 \pm 7	0.995	100	29 \pm 4	0.984	30
	144	51 \pm 4	0.993	54	12 \pm 3	0.979	12
15	47	410 \pm 50	0.992	830	220 \pm 30	0.918	300
	85	100 \pm 20	0.978	120	47 \pm 5	0.987	50
	112	39 \pm 6	0.993	40	17 \pm 2	0.988	17
	144	14 \pm 2	0.989	15	10 \pm 1	0.975	10

3.3. Negative charge flanking the CCT m-AH reduces the electrostatic component of binding.

The results of varying the charge of the protein or the membrane suggested that curvature sensitivity is enhanced by lowering electrostatic attraction. To show that introduction of repulsive negative charges adjacent to the CCT m-AH reduces the electrostatic component of binding, I compared binding of CCT (UP and PM) to 112 nm, 30 mol% PG vesicles as a function of the buffer ionic strength (Figure 3.9) using native Trp fluorescence. The data show low partitioning for CCT (PM) that is nearly independent of ionic strength, but partitioning for CCT (UP) that is strongly ionic strength-dependent (Figure 3.9 B). Thus the binding of CCT (UP) with a neutral tail is affected by changes in electrostatics, whereas CCT (PM) is much less so.

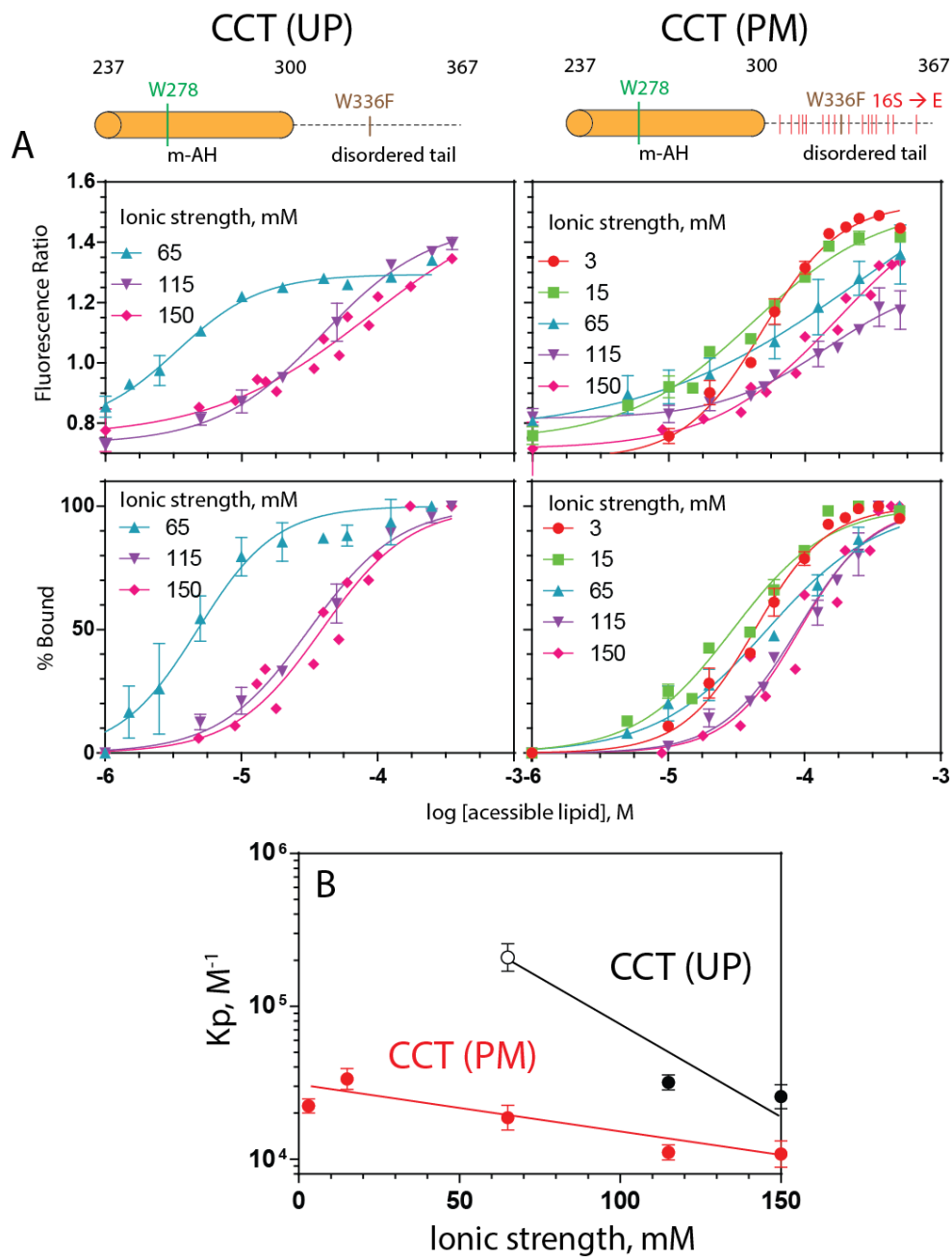


Figure 3.9. Membrane binding of CCT (UP) is sensitive to changes in medium ionic strength whereas CCT (PM) is insensitive.

(A) Binding curves generated from Trp fluorescence ratios. 0% and 100% bound are set to fluorescence ratio in the absence and presence of saturating lipid concentrations, respectively. Proteins were 1 μ M, vesicles were 112 nm in diameter and composed of 30 mol% PG. Error bars represent the \pm S.D. from two independent trials. Curves were fitted using GraphPad Prism sigmoidal-dose response (variable slope). The associated simple schematic of each protein is shown on above its curves. (B) Each data point is the average K_p value \pm 95 % confidence interval for two independent experiments. The open black circle represents a K_p value that is likely underestimated, as there was no excess lipid present at EC50. Thus the ionic strength dependence for CCT (UP) is even stronger than the graph suggests.

Table 3.2. Summary of K_p values for CCT (UP) and (PM) using Trp fluorescence: Varying ionic strength.

Apparent partition coefficients were the log [accessible lipid] when the protein is 50% bound (EC_{50}) as derived from binding curves and equation (2). Curves were fitted using GraphPad Prism 5.0. Errors are \pm 95% confidence interval for two independent binding analyses; R^2 values are taken from curve fits. K_p estimations were based on $1 / [\text{excess lipid}]$ as described in equation (3) of 2.6.5.

Ionic strength, mM	CCT (UP)			CCT (PM)		
	Apparent K_p	R^2	K_p estimation	Apparent K_p	R^2	K_p estimation
		$\times 10^3, M^{-1}$			$\times 10^3, M^{-1}$	
3	-	-	-	23 ± 2	0.986	32
15	-	-	-	33 ± 6	0.974	58
65	209 ± 47	0.940	No excess lipid	19 ± 4	0.975	24
115	32 ± 4	0.987	53	11 ± 1	0.978	13
150	26 ± 5	0.950	38	11 ± 2	0.951	12

3.4. α -Synuclein is less sensitive to electrostatic modulation.

To determine whether charge repulsion adjacent to an m-AH could be a general mechanism augmenting membrane curvature sensitivity, I performed parallel experiments to study the membrane curvature sensing of α -syn. For these experiments, I compared “wild-type” α -syn possessing the highly negatively charged tail (analogous to CCT (PM)) with an α -syn protein that has 12 glutamates and aspartates in the tail region (residues 95-140) mutated to neutral serines (α -syn12S, Figure 1.6 C and Table 2.1). The latter protein is an analog of CCT (UP).

I monitored membrane binding using the fluorescence blue-shifts of an engineered tryptophan to replace valine 37 in the middle of the m-AH (Figure 1.6 B). As shown in the representative spectra, the W37 peak fluorescence shifted from \sim 350 nm in buffer to \sim 325 nm at saturating lipid concentrations, indicating that it had relocated to the hydrophobic environment of the membrane (Figure 3.10). A comparison of the binding to PG/PC SUVs of the W37 variant monitored by Trp fluorescence vs. wild-type α -syn via CD revealed similar Lipid / Protein ratio for half-maximal binding, within a factor of two

(Huang et al., 2013). This suggests the Trp substitution had little effect on partitioning. I tested binding to different sized vesicles made of 30 mol% anionic lipid, as the highly charged membrane revealed the biggest effect of phosphomimicry on the curvature sensing of CCT.

Our results showed that both α -syn and the α -syn12S protein were curvature sensitive under these conditions (Figure 3.11). The α -syn protein showed weak binding to larger vesicles ($d > 85\text{nm}$) and a ≥ 30 -fold improvement in binding with SUVs, a behavior which qualitatively matches the literature reports on the curvature sensitivity of α -syn (Middleton and Rhoades, 2010). α -Syn12S showed a 3 to 4-fold strengthened binding to the larger, flatter vesicles ($d \geq 85\text{nm}$), but retained a strong preference for the very curved SUVs (Figure 3.11 B and Table 3.3). Compared to CCT, reduction of the negative charge flanking the m-AH in α -syn has a weaker impact on curvature dependence. The relative contributions of hydrophobic and electrostatic driving forces in α -syn must differ from the CCT M+P, with α -syn requiring larger modulations of membrane and/or protein charge to affect curvature sensing.

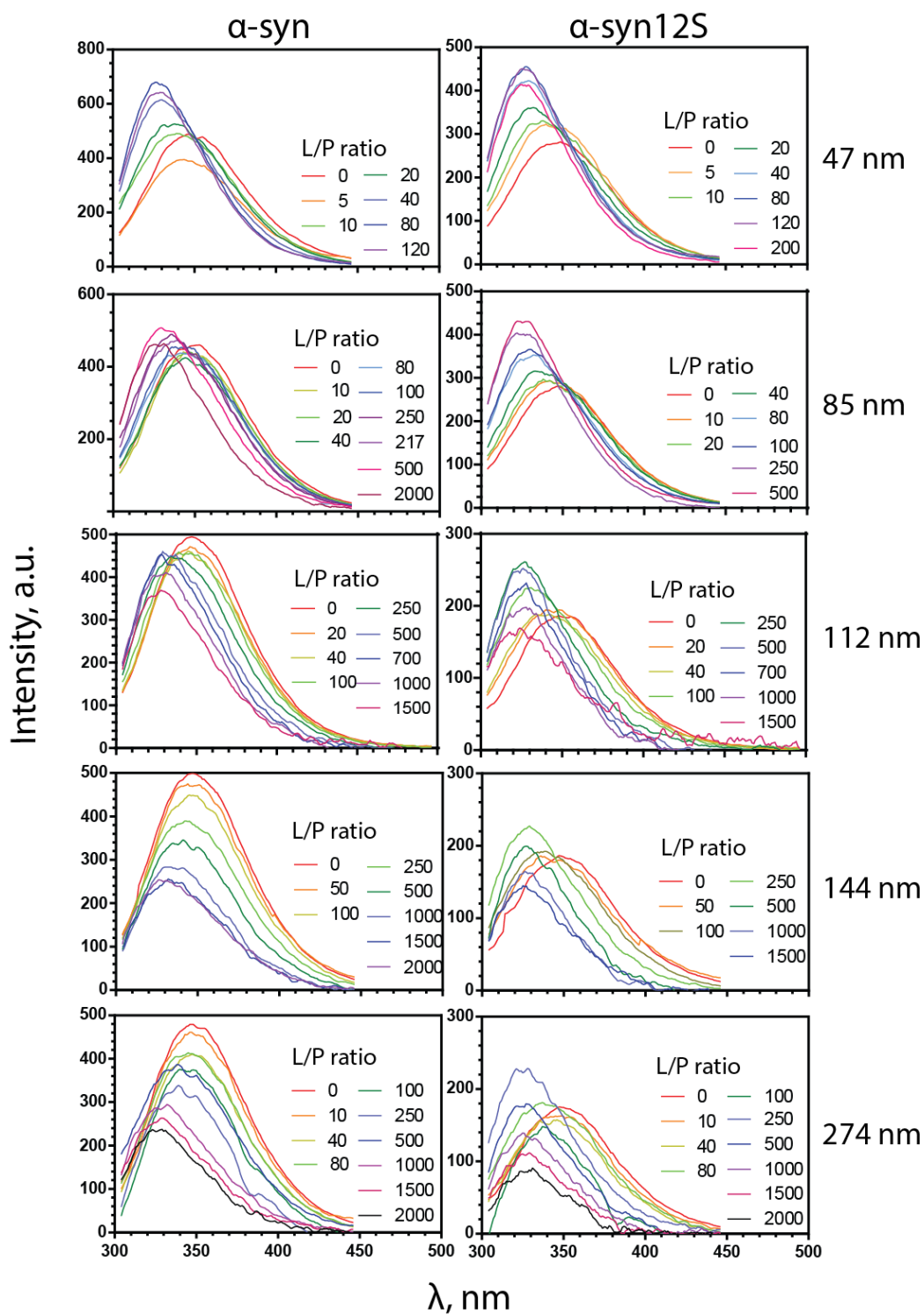


Figure 3.10. The fluorescence of the engineered Trp in α -syn and α -syn12S shows a blue-shift upon titration with vesicles of varying sizes. α -syn and α -syn12S (1 μ M) with 47, 85, 112, 144 and 274nm vesicles (30 mol% PG, ionic strength 115 mM). Spectra were smoothed and background-subtracted. Each set of spectra was repeated with similar results.

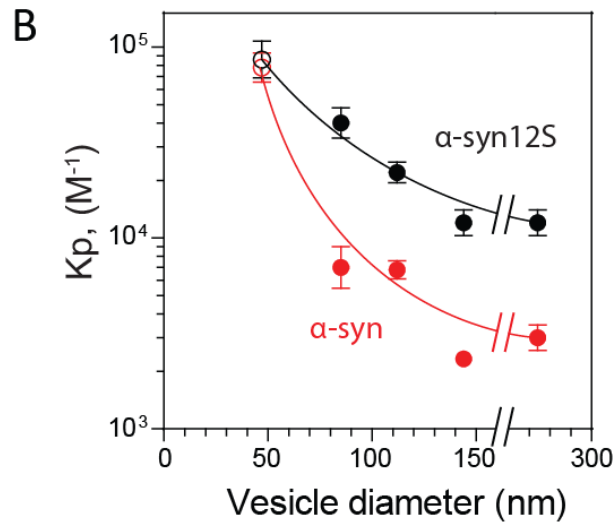
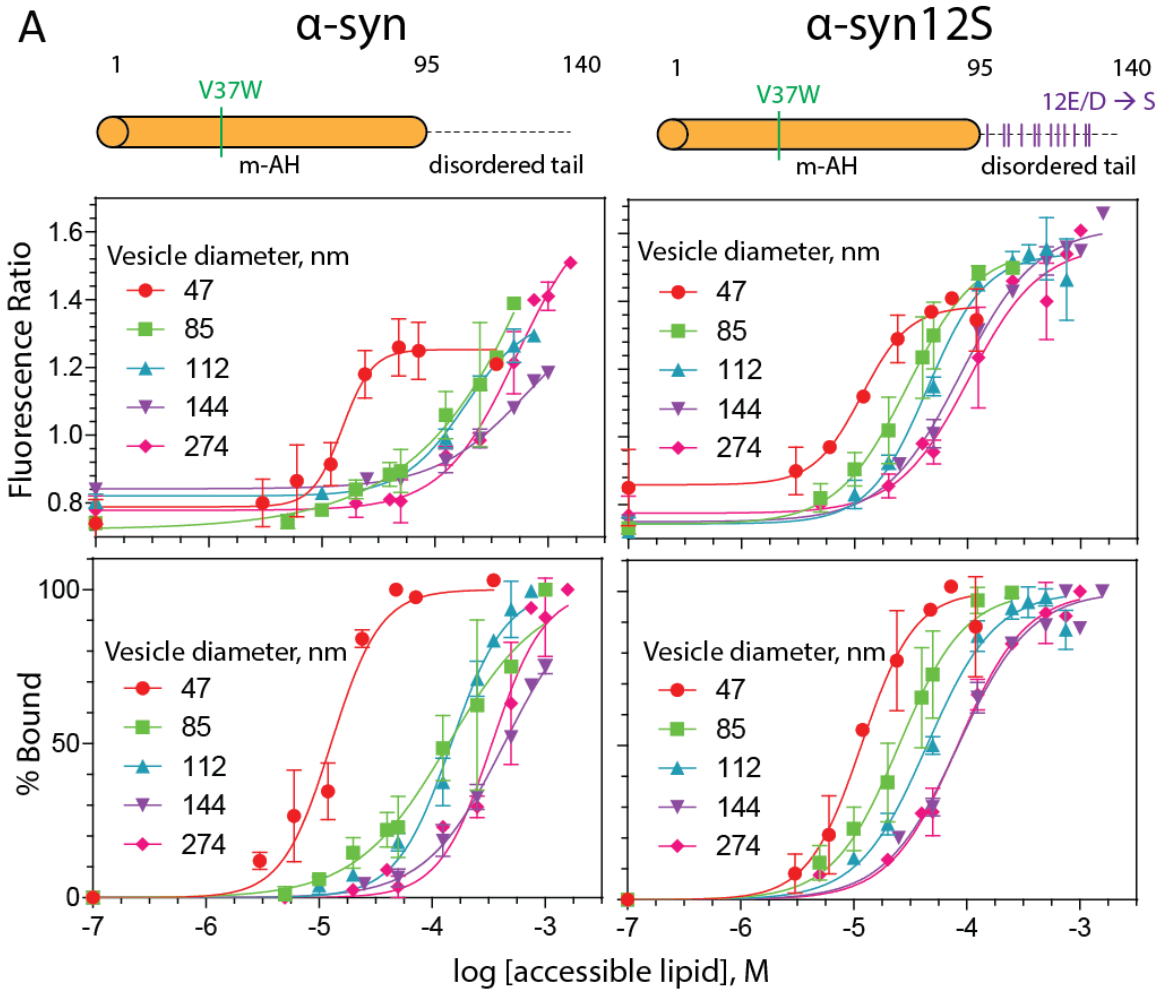


Figure 3.11. Curvature dependence of α -syn and α -syn12S probed by Trp fluorescence.

(A) Binding curves for 1 μ M of α -syn (red curves) or α -syn12S (black curves). Vesicles were composed of 30 mol% PG and the ionic strength was 115 mM. Data were fit to equation (2) using GraphPad Prism 5.0. Error bars represent the \pm S.D. from two independent trials. Curves were fitted using GraphPad Prism sigmoidal-dose response (variable slope). The associated simple schematic of each protein is shown on above its curves. (B) Neutralizing the acidic tail of α -syn increases binding strength. K_p values were determined from the curves of % Bound vs. log [accessible lipid] graph. $K_p = 1 / EC50$. Each data point is the average partition coefficient, $K_p \pm 95\%$ confidence interval for two independent binding analyses. Curves are to facilitate viewing only. The data point in the open red and black circles represent K_p values that are likely underestimated, as there was no excess lipid present at EC50. See sections 2.6.5 and Table 3.2.

Table 3.3. K_p values for α -syn and α -syn12S.

Apparent partition coefficients were the log [accessible lipid] when the protein is 50% bound (EC50) as derived from binding curves and equation (2). Curves were fitted using GraphPad Prism 5.0. Errors are $\pm 95\%$ confidence intervals for two independent binding analyses; R^2 values are taken from curve fits. K_p estimations were based on $1 / [\text{excess lipid}]$ as described in equation (3) of section 2.6.5

Mol % PG	Vesicle diameter, nm	α -syn			α -syn12S		
		Apparent K_p	K_p estimations	R^2	Apparent K_p	K_p estimations	R^2
			$\times 10^3, M^{-1}$			$\times 10^3, M^{-1}$	
30	47	78 ± 15	No excess lipid	0.95 7	86 ± 21	No excess lipid	0.955
	85	7.0 ± 2.0	7.9	0.92 3	40 ± 8	79	0.959
	112	6.8 ± 0.8	7.4	0.98 3	22 ± 3	31	0.981
	144	2.3 ± 0.2	2.4	0.99 2	12 ± 2	14	0.988
	274	3.0 ± 0.5	3.1	0.95 5	12 ± 2	14	0.986

Chapter 4. Concluding Discussion and Future Directions: The significance of curvature sensing for CCT and α -syn proteins

This thesis presents the first explicit demonstration of the curvature sensing feature of the m-AH of CCT in comparison with α -synuclein, a well-described curvature-sensing protein (Jensen et al., 2011; Middleton and Rhoades, 2010; Pranke et al., 2011). My data support the previously introduced idea that curvature sensing by an m-AH can be modulated by changing its charge (Jensen et al., 2011), and specifically provide evidence that curvature sensing can be controlled by charge variation in disordered regions flanking the m-AH. My results suggest a novel potential role for phosphorylation (modeled by phosphomimicry in our experiments) as an electrostatic switch to sensitize an m-AH for curvature sensing. Modulation of curvature dependence by flanking charge was influenced by the hydrophobic character of the m-AH, as shown by the contrasting behaviors of CCT and α -syn.

4.1. Mechanism for modulation of curvature sensing by change in protein electrostatic character

Electrostatic repulsive switches have long been recognized as a means for dampening the binding strength of membrane binding motifs. As discussed in my introduction, the classic example is the binding of polybasic motifs, as in MARCKS and src kinases, which is antagonized by phosphorylation and charge neutralization at several serines within the basic peptide (McLaughlin and Aderem, 1995; McLaughlin and Murray, 2005; Murray et al., 1998). In a study of m-AH curvature sensors, Jensen *et al* (2011) found that curvature sensing in the α -syn m-AH can be affected by amino acid substitutions that alter protein charge. They suggested that curvature sensing is gained when the hydrophobic component of membrane binding exceeds the electrostatic

contribution. Curvature sensing is lost when the electrostatic component dominates. This model was also used to explain the differential targeting of various m-AH containing proteins to flatter plasma membranes vs. highly curved organelle membranes.(Bigay and Antony, 2012)

By contrast, the charge switch I have explored in CCT and α -syn occurs adjacent to, rather than within the m-AH. This charge-switch was most prominent for the CCT m-AH. I propose that an increase in the negative charge of the CCT tail generates electrostatic repulsion with the anionic membrane surface that destabilizes m-AH formation. Antony described m-AH folding and intercalation into lipid membranes as a nucleation-propagation process (Antony, 2011) where insertion of one hydrophobic residue serves as a nucleation point for the remaining AH to fold and intercalate. Instability due to charge repulsion at the C-terminal end of the nascent m-AH may antagonize the nucleation-propagation process. Because its electrostatic character is weakened, m-AH with acidic tails (CCT (PM)) are more dependent on membrane hydrophobicity and curvature.

4.2. The impact of a repulsively charged tail on curvature sensitivity may depend on the electrostatic / hydrophobic balance.

Although the charge switch in the CCT tail affected curvature sensing when membrane charge was strong, it had lesser impact on the curvature sensitivity of α -synuclein. What physico-chemical properties differentiate the behavior of these two m-AH motifs? The membrane binding energy is a composite of contributions from electrostatic and hydrophobic energy terms, as well as changes in membrane and protein entropy (Seelig, 1997; Tamm, 1994). The electrostatic properties of the m-AH motifs in CCT and α -syn are similar. They are both net positive with similar distribution of charged residues (Figure 4.1 and Table 4.1). Basic residues flank the non-polar helical face whereas acidic residues are mostly opposite the non-polar face (Figure 1.6 B). On the other hand, the hydrophobic properties are very different. As discussed in the introduction, the hydrophobic face of the CCT m-AH is richer in large, bulky residues such as tryptophan and phenylalanine whereas the hydrophobic face of the α -syn m-AH

is enriched with smaller residues like valine and alanine (Figure 1.6 B). The mean hydrophobicity of the non-polar face of CCT is twice that of α -syn even though the width of this face is narrower (Table 4.1) (Cornell and Taneva, 2006). The curvature sensitivity of α -syn has been attributed to its very weak non-polar face (Pranke et al., 2011) which would require a strongly hydrophobic (curved) membrane surface to promote binding, even when the repulsive negative charges in its flanking tail have been neutralized.

Table 4.1. Properties of the m-AH in CCT α and α -syn

Table of physicochemical properties modified from Table 1 of (Cornell and Taneva, 2006).

Protein (residues)	Number of amino acids	Negative charges ^a	Positive charges (K, R, H)	Net charge	Aromatic residues (W, Y, F)	Non-polar sector	Mean hydrophobicity of non-polar face (kcal/mol)
CCTα (242-293)	52	10	13	+3	5	120°	0.45
α-syn (1-36)	36	5	7	+2	1	180°	0.27
α-syn (46-82)	37	3	4	+1	0	180°	0.28

¹Assuming the three interfacial glutamates are protonated when the m-AH approaches the acidic membrane interface

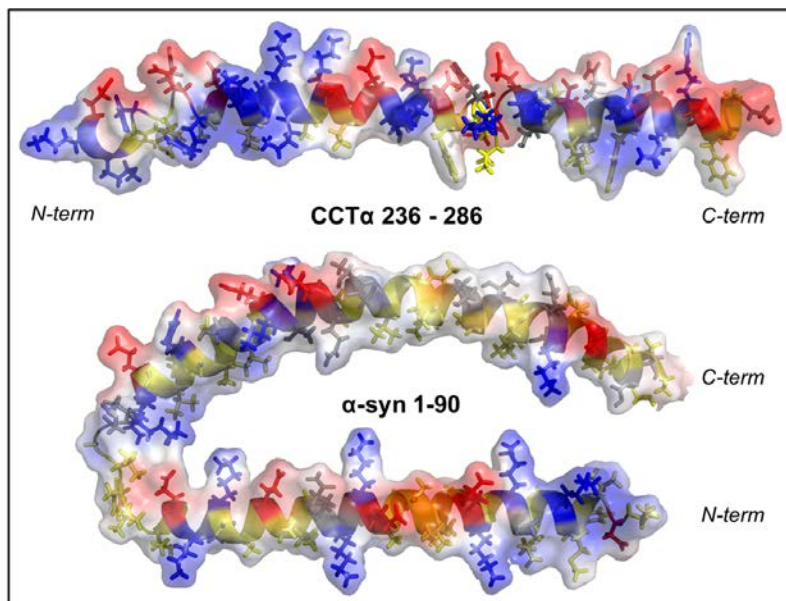


Figure 4.1. The m-AH of CCT α and α -syn have similar distributions of charged residues. Electrostatic surface potential maps generated using Pymol (vacuum electrostatics) for CCT α M domain (residues 236-286; PDB 1peh) and α -syn (residues 1-90; PDB 1xq8). View is from the polar face of the m-AH. Stick rendering for side-chains: blue represents (+) charged residues, red (-) charged, yellow hydrophobic residues and grey represents polar uncharged residues.

In addition, a difference in the electrostatic character of the two proteins may explain their differing responses to the charge neutralization of their tails. There is a greater difference in net charge between CCT (UP) and CCT (PM) as compared to α -syn and α -syn12S which may result in the different curvature sensing behaviours observed in the two sets of proteins. CCT (UP) is much more positively charged compared to α -syn12S (Table 4.2) which may enable binding to anionic membranes indiscriminate of size.

Table 4.2. Δ Net charge of the proteins with negative vs. neutralized tails.

Protein	Neg. Charge ¹	Pos. Charge	Net Charge
CCT(UP)	20	28	+8
CCT (PM)	36	28	-8
		Δ Net charge	16
α -syn12S	12	16	+4
α -syn	24	16	-8
		Δ Net charge	12

¹Assuming the three interfacial glutamates are protonated when the m-AH approaches the acidic membrane interface

4.3. Potential role of acidic tails in targeting m-AH segments to curved or flat membranes in cells

4.3.1. *α -Synuclein may have evolved to have a charged tail to weaken its binding strength.*

There is much literature demonstrating the remarkable curvature sensing of α -syn. But this is the first time a function for the highly negatively charged tail in curvature sensing has been explored. I hypothesized that α -syn evolved an acidic tail to ensure targeting to highly curved synaptic vesicles where it is known to function. My results showed that neutralizing the negative charges flanking the m-AH increased binding affinity towards all vesicles of diameter > 47 nm (Figure 3.11). Thus, without the charged tail α -syn would bind more strongly and with less discrimination between flat and curved organelles in the cell. α -Synuclein can be phosphorylated at four other sites in its acidic tail which may further decrease binding affinity and augment curvature dependence. However, reports on the effects of phosphorylation, phosphomimicry or tyrosine nitration on the tail region of α -syn are somewhat conflicting (Huang et al., 2013; Kuwahara et al., 2012; Paleologou et al., 2008).

4.3.2. Regulation of curvature sensing by phosphorylation of CCT tail could serve to direct CCT to highly curved membranes.

Although CCT has been linked to curvature induction in cells (Gehrig et al., 2008; Gehrig and Ridgway, 2011; Goulbourne et al., 2011; Lagace and Ridgway, 2005; Malhas et al., 2011) its curvature sensing role is more tenuous. As mentioned in the introduction, CCT α is found in the nucleus in many cells, where the inner nuclear membrane is a relatively flat zone rich in anionic lipids (Garnier-Lhomme et al., 2009) resulting in a scenario similar to Figure 3.8 A or B. In such cases, the strong electrostatic force may drive indiscriminate membrane binding of unphosphorylated CCT, but phosphorylation would direct CCT away from the flatter nuclear envelope and onto the curved nucleoplasmic reticulum (Malhas et al., 2011). Lastly, curvature sensing and phosphorylation could facilitate the CCT response to biophysical properties of membranes with a PC deficiency. PC deficiency results in an increase in the density of anionic lipids and non-bilayer favoring lipids, which can augment lipid packing defects (Cornell and Taneva, 2006; Vamparys et al., 2013). Phosphorylation might sensitize CCT to bind only to membrane regions with enhanced packing defects typified by PC deficiency.

4.4. Role of phosphorylation in regions flanking m-AHs on the curvature-sensing of other proteins

Aside from CCT and α -synuclein, there are other proteins containing m-AH motifs whose phosphorylation may modulate membrane binding and/or membrane curvature sensing. Pah1p is a lipin that catalyzes the conversion of phosphatidate to diacylglycerol and contains an ALPS-like m-AH. Its dephosphorylation is crucial for translocation onto membranes, potentially via a membrane curvature sensing mechanism (Karanasios et al., 2010). The membrane tether, Vps41, functions in vesicle-vacuole fusion in yeast. It contains an ALPS motif that can be phosphorylated on serines in its polar face, which weakens binding of the ALPS to the large flat vacuole membrane, and enables a switch to a new protein partner and binding of Vps41 to coated vesicles (Cabrera et al., 2010). A third example, the synaptic vesicle-clustering protein, synapsin, also binds membranes via a curvature-sensing ALPS and its membrane binding is regulated by phosphorylation

(Krabben et al., 2011). How phosphorylation modulates membrane binding of these proteins has not been fully explored. Our results provide a framework for exploring phosphorylation-dependent mechanisms for control of curvature sensing in these and potentially other proteins.

4.5. Critique and Future Work

The *in vitro* work presented in this thesis suggest an intriguing role of phosphorylation in altering the curvature sensing of m-AHs, however parallel *in vivo* studies must be accomplished to gain a complete understanding of the physiological relevance of this role. The first step towards such a goal would involve observing whether there is a difference in the membrane partitioning *in cells* of the m-AH with neutralized vs. acidic tails, and if so whether the differences reflect changes in protein distribution between relatively flat vs. curved membrane systems. For example, does phosphorylation of the CCT α tail direct the enzyme to the nuclear tubules and away from the flat inner nuclear membrane? Though this is not the first time the m-AH of CCT has been studied separate from the full-length CCT, this is the first time curvature sensing has been explored. This study must therefore be expanded to encompass the entire protein, and account for any interactions between the m-AH and the catalytic domain that may influence the curvature sensing behaviour.

In addition, the simplified systems used in my *in vitro* work may have masked certain important subtleties in membrane binding behaviour. For example, though phosphomimicking mutations are commonly used to represent phosphorylated proteins, such mutations are not exact substitutions for the phosphorylated state *in vivo*. Wang and Kent (1995) and Gehrig *et al.* (2009) have used CCT phosphomimic mutations in their studies and observed weakened membrane binding in cells, a result which agrees with the observation that phosphorylation antagonizes membrane binding (Wang et al., 1993; Watkins and Kent, 1991). This suggests that the serine to glutamate mutations may be adequate mimics of phosphorylation. Since this thesis work is concerned about the effect of modifying charge on the curvature sensing of the proteins, the subtleties inherent in phosphomimicry mutations vs. phosphorylated serines may not be so important in the overall conclusions drawn.

There are also limitations to the sensitivity of the methods I used to collect membrane binding data which add complications to the interpretation of my results, in particular, regarding the apparent curvature insensitive binding of CCT (UP) (black line in Figure 3.8 A). As mentioned in the introduction, the bound m-AH can generate curved surfaces in the larger vesicles, therefore, the apparent curvature independent binding of CCT (UP) may actually be a result of remodelling the membrane curvature so as to recruit more CCT. However there is a clear difference in binding strength to large vesicles between CCT (UP) and CCT (PM), although both induce curvature upon binding (Taneva et al., 2012). Although binding of the unphosphorylated form will undoubtedly be promoted by lipid packing defects, its electrostatic attraction to the highly charged vesicles is so strong that an increase in curvature-induced defects would have marginal impact. None-the-less this is a complicating issue that is largely neglected in previous reports on other curvature-sensing proteins, including α -syn. New microscopy-based methods that can directly correlate the vesicle size and bound protein density offer a solution to this problem (Hatzakis et al., 2009; Jensen et al., 2011). In such techniques, vesicles with a wide range of diameters are labelled with a fluorescent lipid and immobilized on a surface. Proteins that are labelled with another fluorescent probe are mixed with these vesicles. The fluorescence signal of a single liposome can be integrated to yield information about its size. An integration of the protein fluorescence associated with that liposome can yield density of bound protein as well as the fraction of liposomes with bound protein. This method is advantageous as it can report binding as a function of curvature with much accuracy.

Finally, though I was able to drastically improve my method of detecting membrane binding with the NBD fluorescence method, I was still unable to obtain reliable partition coefficients for the scenarios where very tight binding occurs (i.e. with the highly curved sonicated vesicles). There are several methods that utilize nanomolar concentrations of proteins that could provide sufficient sensitivity. Biacore Surface Plasmon Resonance translates minute changes in refractive indexes (and therefore changes in the angle of the reflected light) caused by changes in mass at the sensor surface into information about the specificity, affinity and kinetic parameters of a given interaction. In this technique, one can immobilize vesicles on a sensor surface and allow a flow of proteins at various concentrations to interact with the vesicles. From this,

dissociation constants and partition coefficients can be derived for tight interactions that have nanomolar K_D ($10^9 K_D$) (Myszka, 2000) . Furthermore, radiolabelling proteins either by growing cells in media containing radioactive amino acids (e.g. ^{35}S -methionine) or attaching a radioactive group (e.g. using ^3H -N-ethylmaleimide) to the purified protein is an acutely sensitive method that may also be effective in addressing this issue.

References

- Agassandian, M., Zhou, J., Tephly, L.A., Ryan, A.J., Carter, A.B., and Mallampalli, R.K. (2005). Oxysterols inhibit phosphatidylcholine synthesis via ERK docking and phosphorylation of CTP:phosphocholine cytidyltransferase. *J Biol Chem* **280**, 21577-21587.
- Aisenbrey, C., Borowik, T., Bystrom, R., Bokvist, M., Lindstrom, F., Misiak, H., Sani, M.A., and Grobner, G. (2008). How is protein aggregation in amyloidogenic diseases modulated by biological membranes? *Eur Biophys J* **37**, 247-255.
- Antonny, B. (2011). Mechanisms of membrane curvature sensing. *Annu Rev Biochem* **80**, 101-123.
- Arnold, R.S., DePaoli-Roach, A.A., and Cornell, R.B. (1997). Binding of CTP:phosphocholine cytidyltransferase to lipid vesicles: diacylglycerol and enzyme dephosphorylation increase the affinity for negatively charged membranes. *Biochemistry* **36**, 6149-6156.
- Auluck, P.K., Caraveo, G., and Lindquist, S. (2010). alpha-Synuclein: membrane interactions and toxicity in Parkinson's disease. *Annu Rev Cell Dev Biol* **26**, 211-233.
- Bartels, T., Choi, J.G., and Selkoe, D.J. (2011). alpha-Synuclein occurs physiologically as a helically folded tetramer that resists aggregation. *Nature* **477**, 107-110.
- Bartlett, G.R. (1959). Colorimetric assay methods for free and phosphorylated glyceric acids. *J Biol Chem* **234**, 469-471.
- Baumgart, T., Capraro, B.R., Zhu, C., and Das, S.L. (2011). Thermodynamics and mechanics of membrane curvature generation and sensing by proteins and lipids. *Annu Rev Phys Chem* **62**, 483-506.
- Beyer, K., and Ariza, A. (2008). The therapeutical potential of alpha-synuclein antiaggregatory agents for dementia with Lewy bodies. *Curr Med Chem* **15**, 2748-2759.
- Bhatia, V.K., Hatzakis, N.S., and Stamou, D. (2010). A unifying mechanism accounts for sensing of membrane curvature by BAR domains, amphipathic helices and membrane-anchored proteins. *Semin Cell Dev Biol* **21**, 381-390.
- Bigay, J., and Antonny, B. (2012). Curvature, lipid packing, and electrostatics of membrane organelles: defining cellular territories in determining specificity. *Dev Cell* **23**, 886-895.

Bigay, J., Casella, J.F., Drin, G., Mesmin, B., and Antonny, B. (2005). ArfGAP1 responds to membrane curvature through the folding of a lipid packing sensor motif. *EMBO J* 24, 2244-2253.

Bisaglia, M., Tessari, I., Pinato, L., Bellanda, M., Giraudo, S., Fasano, M., Bergantino, E., Bubacco, L., and Mammi, S. (2005). A topological model of the interaction between alpha-synuclein and sodium dodecyl sulfate micelles. *Biochemistry* 44, 329-339.

Bisaglia, M., Trolio, A., Bellanda, M., Bergantino, E., Bubacco, L., and Mammi, S. (2006). Structure and topology of the non-amyloid-beta component fragment of human alpha-synuclein bound to micelles: implications for the aggregation process. *Protein Sci* 15, 1408-1416.

Bogan, M.J., Agnes, G.R., Pio, F., and Cornell, R.B. (2005). Interdomain and membrane interactions of CTP:phosphocholine cytidyltransferase revealed via limited proteolysis and mass spectrometry. *J Biol Chem* 280, 19613-19624.

Bradford, M.M. (1976). A rapid and sensitive method for the quantitation of microgram quantities of protein utilizing the principle of protein-dye binding. *Anal Biochem* 72, 248-254.

Brewer, J.M., Tetley, L., Richmond, J., Liew, F.Y., and Alexander, J. (1998). Lipid vesicle size determines the Th1 or Th2 response to entrapped antigen. *J Immunol* 161, 4000-4007.

Brown, D.R. (2007). Interactions between metals and alpha-synuclein--function or artefact? *FEBS J* 274, 3766-3774.

Burn, P. (1988). Amphitropic proteins: a new class of membrane proteins. *Trends Biochem Sci* 13, 79-83.

Burre, J., Sharma, M., Tsetsenis, T., Buchman, V., Etherton, M.R., and Sudhof, T.C. (2010). Alpha-synuclein promotes SNARE-complex assembly in vivo and in vitro. *Science* 329, 1663-1667.

Buser, C.A., and McLaughlin, S. (1998). Ultracentrifugation technique for measuring the binding of peptides and proteins to sucrose-loaded phospholipid vesicles. *Methods Mol Biol* 84, 267-281.

Buser, C.A., Sigal, C.T., Resh, M.D., and McLaughlin, S. (1994). Membrane binding of myristylated peptides corresponding to the NH2 terminus of Src. *Biochemistry* 33, 13093-13101.

Bussell, R., Jr., and Eliezer, D. (2003). A structural and functional role for 11-mer repeats in alpha-synuclein and other exchangeable lipid binding proteins. *J Mol Biol* 329, 763-778.

- Cabrera, M., Langemeyer, L., Mari, M., Rethmeier, R., Orban, I., Perz, A., Brocker, C., Griffith, J., Klose, D., Steinhoff, H.J., *et al.* (2010). Phosphorylation of a membrane curvature-sensing motif switches function of the HOPS subunit Vps41 in membrane tethering. *J Cell Biol* 191, 845-859.
- Campelo, F., McMahon, H.T., and Kozlov, M.M. (2008). The hydrophobic insertion mechanism of membrane curvature generation by proteins. *Biophys J* 95, 2325-2339.
- Chandra, S., Gallardo, G., Fernandez-Chacon, R., Schluter, O.M., and Sudhof, T.C. (2005). Alpha-synuclein cooperates with CSPalpha in preventing neurodegeneration. *Cell* 123, 383-396.
- Cheng, F., Vivacqua, G., and Yu, S. (2011). The role of alpha-synuclein in neurotransmission and synaptic plasticity. *J Chem Neuroanat* 42, 242-248.
- Choi, B., Choi, M., Kim, J., Yang, Y., Lai, Y., Kweon, D., Lee, N.K., and Shin, Y. (2013). Large α -synuclein oligomers inhibit neuronal SNARE-mediated vesicle docking. *Proc Natl Acad Sci U S A* 110, 4087-4092.
- Conway, K.A., Harper, J.D., and Lansbury, P.T. (1998). Accelerated in vitro fibril formation by a mutant alpha-synuclein linked to early-onset Parkinson disease. *Nat Med* 4, 1318-1320.
- Conway, K.A., Rochet, J.C., Bieganski, R.M., and Lansbury, P.T., Jr. (2001). Kinetic stabilization of the alpha-synuclein protofibril by a dopamine-alpha-synuclein adduct. *Science (New York, NY)* 294, 1346-1349.
- Cooper, A. (2008). Neurodegeneration and Protein Misfolding - What's Gone Wrong with the Cell? *Aus Biochemist* 39, 15 - 18.
- Cornell, R.B. (1991). Regulation of CTP:phosphocholine cytidyltransferase by lipids. 1. Negative surface charge dependence for activation. *Biochemistry* 30, 5873-5880.
- Cornell, R.B., and Northwood, I.C. (2000). Regulation of CTP:phosphocholine cytidyltransferase by amphitropism and relocalization. *TIBS* 25, 441-447.
- Cornell, R.B., and Taneva, S.G. (2006). Amphipathic helices as mediators of the membrane interaction of amphitropic proteins, and as modulators of bilayer physical properties. *Curr Protein Pept Sci* 7, 539-552.
- Cui, H., Lyman, E., and Voth, G.A. (2011). Mechanism of membrane curvature sensing by amphipathic helix containing proteins. *Biophys J* 100, 1271-1279.
- Dathe, M., and Wieprecht, T. (1999). Structural features of helical antimicrobial peptides: their potential to modulate activity on model membranes and biological cells. *Biochim Biophys Acta* 1462, 71-87.
- Davidson, W.S., Jonas, A., Clayton, D.F., and George, J.M. (1998). Stabilization of alpha-synuclein secondary structure upon binding to synthetic membranes. *J Biol Chem* 273, 9443-9449.

- Dennis, M.K., Taneva, S.G., and Cornell, R.B. (2011). The intrinsically disordered nuclear localization signal and phosphorylation segments distinguish the membrane affinity of two cytidylyltransferase isoforms. *J Biol Chem* 286, 12349-12360.
- Ding, T.T., Lee, S.J., Rochet, J.C., and Lansbury, P.T., Jr. (2002). Annular alpha-synuclein protofibrils are produced when spherical protofibrils are incubated in solution or bound to brain-derived membranes. *Biochemistry* 41, 10209-10217.
- Ding, Z., Taneva, S.G., Huang, H.K., Campbell, S.A., Semene, L., Chen, N., and Cornell, R.B. (2012). A 22-mer segment in the structurally pliable regulatory domain of metazoan CTP: phosphocholine cytidylyltransferase facilitates both silencing and activating functions. *J Biol Chem* 287, 38980-38991.
- Dowhan, W. (1997). Molecular basis for membrane phospholipid diversity: why are there so many lipids? *Annu Rev Biochem* 66, 199-232.
- Drescher, M., Veldhuis, G., van Rooijen, B.D., Milikisyants, S., Subramaniam, V., and Huber, M. (2008). Antiparallel arrangement of the helices of vesicle-bound alpha-synuclein. *J Am Chem Soc* 130, 7796-7797.
- Drin, G., and Antonny, B. (2010). Amphipathic helices and membrane curvature. *FEBS Lett* 584, 1840-1847.
- Drin, G., Casella, J.F., Gautier, R., Boehmer, T., Schwartz, T.U., and Antonny, B. (2007). A general amphipathic alpha-helical motif for sensing membrane curvature. *Nat Struct Mol Biol* 14, 138-146.
- Dunne, S.J., Cornell, R.B., Johnson, J.E., Glover, N.R., and Tracey, A.S. (1996). Structure of the membrane binding domain of CTP:phosphocholine cytidylyltransferase. *Biochemistry* 35, 11975-11984.
- Eliezer, D., Kutluay, E., Bussell, R., Jr., and Browne, G. (2001). Conformational properties of alpha-synuclein in its free and lipid-associated states. *J Mol Biol* 307, 1061-1073.
- Escriba, P.V., Ozaita, A., Ribas, C., Miralles, A., Fodor, E., Farkas, T., and Garcia-Sevilla, J.A. (1997). Role of lipid polymorphism in G protein-membrane interactions: nonlamellar-prone phospholipids and peripheral protein binding to membranes. *Proc Natl Acad Sci U S A* 94, 11375-11380.
- Farsad, K., Ringstad, N., Takei, K., Floyd, S.R., Rose, K., and De Camilli, P. (2001). Generation of high curvature membranes mediated by direct endophilin bilayer interactions. *J Cell Biol* 155, 193-200.
- Fink, A.L. (2006). The aggregation and fibrillation of alpha-synuclein. *Acc Chem Res* 39, 628-634.
- Frederick, T.E., Chebukati, J.N., Mair, C.E., Goff, P.C., and Fanucci, G.E. (2009). Bis(monoacylglycero)phosphate forms stable small lamellar vesicle structures: insights into vesicular body formation in endosomes. *Biophys J* 96, 1847-1855.

- Friesen, J.A., Campbell, H.A., and Kent, C. (1999). Enzymatic and cellular characterization of a catalytic fragment of CTP:phosphocholine cytidyltransferase alpha. *J Biol Chem* 274, 13384-13389.
- Frost, A., Unger, V.M., and De Camilli, P. (2009). The BAR domain superfamily: membrane-molding macromolecules. *Cell* 137, 191-196.
- Garnier-Lhomme, M., Byrne, R.D., Hobday, T.M., Gschmeissner, S., Woscholski, R., Poccia, D.L., Dufourc, E.J., and Larijani, B. (2009). Nuclear envelope remnants: fluid membranes enriched in sterols and polyphosphoinositides. *PLoS one* 4, e4255.
- Gehrig, K., Cornell, R.B., and Ridgway, N.D. (2008). Expansion of the nucleoplasmic reticulum requires the coordinated activity of lamins and CTP:phosphocholine cytidyltransferase alpha. *Mol Biol Cell* 19, 237-247.
- Gehrig, K., Morton, C.C., and Ridgway, N.D. (2009). Nuclear export of the rate-limiting enzyme in phosphatidylcholine synthesis is mediated by its membrane binding domain. *J Lipid Res* 50, 966-976.
- Gehrig, K., and Ridgway, N.D. (2011). CTP:phosphocholine cytidyltransferase alpha (CCTalpha) and lamins alter nuclear membrane structure without affecting phosphatidylcholine synthesis. *Biochim Biophys Acta* 1811, 377-385.
- Georgieva, E.R., Ramlall, T.F., Borbat, P.P., Freed, J.H., and Eliezer, D. (2008). Membrane-bound alpha-synuclein forms an extended helix: long-distance pulsed ESR measurements using vesicles, bicelles, and rodlike micelles. *J Am Chem Soc* 130, 12856-12857.
- Georgieva, E.R., Ramlall, T.F., Borbat, P.P., Freed, J.H., and Eliezer, D. (2010). The lipid-binding domain of wild type and mutant alpha-synuclein: compactness and interconversion between the broken and extended helix forms. *J Biol Chem* 285, 28261-28274.
- Gerlach, H., Laumann, V., Martens, S., Becker, C.F., Goody, R.S., and Geyer, M. (2010). HIV-1 Nef membrane association depends on charge, curvature, composition and sequence. *Nat Chem Biol* 6, 46-53.
- Goldenberg, N.M., and Steinberg, B.E. (2010). Surface charge: a key determinant of protein localization and function. *Cancer Res* 70, 1277-1280.
- Goulbourne, C.N., Malhas, A.N., and Vaux, D.J. (2011). The induction of a nucleoplasmic reticulum by prelamin A accumulation requires CTP:phosphocholine cytidyltransferase-alpha. *J Cell Sci* 124, 4253-4266.
- Gruner, S.M., Cullis, P.R., Hope, M.J., and Tilcock, C.P. (1985). Lipid polymorphism: the molecular basis of nonbilayer phases. *Annu Rev Biophys Biophys Chem* 14, 211-238.
- Harlan, J.E., Hajduk, P.J., Yoon, H.S., and Fesik, S.W. (1994). Pleckstrin homology domains bind to phosphatidylinositol-4,5-bisphosphate. *Nature* 371, 168-170.

Hatzakis, N.S., Bhatia, V.K., Larsen, J., Madsen, K.L., Bolinger, P.Y., Kunding, A.H., Castillo, J., Gether, U., Hedegard, P., and Stamou, D. (2009). How curved membranes recruit amphipathic helices and protein anchoring motifs. *Nat Chem Biol* 5, 835-841.

Hejjaoui, M., Butterfield, S., Fauvet, B., Vercruyse, F., Cui, J., Dikiy, I., Prudent, M., Olschewski, D., Zhang, Y., Eliezer, D., *et al.* (2012). Elucidating the role of C-terminal post-translational modifications using protein semisynthesis strategies: alpha-synuclein phosphorylation at tyrosine 125. *J Am Chem Soc* 134, 5196-5210.

Heo, W.D., Inoue, T., Park, W.S., Kim, M.L., Park, B.O., Wandless, T.J., and Meyer, T. (2006). PI(3,4,5)P3 and PI(4,5)P2 lipids target proteins with polybasic clusters to the plasma membrane. *Science* 314, 1458-1461.

Hristova, K., Wimley, W.C., Mishra, V.K., Anantharamiah, G.M., Segrest, J.P., and White, S.H. (1999). An amphipathic alpha-helix at a membrane interface: a structural study using a novel X-ray diffraction method. *J Mol Biol* 290, 99-117.

Hu, J., Shibata, Y., Voss, C., Shemesh, T., Li, Z., Coughlin, M., Kozlov, M.M., Rapoport, T.A., and Prinz, W.A. (2008). Membrane proteins of the endoplasmic reticulum induce high-curvature tubules. *Science* 319, 1247-1250.

Huang, H.K., Taneva, S.G., Lee, J., Silva, L.P., Schriemer, D.C., and Cornell, R.B. (2013). The membrane-binding domain of an amphitropic enzyme suppresses catalysis by contact with an amphipathic helix flanking its active site. *J Mol Biol* 425, 1546-1564.

Hurley, J.H., Newton, A.C., Parker, P.J., Blumberg, P.M., and Nishizuka, Y. (1997). Taxonomy and function of C1 protein kinase C homology domains. *Protein Sci* 6, 477-480.

Iwai, A., Masliah, E., Yoshimoto, M., Ge, N., Flanagan, L., de Silva, H.A., Kittel, A., and Saitoh, T. (1995). The precursor protein of non-A beta component of Alzheimer's disease amyloid is a presynaptic protein of the central nervous system. *Neuron* 14, 467-475.

Jellinger, K.A. (2012). The role of a-synuclein in neurodegeneration - an update. *Translational Neuroscience* 3, 75-122.

Jensen, M.B., Bhatia, V.K., Jao, C.C., Rasmussen, J.E., Pedersen, S.L., Jensen, K.J., Langen, R., and Stamou, D. (2011). Membrane curvature sensing by amphipathic helices: a single liposome study using alpha-synuclein and annexin B12. *J Biol Chem* 286, 42603-42614.

Jensen, P.H., Hager, H., Nielsen, M.S., Hojrup, P., Gliemann, J., and Jakes, R. (1999). alpha-synuclein binds to Tau and stimulates the protein kinase A-catalyzed tau phosphorylation of serine residues 262 and 356. *J Biol Chem* 274, 25481-25489.

Johnson, J.E., and Cornell, R.B. (1999). Amphitropic proteins: regulation by reversible membrane interactions (review). *Mol Membr Biol* 16, 217-235.

Johnson, J.E., Xie, M., Singh, L.M., Edge, R., and Cornell, R.B. (2003). Both acidic and basic amino acids in an amphitropic enzyme, CTP:phosphocholine cytidyltransferase, dictate its selectivity for anionic membranes. *J Biol Chem* 278, 514-522.

Karanasios, E., Han, G.S., Xu, Z., Carman, G.M., and Siniossoglou, S. (2010). A phosphorylation-regulated amphipathic helix controls the membrane translocation and function of the yeast phosphatidate phosphatase. *Proc Natl Acad Sci U S A* 107, 17539-17544.

Kelly, S.M., Jess, T.J., and Price, N.C. (2005). How to study proteins by circular dichroism. *Biochim Biophys Acta* 1751, 119-139.

Kent, C. (1997). CTP:phosphocholine cytidyltransferase. *Biochim Biophys Acta* 1348, 79-90.

Kent, C. (2005). Regulatory enzymes of phosphatidylcholine biosynthesis: a personal perspective. *Biochim Biophys Acta* 1733, 53-66.

Kim, J., Shishido, T., Jiang, X., Aderem, A., and McLaughlin, S. (1994). Phosphorylation, high ionic strength, and calmodulin reverse the binding of MARCKS to phospholipid vesicles. *J Biol Chem* 269, 28214-28219.

Kjaer, L., Giehm, L., Heimborg, T., and Otzen, D. (2009). The influence of vesicle size and composition on alpha-synuclein structure and stability. *Biophys J* 96, 2857-2870.

Krabben, L., Fassio, A., Bhatia, V.K., Pechstein, A., Onofri, F., Fadda, M., Messa, M., Rao, Y., Shupliakov, O., Stamou, D., *et al.* (2011). Synapsin I senses membrane curvature by an amphipathic lipid packing sensor motif. *J Neurosci* 31, 18149-18154.

Krahmer, N., Guo, Y., Wilfling, F., Hilger, M., Lingrell, S., Heger, K., Newman, H.W., Schmidt-Supprian, M., Vance, D.E., Mann, M., *et al.* (2011). Phosphatidylcholine synthesis for lipid droplet expansion is mediated by localized activation of CTP:phosphocholine cytidyltransferase. *Cell Metab* 14, 504-515.

Kutateladze, T.G. (2010). Translation of the phosphoinositide code by PI effectors. *Nat Chem Biol* 6, 507-513.

Kuwahara, T., Tonegawa, R., Ito, G., Mitani, S., and Iwatsubo, T. (2012). Phosphorylation of alpha-synuclein protein at Ser-129 reduces neuronal dysfunction by lowering its membrane binding property in *Caenorhabditis elegans*. *J Biol Chem* 287, 7098-7109.

Ladokhin, A.S., Jayasinghe, S., and White, S.H. (2000). How to measure and analyze tryptophan fluorescence in membranes properly, and why bother? *Anal Biochem* 285, 235-245.

Lagace, T.A., and Ridgway, N.D. (2005). The rate-limiting enzyme in phosphatidylcholine synthesis regulates proliferation of the nucleoplasmic reticulum. *Mol Biol Cell* 16, 1120-1130.

Lee, H.J., Choi, C., and Lee, S.J. (2002). Membrane-bound alpha-synuclein has a high aggregation propensity and the ability to seed the aggregation of the cytosolic form. *J Biol Chem* 277, 671-678.

Lee, J. (2011). The regulatory domain of CTP:phosphocholine cytidyltransferase (CCT): Structure, membrane interactions, and similarity to alpha-synuclein. In *Molecular Biology and Biochemistry* (Burnaby, B. C., Simon Fraser University), pp. 1-118.

Lee, J., Johnson, J., Ding, Z., Paetzel, M., and Cornell, R.B. (2009). Crystal structure of a mammalian CTP: phosphocholine cytidyltransferase catalytic domain reveals novel active site residues within a highly conserved nucleotidyltransferase fold. *J Biol Chem* 284, 33535-33548.

Lee, M.C., Orci, L., Hamamoto, S., Futai, E., Ravazzola, M., and Schekman, R. (2005). Sar1p N-terminal helix initiates membrane curvature and completes the fission of a COPII vesicle. *Cell* 122, 605-617.

Lenarcic, R., Halbedel, S., Visser, L., Shaw, M., Wu, L.J., Errington, J., Marenduzzo, D., and Hamoen, L.W. (2009). Localisation of DivIVA by targeting to negatively curved membranes. *Embo J* 28, 2272-2282.

Leong, S.L., Cappai, R., Barnham, K.J., and Pham, C.L. (2009). Modulation of alpha-synuclein aggregation by dopamine: a review. *Neurochem Res* 34, 1838-1846.

Leventis, P.A., and Grinstein, S. (2010). The distribution and function of phosphatidylserine in cellular membranes. *Annu Rev Biophys* 39, 407-427.

Li, Z., and Vance, D.E. (2008). Phosphatidylcholine and choline homeostasis. *J Lipid Res* 49, 1187-1194.

Liu, S.T.H., Sharon-Frilling, R., Ivanova, P., Milne, S.B., Myers, D.S., Rabinowitz, J.D., Brown, H.A., and Shenk, T. (2011). Synaptic vesicle-like lipidome of human cytomegalovirus virions reveals a role for SNARE machinery in virion egress. *Proc Natl Acad Sci U S A* 108, 12869-12874.

Lykidis, A., Baburina, I., and Jackowski, S. (1999). Distribution of CTP:phosphocholine cytidyltransferase (CCT) isoforms. Identification of a new CCTbeta splice variant. *J Biol Chem* 274, 26992-27001.

MacDonald, J.I., and Kent, C. (1994). Identification of phosphorylation sites in rat liver CTP: phosphocholine cytidyltransferase. *J Biol Chem* 269, 10529-10537.

Malhas, A., Goulbourne, C., and Vaux, D.J. (2011). The nucleoplasmic reticulum: form and function. *Trends Cell Biol* 21, 362-373.

Martens, S., Kozlov, M.M., and McMahon, H.T. (2007). How synaptotagmin promotes membrane fusion. *Science (New York, NY)* 316, 1205-1208.

Martens, S., and McMahon, H.T. (2008). Mechanisms of membrane fusion: disparate players and common principles. *Nat Rev Mol Cell Biol* 9, 543-556.

- Matsuzaki, K. (1998). Magainins as paradigm for the mode of action of pore forming polypeptides. *Biochim Biophys Acta* 1376, 391-400.
- Matsuzaki, K., Murase, O., Sugishita, K., Yoneyama, S., Akada, K., Ueha, M., Nakamura, A., and Kobayashi, S. (2000). Optical characterization of liposomes by right angle light scattering and turbidity measurement. *Biochim Biophys Acta* 1467, 219-226.
- Mayer, L.D., Hope, M.J., and Cullis, P.R. (1986). Vesicles of variable sizes produced by a rapid extrusion procedure. *Biochim Biophys Acta* 858, 161-168.
- McLaughlin, S., and Aderem, A. (1995). The myristoyl-electrostatic switch: a modulator of reversible protein-membrane interactions. *TIBS* 20, 272-276.
- McLaughlin, S., and Murray, D. (2005). Plasma membrane phosphoinositide organization by protein electrostatics. *Nature* 438, 605-611.
- McMahon, H.T., and Gallop, J.L. (2005). Membrane curvature and mechanisms of dynamic cell membrane remodeling. *Nature* 438, 590-596.
- Mesmin, B., Drin, G., Levi, S., Rawet, M., Cassel, D., Bigay, J., and Antonny, B. (2007). Two lipid-packing sensor motifs contribute to the sensitivity of ArfGAP1 to membrane curvature. *Biochemistry* 46, 1779-1790.
- Middleton, E.R., and Rhoades, E. (2010). Effects of curvature and composition on alpha-synuclein binding to lipid vesicles. *Biophys J* 99, 2279-2288.
- Murray, D., Hermida-Matsumoto, L., Buser, C.A., Tsang, J., Sigal, C.T., Ben-Tal, N., Honig, B., Resh, M.D., and McLaughlin, S. (1998). Electrostatics and the membrane association of Src: theory and experiment. *Biochemistry* 37, 2145-2159.
- Myszka, D.G. (2000). Kinetic, equilibrium, and thermodynamic analysis of macromolecular interactions with BIACORE. *Methods Enzymol* 323, 333-340.
- Nuscher, B., Kamp, F., Mehnert, T., Odoy, S., Haass, C., Kahle, P.J., and Beyer, K. (2004). Alpha-synuclein has a high affinity for packing defects in a bilayer membrane: a thermodynamics study. *J Biol Chem* 279, 21966-21975.
- Paleologou, K.E., Schmid, A.W., Rospigliosi, C.C., Kim, H.Y., Lamberto, G.R., Fredenburg, R.A., Lansbury, P.T., Jr., Fernandez, C.O., Eliezer, D., Zweckstetter, M., *et al.* (2008). Phosphorylation at Ser-129 but not the phosphomimics S129E/D inhibits the fibrillation of alpha-synuclein. *J Biol Chem* 283, 16895-16905.
- Peter, B.J., Kent, H.M., Mills, I.G., Vallis, Y., Butler, P.J., Evans, P.R., and McMahon, H.T. (2004). BAR domains as sensors of membrane curvature: the amphiphysin BAR structure. *Science* 303, 495-499.
- Pranke, I.M., Morello, V., Bigay, J., Gibson, K., Verbavatz, J.M., Antonny, B., and Jackson, C.L. (2011). alpha-Synuclein and ALPS motifs are membrane curvature sensors whose contrasting chemistry mediates selective vesicle binding. *J Cell Biol* 194, 89-103.

- Rapaport, D., and Shai, Y. (1991). Interaction of fluorescently labeled pardaxin and its analogues with lipid bilayers. *J Biol Chem* 266, 23769-23775.
- Rebecchi, M.J., and Scarlata, S. (1998). Pleckstrin homology domains: a common fold with diverse functions. *Annu Rev Biophys Biomol Struct* 27, 503-528.
- Recchia, A., Debetto, P., Negro, A., Guidolin, D., Skaper, S.D., and Giusti, P. (2004). Alpha-synuclein and Parkinson's disease. *FASEB J* 18, 617-626.
- Richnau, N., Fransson, A., Farsad, K., and Aspenstrom, P. (2004). RICH-1 has a BIN/Amphiphysin/Rvsp domain responsible for binding to membrane lipids and tubulation of liposomes. *Biochem Biophys Res Commun* 320, 1034-1042.
- Rizo, J., and Sudhof, T.C. (1998). C2-domains, structure and function of a universal Ca²⁺-binding domain. *J Biol Chem* 273, 15879-15882.
- Roux, A., Koster, G., Lenz, M., Sorre, B., Manneville, J.B., Nassoy, P., and Bassereau, P. (2010). Membrane curvature controls dynamin polymerization. *Proc Natl Acad Sci U S A* 107, 4141-4146.
- Salaun, C., Greaves, J., and Chamberlain, L.H. (2010). The intracellular dynamic of protein palmitoylation. *J Chem Biol* 191, 1229-1238.
- Seelig, J. (1997). Titration calorimetry of lipid-peptide interactions. *Biochim Biophys Acta* 1331, 103-116.
- Shai, Y. (1999). Mechanism of the binding, insertion and destabilization of phospholipid bilayer membranes by alpha-helical antimicrobial and cell non-selective membrane-lytic peptides. *Biochim Biophys Acta* 1462, 55-70.
- Sousa, V.L., Bellani, S., Giannandrea, M., Yousuf, M., Valtorta, F., Meldolesi, J., and Chieregatti, E. (2009). {alpha}-synuclein and its A30P mutant affect actin cytoskeletal structure and dynamics. *Mol Biol Cell* 20, 3725-3739.
- Sreerama, N., and Woody, R.W. (2000). Estimation of protein secondary structure from circular dichroism spectra: comparison of CONTIN, SELCON, and CDSSTR methods with an expanded reference set. *Anal Biochem* 287, 252-260.
- Stachowiak, J.C., Hayden, C.C., and Sasaki, D.Y. (2010). Steric confinement of proteins on lipid membranes can drive curvature and tubulation. *Proc Natl Acad Sci U S A* 107, 7781-7786.
- Tamm, L.K. (1994). Physical Studies of Peptide—Bilayer Interactions. In *Membrane Protein Structure*, S.H. White, ed. (Springer New York), pp. 283-313.
- Taneva, S.G., Lee, J.M., and Cornell, R.B. (2012). The amphipathic helix of an enzyme that regulates phosphatidylcholine synthesis remodels membranes into highly curved nanotubules. *Biochim Biophys Acta* 1818, 1173-1186.

- Thelen, M., Rosen, A., Nairn, A.C., and Aderem, A. (1991). Regulation by phosphorylation of reversible association of a myristoylated protein kinase C substrate with the plasma membrane. *Nature* *351*, 320-322.
- Trexler, A.J., and Rhoades, E. (2009). Alpha-synuclein binds large unilamellar vesicles as an extended helix. *Biochemistry* *48*, 2304-2306.
- Uversky, V.N., Li, J., and Fink, A.L. (2001). Evidence for a partially folded intermediate in alpha-synuclein fibril formation. *J Biol Chem* *276*, 10737-10744.
- Vamparys, L., Gautier, R., Vanni, S., Bennett, W.F., Tieleman, D.P., Antony, B., Etchebest, C., and Fuchs, P.F. (2013). Conical lipids in flat bilayers induce packing defects similar to that induced by positive curvature. *Biophys J* *104*, 585-593.
- van Meer, G., Voelker, D.R., and Feigenson, G.W. (2008). Membrane lipids: where they are and how they behave. *Nat Rev Mol Cell Biol* *9*, 112-124.
- Varkey, J., Isas, J.M., Mizuno, N., Jensen, M.B., Bhatia, V.K., Jao, C.C., Petrlova, J., Voss, J.C., Stamou, D.G., Steven, A.C., *et al.* (2010). Membrane curvature induction and tubulation are common features of synucleins and apolipoproteins. *J Biol Chem* *285*, 32486-32493.
- Vilar, M., Chou, H.T., Luhrs, T., Maji, S.K., Riek-Loher, D., Verel, R., Manning, G., Stahlberg, H., and Riek, R. (2008). The fold of alpha-synuclein fibrils. *Proc Natl Acad Sci U S A* *105*, 8637-8642.
- Volles, M.J., and Lansbury, P.T., Jr. (2003). Zeroing in on the pathogenic form of alpha-synuclein and its mechanism of neurotoxicity in Parkinson's disease. *Biochemistry* *42*, 7871-7878.
- Volles, M.J., Lee, S.J., Rochet, J.C., Shtilerman, M.D., Ding, T.T., Kessler, J.C., and Lansbury, P.T., Jr. (2001). Vesicle permeabilization by protofibrillar alpha-synuclein: implications for the pathogenesis and treatment of Parkinson's disease. *Biochemistry* *40*, 7812-7819.
- Voth, G.A. (2013). New and notable: key new insights into membrane targeting by proteins. *Biophys J* *104*, 517-519.
- Wang, Y., and Kent, C. (1995). Effects of altered phosphorylation sites on the properties of CTP:phosphocholine cytidyltransferase. *J Biol Chem* *270*, 17843-17849.
- Wang, Y., MacDonald, J.I., and Kent, C. (1993.) Regulation of CTP:phosphocholine cytidyltransferase in HeLa cells. Effect of oleate on phosphorylation and intracellular localization. *J Biol Chem* *268*, 5512-5518.
- Watkins, J.D., and Kent, C. (1991). Regulation of CTP:phosphocholine cytidyltransferase activity and subcellular location by phosphorylation in Chinese hamster ovary cells. The effect of phospholipase C treatment. *The Journal of biological chemistry* *266*, 21113-21117.

Weinreb, P.H., Zhen, W., Poon, A.W., Conway, K.A., and Lansbury, P.T., Jr. (1996). NACP, a protein implicated in Alzheimer's disease and learning, is natively unfolded. *Biochemistry* 35, 13709-13715.

Westphal, C.H., and Chandra, S.S. (2013). Monomeric synucleins generate membrane curvature. *J Biol Chem* 288, 1829-1840.

Wieprecht, M., Wieder, T., Paul, C., Geilen, C.C., and Orfanos, C.E. (1996). Evidence for phosphorylation of CTP:phosphocholine cytidyltransferase by multiple proline-directed protein kinases. *J Biol Chem* 271, 9955-9961.

Wieprecht, T., Apostolov, O., Beyermann, M., and Seelig, J. (2000). Interaction of a mitochondrial presequence with lipid membranes: role of helix formation for membrane binding and perturbation. *Biochemistry* 39, 15297-15305.

Zhang, B., Koh, Y.H., Beckstead, R.B., Budnik, V., Ganetzky, B., and Bellen, H.J. (1998). Synaptic vesicle size and number are regulated by a clathrin adaptor protein required for endocytosis. *Neuron* 21, 1465-1475.

Zhu, M., and Fink, A.L. (2003). Lipid binding inhibits alpha-synuclein fibril formation. *J Biol Chem* 278, 16873-16877.

Zimmerberg, J., and Kozlov, M.M. (2006). How proteins produce cellular membrane curvature. *Nat Rev Mol Cell Biol* 7, 9-19.